

Thermal transport in low dimensions

THÈSE N° 6950 (2016)

PRÉSENTÉE LE 1^{ER} MARS 2016

À LA FACULTÉ DES SCIENCES ET TECHNIQUES DE L'INGÉNIEUR
LABORATOIRE DE THÉORIE ET SIMULATION DES MATÉRIAUX
PROGRAMME DOCTORAL EN SCIENCE ET GÉNIE DES MATÉRIAUX

ÉCOLE POLYTECHNIQUE FÉDÉRALE DE LAUSANNE

POUR L'OBTENTION DU GRADE DE DOCTEUR ÈS SCIENCES

PAR

Andrea CEPELLOTTI

acceptée sur proposition du jury:

Prof. P. Muralt, président du jury
Prof. N. Marzari, directeur de thèse
Prof. M. Verstraete, rapporteur
Prof. D. G. Cahill, rapporteur
Prof. O. Yazyev, rapporteur



ÉCOLE POLYTECHNIQUE
FÉDÉRALE DE LAUSANNE

Suisse
2016

Thermodynamics is a funny subject.
The first time you go through it, you don't understand it at all.
The second time you go through it, you think you understand it,
except for one or two small points.
The third time you go through it, you know you don't understand it,
but by that time you are so used to it, it doesn't bother you any more.
— Arnold Sommerfeld

Dedicated to my parents

Acknowledgements

The Thesis is the end of a long journey, which I wouldn't have completed if not for the support of many people that I encountered in the last years.

Firstly, I thank my supervisor, Prof. Nicola Marzari, for accepting me as a PhD student and for giving me the possibility of investigating transport properties and the issues of data management. I truly appreciated the freedom he granted in my studies and his guidance for conducting research in an effective way.

A special mention goes to my ever tireless friend Giovanni Pizzi, which I have to thank for the countless discussions we had in the last years and for teaching me the proper way of writing software in an object-oriented style.

There are many other people which have been involved in AiiDA, in particular Boris Kozinsky with valuable thoughts and insights. Moreover the project has been growing steadily and I want to thank all the people that have contributed to the project (in random order): Nicolas Mounet, Andrius Merkys, Giovanni 'Gustav' Borghi, Marco Gibertini, Philippe Schwaller, Riccardo Sabatini, Valentin Bersier, Spyros Zoupanos, Snehal Waychal, Martin Uhrin, Leonid Kahle and many other more that are believing in this software and are working for its success.

The collaboration with the group of Prof. Francesco Mauri has been for me an important moment of my education, and I have to thank him and all his coworkers, Giorgia Fugallo for the valuable discussions, Lorenzo Paulatto for its work on Quantum ESPRESSO and Prof. Michele Lazzeri.

I would like to thank all the members of the THEOS group which made enjoyable my time at EPFL, those mentioned above and Daniele, Anand, all the Nicola's, Oliviero, David, James, Linh, Emine, Gianluca, Antimo, Aris, Matteo, Ivano, Eva, Irène, Riccarda, Lidia and Elisabeth and all the visiting people that passed by the group.

Last but not least, I would like to thank my family for their support: my brother Mauro and my parents Paolo and Rosa Anna, to whom I dedicate my Thesis.

Lausanne, 25 January 2016

A. C.

Abstract

Lattice vibrations are the microscopic mechanism responsible for a large, if not dominant, contribution to heat transport in crystalline insulators. These vibrations are described in terms of phonons, collective excitations (or quasiparticles) in the form of waves of atomic displacements inside a crystal. Phonons are traditionally considered to be the quasiparticles responsible for carrying heat through the material. Heat transport is considered as a flux of a phonon gas, diffusing from hot areas (high phonon densities) to cold areas (low phonon densities) in an attempt to reestablish equilibrium, with phonon collisions being the source of heat flux dissipation. However, as dimensionality is reduced, the motion of phonons stimulated by temperature perturbations becomes correlated and this gas-like picture of thermal transport in terms of phonons becomes invalid.

In this Thesis, we lay out an interpretation of thermal transport in 2D materials based on the Boltzmann transport equation in the form of collective excitations of phonons. These collective phonon excitations give rise to complex phenomena, such as high thermal conductivities, that are otherwise unexplained. As another example, collective excitations, at variance with conventional diffusive transport, can induce wave-like heat propagation, or second sound. This had been found only in a few exotic materials at cryogenic temperatures, but is present instead routinely in 2D materials at room temperature.

The correlated-phonon description of heat transfer can be rationalised by introducing a new collective excitation, called 'relaxon', which is defined as the eigenstate of the collision operator. Whereas only oversimplifying assumptions endow phonons with well defined relaxation times (the average interval of time between collisions), relaxons have always well defined relaxation times and permit an exact description of thermal transport. The complex dynamic of heat transport in 2D is thus greatly simplified and a kinetic gas theory of thermal transport still applies, provided that the gas is not constituted by phonons, but by relaxons.

Our work on thermal transport is part of a larger effort, aiming at the creation of a database of numerically computed properties of materials. The high-throughput production of simulated properties is a challenging task, since it necessitates the understanding of a physical model, but it also needs to face a myriad of technicalities and problems that hinder the execution of a large number of calculations. In order to allow the creation of computational materials databases, we developed AiiDA, an open-source automated interactive infrastructure and database for computational science. This platform tackles the problems of creation, management, analysis and sharing of data and simulations, summarized in the pillars of Automation, Data, Environment and Sharing. Automation is achieved by management of remote computational

Acknowledgements

resources and the encoding of workflows, that allows the execution of complex sequences of calculations. The tight coupling between automation and data storage, handled by the platform, enables full reproducibility of the results and a suitable database design allows for efficient data analysis tools. Sharing of scientific knowledge is addressed by providing tools for distribution of data and of the underlying workflows that generated them, creating an ecosystem for computational materials science.

Keywords: thermal conductivity, heat, transport, first principles, automation

Riassunto

Le vibrazioni atomiche sono il principale meccanismo responsabile per il trasporto termico in un cristallo dielettrico. Queste vibrazioni sono descritte in termini di fononi, cioè eccitazioni collettive di atomi (o quasiparticelle) in forma di onde di vibrazioni atomiche nel cristallo. Tradizionalmente i fononi sono considerati le quasiparticelle responsabili del trasporto di calore in un materiale, modellizzato come il flusso di un gas che diffonde da zone calde (ad alta concentrazione di fononi) a fredde (a bassa concentrazione di fononi), nel tentativo di ristabilire l'equilibrio termico attraverso collisioni tra quasiparticelle che dissipano il flusso di calore. Tuttavia, riducendo la dimensionalità, il moto dei fononi stimolato da una perturbazione termica diventa correlato e non è più possibile descrivere il trasporto termico di fononi come quello di un gas.

Nel corso di questa Tesi proporremo, usando l'equazione del trasporto di Boltzmann, un'interpretazione del trasporto termico nei cristalli 2D in termini di eccitazioni collettive di fononi. Queste possono dar luogo a fenomeni complessi, come conducibilità termiche elevate altrimenti inspiegabili. Inoltre, possono propagare il calore in forma di onde termiche, a differenza della più comune diffusione di calore, un fenomeno finora osservato solo in pochi materiali esotici a temperature prossime allo zero assoluto, ma comune in materiali 2D a temperatura ambiente.

Il trasporto termico può essere spiegato formalmente introducendo una nuova eccitazione collettiva, il rilassone, definita dagli autostati dell'operatore di collisione. Al contrario dei fononi, per i quali si possono definire tempi di rilassamento (cioè il tempo medio tra eventi di collisione) solo entro certe approssimazioni, i rilassoni hanno tempi di rilassamento ben definiti e permettono una descrizione esatta del trasporto termico. La dinamica del trasporto termico può così essere semplificata, ottenendo una descrizione simile alla teoria cinetica del trasporto nei gas, a patto di non utilizzare i fononi come il gas di eccitazioni rilevanti per il trasporto termico, bensì i rilassoni.

Il nostro lavoro sul trasporto termico fa parte di un progetto più vasto, che punta a realizzare una banca dati di proprietà di materiali calcolate numericamente. L'esecuzione su larga scala di simulazioni è una sfida intricata, e richiede non solo la comprensione dei modelli fisici, ma deve anche far fronte ad una miriade di problemi e tecnicismi che ostacolano il calcolo di un grande numero di proprietà. Per permettere la creazione di una tale banca dati, abbiamo sviluppato AiiDA, un'infrastruttura informatica per automatizzare la scienza computazionale. Questa piattaforma è costruita attorno ai concetti chiave di creazione, gestione, analisi e condivisione dei dati e delle simulazioni. L'automatizzazione viene realizzata con

Acknowledgements

un controllo delle risorse computazionali remote e dalla scrittura programmatica di flussi di lavoro che permettono l'esecuzione di una serie complessa di calcoli. La gestione condivisa di automatizzazione e salvataggio dati permette la completa riproducibilità dei risultati, mentre un'architettura adeguata della banca dati consente la realizzazione di strumenti per l'analisi dati ad alte prestazioni. La condivisione della conoscenza scientifica è affrontata rilasciando funzionalità per la distribuzione dei dati e dei flussi di lavoro che li hanno generati, creando così un'ecosistema per la scienza computazionale dei materiali.

Parole chiave: conducibilità termica, calore, trasporto, principi primi, automazione

Contents

Acknowledgements	i
Abstract (English/Italiano)	iii
List of figures	ix
List of tables	xi
Introduction	1
1 Phonons	5
1.1 The crystal lattice and the reciprocal lattice	5
1.2 Harmonic approximation	9
1.3 Equilibrium distributions	13
1.4 Ab initio treatment	15
2 Phonon scattering	21
2.1 Phonon-phonon interaction	21
2.2 Normal and Umklapp scattering	24
2.3 Three-phonon scattering rate	25
2.4 Ab initio evaluation	26
2.5 Mass disorder scattering	27
3 The phonon Boltzmann transport equation	31
3.1 Formal derivation	32
3.2 Conductivity without scattering	37
3.3 Variational principle	38
3.4 Matthiessen rule	40
4 Solutions of the Boltzmann transport equation	43
4.1 Single mode relaxation time approximation	44
4.2 Callaway approximation	46
4.3 Iterative method	49
4.4 Variational method	50
4.5 Relaxons	52
	vii

Contents

4.6	Technical details	55
5	Surface scattering	57
5.1	Definition of the problem	58
5.2	SMA surface scattering	60
6	Transport in 2D materials	63
6.1	Failure of the relaxation time approximation	65
6.2	Phonon transport regimes	69
6.3	Testing the Callaway approximation	72
7	Fourier's law failures	75
7.1	Size dependent conductivity	76
7.2	Second sound	79
8	Relaxons in graphene	89
8.1	Relaxon properties	90
8.2	Failure of the Matthiessen rule	94
8.3	Divergence of iterative methods	95
9	AiiDA	97
9.1	The ADES model for computational science	98
9.2	The AiiDA infrastructure	102
9.3	Automation in AiiDA	103
9.4	Data in AiiDA: database, storage and provenance	105
9.5	The scientific environment in AiiDA	110
9.6	Sharing in AiiDA	116
	Conclusion	119
A	Computational parameters	121
	Bibliography	131
	Curriculum Vitae	133

List of Figures

1.1	Graphene's crystal	6
1.2	Graphene Brillouin zone	9
1.3	Phonon dispersion of graphene	19
2.1	3-phonon scatterings	24
2.2	Normal and Umklapp scattering	25
5.1	Geometry of a finite 2D material	58
6.1	Thermal conductivity of graphene, bilayer graphene and graphite	64
6.2	Thermal conductivities of 2D materials	66
6.3	Thermal conductivities of transition metal dichalcogenides	67
6.4	Strain engineering of the thermal conductivity in graphene	68
6.5	Average lifetimes of 2D materials	70
6.6	Thermal conductivity regimes in graphene	72
6.7	Callaway's approximation to thermal conductivity in 2D materials	73
6.8	Callaway's approximation to thermal conductivity in transition metal dichalco- genides	73
7.1	Study of mean free paths in graphene, bilayer graphene and graphite	77
7.2	Schematic description of extrinsic scattering sources	78
7.3	Out-of-equilibrium phonon distribution in graphene	84
7.4	Drifting component of the out-of-equilibrium phonon distribution	85
7.5	Second sound relaxation times	86
7.6	Second sound and first sound velocities	87
7.7	Second sound propagation lengths	88
8.1	The longest lived relaxon	90
8.2	Phonon and relaxon lifetimes	91
8.3	Phonon and relaxon velocities	92
8.4	Phonon and relaxon mean free paths	93
8.5	Failure of the Matthiessen rule	94
8.6	Divergence of the iterative method	96
9.1	The ADES model for computational science	99

List of Figures

9.2	The architecture of AiiDA	103
9.3	A Quantum ESPRESSO calculation in AiiDA	105
9.4	Main tables of the AiiDA database schema	106
9.5	The element attribute value table	107
9.6	An AiiDA graph example	109
9.7	The AiiDA documentation	116

List of Tables

6.1	Classification of thermal transport regimes	71
A.1	Ab-initio computational parameters	122
A.2	Boltzmann equation computational parameters	122

Introduction

The development of contemporary hardware architectures is encountering enormous challenges in the thermal and energy management. The increasing device density in electronic chips leads to the formation of hot spots, i.e. areas where the operating temperature grows so high that causes damage or melting. In fact, dissipated heat fluxes have become so high that contemporary CPUs are not designed anymore to maximise their computational power, but rather to minimise the energy cost to solution. For these reasons thermal management is a key factor to sustain the evolution of modern electronics.

Much work had been done in the 1950s-1960s to explain thermal transport in conventional semiconductor crystals, such as silicon. This work set the foundations for the characterisation of thermal conductivity, i.e. the capability of a material to conduct heat, and has constituted the backbone to understand heat management in semiconductors in the following decades. In the last few years, the study of heat transport found renewed interest [36, 46], driven by the miniaturisation of microchips, novel experimental techniques, and the emergence of two-dimensional (2D) materials. In particular, the highest thermal conductivity among known materials has been measured in graphene [37]. Despite this, there is not, to-date, a universal consensus on its precise value, with theoretical and experimental estimates varying by at least an order of magnitude.

The large uncertainty in quantifying thermal conductivities of 2D materials originates from a different phenomenology for thermal transport that is not present in conventional bulk crystals, but emerges when the relevant sizes are brought to the nanoscale, or when dimensionality is reduced. Several assumptions, correct in bulk crystals, lose their validity in 2D. At the same time, the computational capabilities of modern computers have made possible to solve the Boltzmann transport equation with high accuracy and to abandon oversimplifying approximations. Therefore, we are now in an ideal situation to reconsider the prevalent approaches to thermal transport.

In dielectric crystals, lattice vibrations are responsible for the largest contribution to thermal conductivity. However, analysing these and extracting the value of thermal conductivity is a quite formidable task and in fact there is no universal theory of heat transport that holds at any temperature or that can be solved taking into account all possible effects. In this Thesis we will use exclusively the Boltzmann transport equation, which is a formalism that gives an excellent

List of Tables

description of thermal transport around room temperature conditions, the most interesting for applications. We will not discuss the limits of validity of the Boltzmann equation in this Thesis, as it is a fairly broad and complex topic still subject of active research; we will just mention that methods like the Green's function approach have greater generality [80] (at the price of substantially increased complexity). Luckily, the theory has proved in many cases to be an adequate approximation and is one of the most useful theoretical frameworks for interpreting thermal transport.

The vibrations of atoms in crystals are described in terms of phonons, collective excitations of atoms describing waves of atomic displacements that propagate inside the crystal. The dynamics of the phonon wavepackets is the subject of investigation of the Boltzmann equation and the knowledge of their populations allows the quantification of thermal conductivity. Thermal transport is traditionally modeled according to the kinetic theory of gases: the hot and cold areas of the crystals correspond to location of higher and lower densities of phonons and the system evolves according to the second law of thermodynamics, trying to reestablish a homogeneous density in an attempt of maximising the entropy. To each phonon is assigned a specific heat (the energy necessary for changing the temperature by 1 degree), a velocity and a mean free path (the average distance between phonon scattering events); the thermal conductivity is related to the product of these three quantities. However, whereas the specific heat and the velocity of phonons are well defined, the phonon mean free path is only an approximated concept. The motion of phonons is correlated by the presence of scattering events and it is not possible to identify a distance between phonon scatterings, since this depends also on the many-body dynamics of phonons. Only within some approximations it is possible to define a phonon mean free path. Although these approximations typically hold in conventional 3D crystals, they fail in lower dimensionality or low temperatures, and an improved description of thermal transport is needed.

In this Thesis we provide a novel interpretation for thermal transport that is based on collective excitations of phonons. First we show that heat transport in low dimensional materials is dominated by the presence of normal scattering events. These collisions preserve heat flux, with heat being mostly shuttled between phonon modes. The correct correlated phonon dynamics can only be described by going beyond the common approximation that describe heat transport as being carried by single phonon excitations, and only the inclusion of collective phonon excitations allows a quantitative characterisation of thermal properties, e.g. the extremely high thermal conductivity found in graphene. Correlated dynamics also leads to the failure of Fourier's law, which describes the relation between heat flux and the temperature profile inside the material. A first failure is found when thermal conductivity depends on the sample size, since the mean free paths of collective excitations are comparable with typical crystal sizes. Moreover, collective excitations admit the propagation of heat in the form of heat waves (second sound) rather than heat diffusion, a phenomenon that has been observed up to now only in few exotic bulk crystals at cryogenic temperatures, but that instead we find common in 2D materials. Finally, we rationalise the collective behavior by introducing the concept of relaxons, a new set of collective excitations that are eigenstates of the collisions

operator. Thermal transport can then be described exactly using the kinetic theory of gas, with the relevant gas for thermal excitations being made not by phonons, but by relaxons.

Many insights on thermal transport that are given in this Thesis have been possible only thanks to computational experiments. Although increasing computational capabilities allow us to solve physical models with improved accuracy, they can impose a myriad of problems and technicalities when running simulations. As a result, most of the time is spent on managing the computational effort and on handling data, rather than focusing on the scientific content. This suggests the need for a dedicated software infrastructure that speeds up the productivity of a researcher. The development of such platform is however technically challenging, as an implementation must be flexible and general, while being also easy to use. In addition, a software infrastructure should also tackle the problem of reproducibility of numerical simulations (often missed in several publications) and facilitate the sharing of data. With this vision in mind we developed the platform AiiDA, an open-source software that we tuned first to the demands of materials science, and built around the pillars of automation, data, environment and sharing. Many of the results presented in this Thesis have indeed been realized with AiiDA workflows.

The Thesis will be structured as follows.

In Chapter 1 we briefly recall the definition of a crystal and the harmonic lattice, introducing the concept of phonons. Phonons can nowadays be routinely computed from first principles using density-functional perturbation theory, which has been used to compute all the lattice properties of this Thesis; we report here the basic notions of this technique. We also show with simple arguments drawn from statistical mechanics how we can obtain the distribution of phonons at equilibrium.

Phonon scattering is introduced in Chapter 2. We mainly focus on the role of three-phonon processes and phonon-isotope scattering, that in most crystals at room temperature are the most important sources of thermal resistivity. We also introduce the distinction between normal and Umklapp scattering that will be used later in the analysis of the collective phonon excitations.

In Chapter 3 we present the Boltzmann transport equation. This is the theoretical framework that we will use to study phonons in out-of-equilibrium conditions and show how this equation, combined with the scatterings probabilities, can be used to compute thermal conductivity. Moreover, we will also recall the variational interpretation of the Boltzmann equation and the Matthiessen rule.

Chapter 4 focuses on approximations and algorithms for solving the Boltzmann transport equation. First we summarize two common approaches, the single-mode relaxation time approximation and the Callaway approximation. Secondly, we show three methods for solving exactly the Boltzmann equation with iterative, variational and diagonalisation methods. In connection with the latter, we introduce the concept of relaxons.

List of Tables

Surface effects are introduced in Chapter 5. We explain why surface scattering cannot be treated at the same level of other intrinsic phonon processes and show how the thermal conductivity of a finite sample can be computed in absence of intrinsic scattering or within the single-mode relaxation time approximation.

We start presenting our numerical results in Chapter 6, where we show that the single-mode relaxation time approximation is violated in many layered and two-dimensional materials, and introduce the concept of collective phonon excitations. We show that normal scattering events are dominant in 2D materials at any temperature, at variance with 3D solids where this can only happen at cryogenic temperatures. Under these conditions, hydrodynamic regimes emerge and the Callaway model becomes a good approximation for thermal transport.

In Chapter 7 we discuss two cases in which Fourier's law does not describe thermal transport. The first case is found when the size of the sample becomes comparable or much smaller than the mean free paths of the heat flux excitations, as it is often the case for the size of 2D samples used in experiments. Another case is the response to temperature oscillations, and we will see that collective excitations induce a response of thermal waves (also called second sound), typically negligible in most materials at room temperature and instead common in 2D materials.

The concept of relaxons is numerically investigated in Chapter 8, illustrating the relaxon properties that can be obtained from the diagonalisation of the scattering matrix. We show that Matthiessen's rule is violated in 2D materials and that the iterative method gives divergent results for graphene at room temperature.

Finally, Chapter 9 contains an overview of the efforts in the automatisisation of simulations. We introduce the ADES model and the four pillars that a computational platform should meet in order to be an effective tool in computational science; then we discuss their implementation in the AiiDA platform we developed (www.aiida.net).

1 Phonons

A Thesis about lattice thermal transport necessarily needs to start with an introduction on the quantum theory of atomic vibrations in crystals. The characterising property of a crystal is that atoms belonging to this material occupy an ordered lattice of positions in space. However, the atoms in the crystal are not perfectly frozen and stand still at these positions; instead they typically oscillate around their equilibrium positions. The temperature is in fact a measure of the amplitude of the atomic vibrations: as temperature increases, so does the amplitude of the atomic motion. A direct discussion of how each atom is moving is not practically viable, it is instead much more convenient to introduce collective variables and study the displacement of atoms in the form of waves, called phonons.

In this chapter, we will give a brief overview of phonon properties. The breadth of the topic is such that extends beyond the purpose of this Thesis; we will simply present the main results that are needed for the later developments on thermal transport. Fortunately, there are many good books on the subject (Refs. [34, 132, 123] among the various) where the reader can find complementary and additional discussions on phonons. We will start recalling in Section 1.1 the definition of a crystal lattice and its reciprocal lattice. In Section 1.2 we consider the lattice Hamiltonian and solve it in the harmonic approximation, introducing the concept of a phonon and its characteristic properties. The temperature is then introduced in Section 1.3, explaining how the quantum numbers of phonons can be determined with the help of basic statistical physics. Finally, we will briefly overview in Section 1.4 how the parameters entering the lattice Hamiltonian (the force constants) can be computed using density functional theory, a successful theory that allows to get microscopic parameters with a favorable quality/cost ratio and without the need for empirical parameters.

1.1 The crystal lattice and the reciprocal lattice

A crystal structure is a highly ordered arrangement of atoms. The space occupied by the crystal can be partitioned in unit cells, which is a volume of the 3D space defined by three lattice vectors ($\mathbf{a}_1, \mathbf{a}_2, \mathbf{a}_3$). A unit cell, if repeated throughout the space, is such that the complete

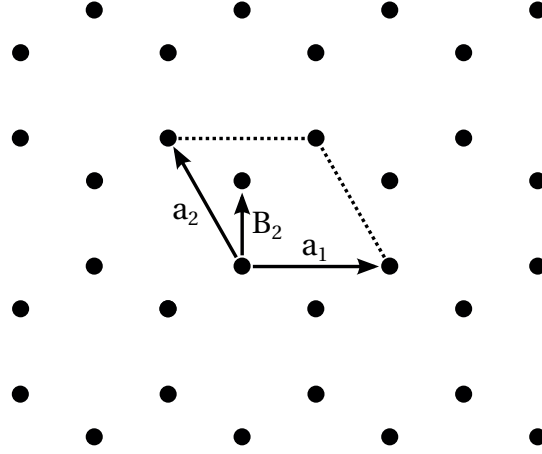


Figure 1.1 – The crystal of graphene. The vectors \mathbf{a}_i are the lattice vectors defining the periodically repeated unit cell (enclosed in lines), and the vectors $\mathbf{B}_1 = (0, 0)$ and \mathbf{B}_2 define the position of the atoms in each unit cell.

crystal can be recovered. More precisely, we define the Bravais lattice as an infinite set of points defined by the lattice vectors:

$$\mathbf{R}_l = l_1 \mathbf{a}_1 + l_2 \mathbf{a}_2 + l_3 \mathbf{a}_3, \quad (1.1)$$

where the three vectors \mathbf{a}_i , that do not lie in the same plane, are known as primitive vectors and l_i are any integer. The original crystal can be recovered by placing one unit cell at each point of the Bravais lattice. An important property of the Bravais lattice is the translational invariance, that is, regardless of where one sets the origin of the reference system (\mathbf{R}_0), the crystal still looks the same. On top of the Bravais lattice, which is merely a geometric construction, we place atoms in the positions specified by the vectors:

$$\mathbf{R}_l + \mathbf{B}_b, \quad (1.2)$$

where b is a label over the basis of atoms, i.e. the atoms present in each unit cell whose positions are identified by the basis vectors \mathbf{B}_b .

In materials of lowered dimensionality, such as graphene in 2D, the same arguments of above hold, but the vectors span only a 2D space and \mathbf{a}_3 is not needed anymore. As an example it is easy to see that the crystal of graphene, of great interest for this Thesis, can be defined as (see

Figure 1.1):

$$\begin{aligned}
 \mathbf{a}_1 &= \sqrt{3}a(1, 0), \\
 \mathbf{a}_2 &= \sqrt{3}a\left(-\frac{1}{2}, \frac{\sqrt{3}}{2}\right), \\
 \mathbf{B}_1 &= a(0, 0), \\
 \mathbf{B}_2 &= a(0, 1).
 \end{aligned}
 \tag{1.3}$$

However, it should be pointed out that the choice of \mathbf{a}_i and \mathbf{B}_i is not unique, and several equivalent choices exist to describe the same crystal.

A number of physical properties of a lattice, phonons included, are conveniently described as waves of the form $e^{i\mathbf{k}\cdot\mathbf{r}}$. To this aim, it is convenient to build the reciprocal lattice, i.e. the set of wave vectors that yield plane waves with a periodicity compatible with a given Bravais lattice. Therefore, we try to find all vectors \mathbf{G} such that

$$e^{i\mathbf{G}\cdot(\mathbf{r}+\mathbf{R})} = e^{i\mathbf{G}\cdot\mathbf{r}}, \tag{1.4}$$

for any Bravais lattice vector \mathbf{R} (we drop the labeling l for simplicity) or equivalently

$$e^{i\mathbf{G}\cdot\mathbf{R}} = 1. \tag{1.5}$$

We don't provide a constructive proof to find the vectors \mathbf{G} , however we introduce three reciprocal lattice vectors:

$$\begin{aligned}
 \mathbf{b}_1 &= 2\pi \frac{\mathbf{a}_2 \times \mathbf{a}_3}{\mathbf{a}_1 \cdot (\mathbf{a}_2 \times \mathbf{a}_3)} \\
 \mathbf{b}_2 &= 2\pi \frac{\mathbf{a}_3 \times \mathbf{a}_1}{\mathbf{a}_1 \cdot (\mathbf{a}_2 \times \mathbf{a}_3)} \\
 \mathbf{b}_3 &= 2\pi \frac{\mathbf{a}_1 \times \mathbf{a}_2}{\mathbf{a}_1 \cdot (\mathbf{a}_2 \times \mathbf{a}_3)}.
 \end{aligned}
 \tag{1.6}$$

Since the vectors \mathbf{b}_i satisfy the relation

$$\mathbf{a}_i \cdot \mathbf{b}_j = 2\pi\delta_{ij}, \tag{1.7}$$

it can be shown that any reciprocal lattice vector \mathbf{G} must be of the form

$$\mathbf{G} = g_1\mathbf{b}_1 + g_2\mathbf{b}_2 + g_3\mathbf{b}_3, \tag{1.8}$$

with g_i any integer. Just like the direct lattice vectors \mathbf{a}_i define a unit cell in real space, so the reciprocal lattice vectors \mathbf{b}_i define a cell in the reciprocal lattice.

We shall see that the atoms in the crystal move under the presence of a potential $V(\mathbf{r})$, \mathbf{r} being the position vector, which has itself the same periodicity of the underlying lattice: $V(\mathbf{r}+\mathbf{R}) = V(\mathbf{r})$, for any lattice vector \mathbf{R} . This constrain arises from the translational invariance

Chapter 1. Phonons

of the crystal. The non-interacting atom moving in a periodic potential are characterised by the Bloch theorem [34]:

Theorem: The eigenstates ψ of a single-particle Hamiltonian $H = -\frac{\hbar^2}{2m}\nabla^2 + V(\mathbf{r})$, where $V(\mathbf{r}) = V(\mathbf{r} + \mathbf{R})$ for all \mathbf{R} in a Bravais lattice, can be chosen so that associated to each ψ is a wave vector \mathbf{q} such that:

$$\psi(\mathbf{r} + \mathbf{R}) = e^{i\mathbf{q}\cdot\mathbf{r}}\psi(\mathbf{r}). \quad (1.9)$$

The theorem naturally introduces the wave-vector \mathbf{q} as a quantum number stemming from the periodicity of the Hamiltonian. One can thus infer that rather than working in the direct lattice, the system can be solved in the reciprocal lattice (the clear advantage of this operation will be explained in the next section). To make this transformation, we start by considering a Bravais lattice of finite size (practical constraints impose that we can only work with a finite number of atoms), in which the integer number l_i appearing in Eq. 1.1 can only assume values from 0 to N_i . Since we are interested in an infinite crystal, we reduce the finite size artifacts by imposing the Born–Von Karman boundary conditions:

$$\psi(\mathbf{r} + N_i \mathbf{a}_i) = \psi(\mathbf{r}), \quad \forall i. \quad (1.10)$$

It can be shown that the properties of the infinite crystal are recovered when N_i goes to infinity. Therefore, we will always work (at least implicitly) with a crystal of finite size whose volume is given by $\mathcal{V} = N_1 \mathbf{a}_1 \cdot (N_2 \mathbf{a}_2 \times N_3 \mathbf{a}_3)$ and that contains $N = N_1 N_2 N_3$ unit cells.

Combining the Bloch theorem with the boundary condition, we find:

$$\psi_{\mathbf{q}}(\mathbf{r} + N_i \mathbf{a}_i) = e^{iN_i \mathbf{q} \cdot \mathbf{a}_i} \psi_{\mathbf{q}}(\mathbf{r}), \quad \forall i, \quad (1.11)$$

which requires:

$$e^{iN_i \mathbf{q} \cdot \mathbf{a}_i} = 1. \quad (1.12)$$

This condition is very close to the one defining the reciprocal lattice. The only allowed values of the wave vector \mathbf{q} are:

$$\mathbf{q} = \frac{n_1}{N_1} \mathbf{b}_1 + \frac{n_2}{N_2} \mathbf{b}_2 + \frac{n_3}{N_3} \mathbf{b}_3, \quad (1.13)$$

where n_i are any integer from 0 to N_i . Wave vectors defined by other values of n_i are unnecessary, since the periodicity of the complex exponential will lead to terms already described by the numbers in the chosen range. Therefore, all the eigenstates of the Hamiltonian are labeled with a quantum number \mathbf{q} that does not span an infinite range of values, but is instead limited to the values inside the cell defined by the reciprocal lattice vectors. Actually, rather than the cell defined by the vectors \mathbf{b}_i , it is customary to work with the Brillouin zone. Given the reciprocal lattice, the Brillouin zone is built as the locus of points that are closer to the origin

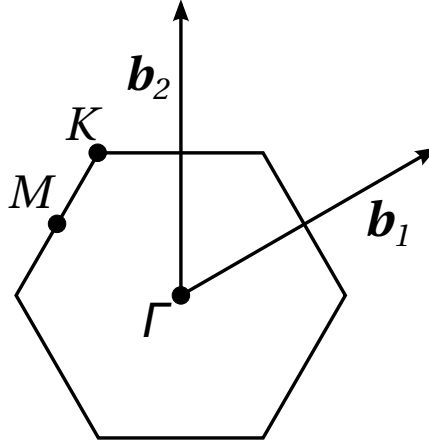


Figure 1.2 – The reciprocal lattice vectors of a crystal of graphene $\mathbf{b}_1 = \frac{2\pi}{a}(\frac{\sqrt{3}}{3}, \frac{1}{3})$, $\mathbf{b}_2 = \frac{2\pi}{a}(0, \frac{2}{3})$, the corresponding hexagonal Brillouin zone and the high symmetry points relevant for phonon properties.

of the reciprocal lattice than to any other reciprocal lattice points. For example, the Brillouin zone of graphene is reported in Figure 1.2, together with the reciprocal lattice vectors.

The last two properties recalled in this section, useful for later, are two summations:

$$\sum_{\mathbf{q}} e^{i\mathbf{q}\cdot\mathbf{R}_l} = \begin{cases} 0 & (\mathbf{R}_l \neq 0) \\ N & (\mathbf{R}_l = 0) \end{cases}$$

$$\sum_l e^{i\mathbf{q}\cdot\mathbf{R}_l} = \begin{cases} 0 & (\mathbf{q} \neq \mathbf{G}) \\ N & (\mathbf{q} = \mathbf{G}) \end{cases} . \quad (1.14)$$

These results state that the phase factors cancel out each other in the summation, unless they are computed at particular values of \mathbf{q} or \mathbf{R} . Hence, the points of the reciprocal or direct lattice are the only locus of points for which many integrals will have a non zero value.

1.2 Harmonic approximation

The atoms in a crystal are described by the following lattice Hamiltonian:

$$H = \sum_{lb} \frac{p^2(lb)}{2m_b} + V(\mathbf{x}_{l_1 b_1}, \mathbf{x}_{l_2 b_2}, \dots), \quad (1.15)$$

where $\mathbf{x}_{lb} = \mathbf{R}_l + \mathbf{B}_b$ and \mathbf{p}_{lb} identify the position and the momentum of every atom (lb) in the crystal, and V is the potential energy surface felt by the atoms, in general a function of the atomic positions. This Hamiltonian can be justified at a fundamental level, since it is the Hamiltonian to which the atoms are subject under the Born-Oppenheimer approximation.

Chapter 1. Phonons

The solution of the general Hamiltonian is an extremely complicated task for a generic potential V . The typical procedure is to study the system in the limiting case of atoms sitting on their equilibrium site and vibrating by small oscillations around their equilibrium positions. In this case, we introduce the displacement $\mathbf{u}(lb)$:

$$\mathbf{u}(lb) = \mathbf{x}_{lb} - (\mathbf{R}_l + \mathbf{B}_b), \quad (1.16)$$

and work in the limit for which $\mathbf{u}(lb)$ is small for every atom. Let us then expand the potential V in a Taylor series around the equilibrium positions ($\mathbf{u}(lb) = 0$):

$$\begin{aligned} V &= V_0 + \sum_{lb\alpha} \frac{\partial V}{\partial u_\alpha(lb)} \Big|_0 u_\alpha(lb) + \frac{1}{2} \sum_{lb\alpha l'\beta} \frac{\partial^2 V}{\partial u_\alpha(lb) \partial u_\beta(l'b')} \Big|_0 u_\alpha(lb) u_\beta(l'b') \\ &+ \frac{1}{3!} \sum_{lb\alpha l'\beta l''\gamma} \frac{\partial^3 V}{\partial u_\alpha(lb) \partial u_\beta(l'b') \partial u_\gamma(l''b'')} \Big|_0 u_\alpha(lb) u_\beta(l'b') u_\gamma(l''b'') + \dots \\ &= V_0 + V_1 + V_2 + V_3 + \dots \end{aligned} \quad (1.17)$$

where we use the greek letters to label the cartesian directions. The first term V_0 is a constant term of the energy that can be set to zero without loss of generality. The term V_1 corresponds to the forces acting on the atoms, which at the equilibrium positions need to be zero. The first non-zero term is V_2 , which describes the second derivatives of the potential with respect to the atomic displacements. For the rest of this chapter we will stop at the term V_2 which identifies the harmonic Hamiltonian, but the higher order term will be reintroduced later.

Let us therefore consider the harmonic crystal Hamiltonian:

$$H = \sum_{lb} \frac{p^2(lb)}{2m_b} + \frac{1}{2} \sum_{lb\alpha l'\beta} \phi_{\alpha\beta}(lb, l'b') u_\alpha(lb) u_\beta(l'b'), \quad (1.18)$$

where we simplified the notation introducing the dynamical matrix ϕ :

$$\phi_{\alpha\beta}(lb, l'b') = \frac{\partial^2 V}{\partial u_\alpha(lb) \partial u_\beta(l'b')} \Big|_0, \quad (1.19)$$

where these matrix terms are also called force constants, due to the similarity with the Hamiltonian of a spring. Among the various properties of the dynamical matrix, we recall that, by translational symmetry, the terms of the dynamical matrix must only depend on the distance between the Bravais lattice sites:

$$\phi_{\alpha\beta}(lb, l'b') = \phi_{\alpha\beta}(0b, (l' - l)b'). \quad (1.20)$$

Even if the harmonic Hamiltonian is simpler than the original one, the solution in the position and momentum representation is still not self-evident. The difficulty arise due to the fact that the force constants couple the motion of the atoms. However, the motion of the atoms can be decoupled if instead of studying their motion atoms by atoms, we study their motion as waves

of displacements, or, in other words, we look for solution in the form of waves. To this aim, we switch to a reciprocal space representation by introducing a set of collective variables:

$$\begin{aligned} \mathbf{u}(lb) &= \frac{1}{\sqrt{\mathcal{V}}} \sum_{\mathbf{q}} \mathbf{X}(\mathbf{q}b) e^{i\mathbf{q}\cdot\mathbf{R}_l}, \\ \mathbf{p}(lb) &= \frac{1}{\sqrt{\mathcal{V}}} \sum_{\mathbf{q}} \mathbf{P}(\mathbf{q}b) e^{-i\mathbf{q}\cdot\mathbf{R}_l}. \end{aligned} \quad (1.21)$$

Now, each displacement and momentum is thought as a superposition of waves, each with wave vector \mathbf{q} . Mathematically, this procedure corresponds to applying a Fourier transform of the coordinates. Adopting these coordinates, the harmonic Hamiltonian becomes:

$$H = \frac{1}{\mathcal{V}} \sum_{\mathbf{q}b} \frac{\mathbf{P}(\mathbf{q}b) \cdot \mathbf{P}^\dagger(\mathbf{q}b)}{2m_b} + \frac{1}{2\mathcal{V}} \sum_{\mathbf{q}bb'\alpha\beta} \phi_{\alpha\beta}(bb'|\mathbf{q}) X_\alpha(\mathbf{q}b) X_\beta^\dagger(\mathbf{q}b'), \quad (1.22)$$

where we Fourier transformed the dynamical matrix as:

$$\phi_{\alpha\beta}(bb'|\mathbf{q}) = \sum_{l'} \phi_{\alpha\beta}(0b, l'b') e^{-i\mathbf{q}\cdot\mathbf{R}_{l'}}. \quad (1.23)$$

The transformation carries a great advantage over the previous representation. Whereas previously the potential term was correlating all atoms, with the reciprocal space description instead the waves of different wave vector are decoupled. Therefore, the problem is greatly simplified and rather than solving one large equation involving all the atomic coordinates, now we can solve much simpler equations (in fact we will solve them analytically), each for every wave vector \mathbf{q} . More rigorously, the Hamiltonian now is a sum of separate terms:

$$H = \sum_{\mathbf{q}} H_{\mathbf{q}}, \quad (1.24)$$

where each $H_{\mathbf{q}}$ can be solved separately. The Bloch theorem also comes at hand now, since one of its consequences is that the only relevant wave vectors \mathbf{q} are those belonging to the Brillouin zone.

To proceed, we diagonalise the dynamical matrix at each \mathbf{q} -point:

$$\sum_{b'\beta} \frac{1}{\sqrt{m_b m_{b'}}} \phi_{\alpha\beta}(bb'|\mathbf{q}) e_\beta(b'|\mathbf{q}s) = \omega_{\mathbf{q}s}^2 e_\alpha(b|\mathbf{q}s), \quad (1.25)$$

where $s = 1, 3N_{\text{at}}$ is a set of eigenvalue indices, N_{at} is the number of atoms in the basis, ω^2 are the eigenvalues and e the eigenvectors.

Although we could solve the Hamiltonian just with these transformations, it will be useful for

later discussion to introduce another set of operators as:

$$\begin{aligned} X(\mathbf{q}b) &= -i \sum_s \sqrt{\frac{\hbar}{2m_b \omega_{\mathbf{q}s}}} e(b|\mathbf{q}s) (a_{\mathbf{q}s}^\dagger - a_{-\mathbf{q}s}), \\ P(\mathbf{q}b) &= \sum_s \sqrt{\frac{\hbar m_b \omega_{\mathbf{q}s}}{2}} e^*(b|\mathbf{q}s) (a_{\mathbf{q}s} + a_{-\mathbf{q}s}^\dagger), \end{aligned} \quad (1.26)$$

expressing the X and P operators in terms of the so called creation and annihilation operators. In this representation, the Hamiltonian has taken the form of an ensemble of harmonic oscillators in the second quantization:

$$H_{\text{harm}} = \sum_{\mathbf{q}s} \hbar \omega_{\mathbf{q}s} \left(\frac{1}{2} + a_{\mathbf{q}s}^\dagger a_{\mathbf{q}s} \right), \quad (1.27)$$

where from the commutation relations of the position and momentum:

$$[u_\alpha(l, b), p_\beta(l', b')] = i\hbar \delta_{l,l'} \delta_{b,b'} \delta_{\alpha,\beta}, \quad (1.28)$$

we can obtain the commutation relations for the creation and annihilation operators:

$$[a_{\mathbf{q}s}, a_{\mathbf{q}'s'}^\dagger] = \delta_{\mathbf{q},\mathbf{q}'} \delta_{s,s'}, \quad (1.29)$$

indicating a bosonic statistic for the waves of atomic displacements. Starting from the commutation relations, the Hamiltonian of the harmonic oscillator can be solved exactly (for a detailed explanation, see for example Ref. [54]). The main results are that the state of the system is represented by the state:

$$|n_{\mathbf{q}_1 s_1}, n_{\mathbf{q}_2 s_2}, \dots\rangle = |n_{\mathbf{q}_1 s_1}\rangle \otimes |n_{\mathbf{q}_2 s_2}\rangle \otimes \dots, \quad (1.30)$$

where $|n_{\mathbf{q}s}\rangle$ denotes the eigenstates of the operator $a_{\mathbf{q}s}^\dagger a_{\mathbf{q}s}$, also eigenstates of the Hamiltonian, which are the phonons. The eigenvalues $n_{\mathbf{q}s}$ of the operator $a_{\mathbf{q}s}^\dagger a_{\mathbf{q}s}$ are called the phonon excitation number. The eigenvalues of the Hamiltonian are $\hbar \omega_{\mathbf{q}s} (n_{\mathbf{q}s} + \frac{1}{2})$, so that the total energy of the system is just the sum of the separate oscillators:

$$E = \sum_{\mathbf{q}s} \left(n_{\mathbf{q}s} + \frac{1}{2} \right) \hbar \omega_{\mathbf{q}s}, \quad (1.31)$$

showing how the total energy of the system is directly related with the excitation number $n_{\mathbf{q}s}$. Each excitation number, i.e. each quantum of energy, defines a phonon.

The name of the operators a^\dagger and a , the creation and annihilation operators, come from noting two properties:

$$\begin{aligned} a_{\mathbf{q}s}^\dagger |n_{\mathbf{q}s}\rangle &= \sqrt{n_{\mathbf{q}s} + 1} |n_{\mathbf{q}s} + 1\rangle \\ a_{\mathbf{q}s} |n_{\mathbf{q}s}\rangle &= \sqrt{n_{\mathbf{q}s}} |n_{\mathbf{q}s} - 1\rangle. \end{aligned} \quad (1.32)$$

Therefore, we call a^\dagger the creation operator, since its action on the state of the system creates one phonon excitation (and thus increases the total energy). Similarly, the action of a destroys a phonon and is thus called the annihilation operator.

Before moving on, there are some properties not necessary to understand the harmonic oscillator but of great help in later chapters. Applying backwards the various coordinate transformations, the time dependent displacement of an atom (lb) can be expressed in terms of the creation and annihilation operators as:

$$u_\alpha(lb)(t) = \sum_{\mathbf{q}_s} \left(\frac{\hbar}{2\mathcal{V} m_b \omega_{\mathbf{q}_s}} \right)^{\frac{1}{2}} (a_{\mathbf{q}_s} - a_{-\mathbf{q}_s}^\dagger) e_\alpha(b|\mathbf{q}_s) e^{i(\mathbf{q} \cdot \mathbf{R}_l - \omega_{\mathbf{q}_s} t)}. \quad (1.33)$$

In this expression it is also more clearly stated that the displacement of an atom is a superposition of monochromatic waves and that, since it is not linear in $a^\dagger a$, it is not an eigenstate of the Hamiltonian.

The group velocity of the monochromatic wave, i.e. the phonon group velocity, is:

$$v_{\mathbf{q}_s} = \frac{\partial \omega_{\mathbf{q}_s}}{\partial \mathbf{q}}. \quad (1.34)$$

Finally, there are some useful symmetry properties of the phonons, all coming from the hermiticity of the matrix ϕ :

$$\phi_{\alpha\beta}^*(bb'|\mathbf{q}) = \phi_{\beta\alpha}(b'b|\mathbf{q}). \quad (1.35)$$

In particular, we note that:

$$\begin{aligned} e_\alpha^*(b|-\mathbf{q}_s) &= e^{i\xi} e_\alpha(b|\mathbf{q}_s) \\ v_{-\mathbf{q}_s} &= -v_{\mathbf{q}_s} \\ \omega_{-\mathbf{q}_s} &= \omega_{\mathbf{q}_s}, \end{aligned}$$

where ξ is any real number. Therefore, phonon energies/velocities are even/odd under inversion of wave vector.

1.3 Equilibrium distributions

In the previous section we learned that the energy of the harmonic crystal is determined by the knowledge of the force constants ϕ and of the phonon occupation numbers. In this section we focus on how to obtain the latter. The second quantization of quantum mechanics alone does not prescribe a way to determine the phonon occupation numbers. Also, they are not directly related with the atomistic details of the system, which instead determine the phonon frequencies. We have to introduce some fundamental knowledge of statistical physics

Chapter 1. Phonons

to predict what is the most likely number of phonons. As a matter of fact, most of the problem of thermal transport consists in trying to find a good guess for $n_{\mathbf{q}s}$ in presence of a gradient of temperature.

At equilibrium conditions the problem is much simpler and can be solved with few considerations. In this case, the most likely phonon occupation number, i.e. the thermal equilibrium, can be found by entropy maximisation (which is a fundamental law of thermodynamics). It can be shown that the entropy of an ensemble of non-interacting bosons (as it is the case for the harmonic crystal) is [90]:

$$\frac{S}{k_B} = \sum_{\mathbf{q}s} [(n_{\mathbf{q}s} + 1) \log(n_{\mathbf{q}s} + 1) - n_{\mathbf{q}s} \log(n_{\mathbf{q}s})]. \quad (1.36)$$

Before maximising the entropy, we impose a constrain that keeps the energy constant to a value E :

$$\mathcal{L} = \sum_{\mathbf{q}s} [(n_{\mathbf{q}s} + 1) \log(n_{\mathbf{q}s} + 1) - n_{\mathbf{q}s} \log(n_{\mathbf{q}s})] - \beta E, \quad (1.37)$$

where the Lagrange multiplier $\beta = \frac{1}{k_B T}$, defining the temperature of the system T , is the parameter that controls the total energy. Therefore, we look for the extremal value of the functional \mathcal{L} :

$$\frac{\delta \mathcal{L}}{\delta n_{\mathbf{q}s}} = 0 \quad (1.38)$$

$$\log(n_{\mathbf{q}s} + 1) - \log(n_{\mathbf{q}s}) - \beta \hbar \omega_{\mathbf{q}s} = 0. \quad (1.39)$$

Inverting the relation, we obtain the Bose–Einstein distribution, i.e. the phonon excitation number at thermal equilibrium:

$$\bar{n}_{\mathbf{q}s} = \frac{1}{e^{\beta \hbar \omega_{\mathbf{q}s}} - 1}. \quad (1.40)$$

With this result we can compute the expectation value of several quantities at thermal equilibrium (in the harmonic approximation). For example, the internal energy of a harmonic crystal at temperature T is:

$$U = \frac{1}{N} \sum_{\mathbf{q}s} \hbar \omega_{\mathbf{q}s} \left(\bar{n}_{\mathbf{q}s} + \frac{1}{2} \right) = \frac{1}{N} \sum_{\mathbf{q}s} \frac{\hbar \omega_{\mathbf{q}s}}{2} + \frac{1}{N} \sum_{\mathbf{q}s} \frac{\hbar \omega_{\mathbf{q}s}}{e^{\beta \hbar \omega_{\mathbf{q}s}} - 1}. \quad (1.41)$$

The specific heat at constant volume can also be obtained from the previous relation:

$$C_v = \frac{\partial U}{\partial T} = \frac{1}{N} \sum_{\mathbf{q}s} \frac{\partial}{\partial T} \frac{\hbar \omega_{\mathbf{q}s}}{e^{\beta \hbar \omega_{\mathbf{q}s}} - 1} = \frac{1}{N} \sum_{\mathbf{q}s} \bar{n}_{\mathbf{q}s} (\bar{n}_{\mathbf{q}s} + 1) \frac{(\hbar \omega_{\mathbf{q}s})^2}{k_B T^2} = \frac{1}{N} \sum_{\mathbf{q}s} C_{\mathbf{q}s}. \quad (1.42)$$

Another important distribution is the most probable under the constrain of conservation of

energy and momentum. To this aim, we maximise the functional:

$$\mathcal{L} = \sum_{\mathbf{q}_s} [(n_{\mathbf{q}_s} + 1) \log(n_{\mathbf{q}_s} + 1) - n_{\mathbf{q}_s} \log(n_{\mathbf{q}_s})] - \beta E - \mathbf{\Lambda} \cdot \mathbf{P} \quad (1.43)$$

where we introduced an additional Lagrange multiplier $\mathbf{\Lambda}$ with the purpose to keep constant the momentum \mathbf{P} :

$$\mathbf{P} = \sum_{\mathbf{q}_s} \mathbf{q} n_{\mathbf{q}_s} . \quad (1.44)$$

We set to zero the functional derivative:

$$\frac{\delta \mathcal{L}}{\delta n_{\mathbf{q}_s}} = 0 \quad (1.45)$$

$$-[\log(n_{\mathbf{q}_s} + 1) - \log(n_{\mathbf{q}_s})] - \beta \hbar \omega_{\mathbf{q}_s} - \mathbf{\Lambda} \cdot \mathbf{q} = 0 . \quad (1.46)$$

Inverting the previous relation, we obtain the drifting distribution:

$$n_{\mathbf{q}_s}^{\text{drift}} = \frac{1}{e^{\beta \hbar \omega_{\mathbf{q}_s} - \mathbf{\Lambda} \cdot \mathbf{q}} - 1} = \frac{1}{e^{\beta (\hbar \omega_{\mathbf{q}_s} - \mathbf{V}^{\text{drift}} \cdot \mathbf{q})} - 1} , \quad (1.47)$$

where in the last equality we introduced the drifting velocity $\mathbf{V}^{\text{drift}}$ such that $\mathbf{V}^{\text{drift}} \beta = \mathbf{\Lambda}$, which is sometimes more convenient for a physical interpretation. The equilibrium distribution for a momentum conserving distribution is therefore quite similar to the Bose–Einstein one, but "displaced" by the action of the drift velocity.

1.4 Ab initio treatment

Statistical physics gives us the tool to compute the phonon excitation numbers. The last missing ingredient is to find a good estimate of the force constants ϕ , which is ultimately related with the phonon frequencies ω . Density functional theory (DFT) [79, 87] nowadays offers the best tradeoff between cost and accuracy to compute microscopic parameters without the introduction of any empirical parameter. As a proof of its success, twelve papers in the top-100 list of the most cited papers are related with this theory [127], and 2 of them are in the top 10. Let us then show how density functional theory enters the computation of the force constants and sketch the main ideas behind the method. The topic is still relatively recent but quite broad and still under active development, therefore we refer to dedicated books for more details, for example Refs. [101, 64].

The exact state of the crystal is in principle described by the Schrödinger equation for a system of N_{at} atoms and N_e electrons. The problem is in practice almost impossible to solve exactly except for a very few simple cases. Therefore, one tries to simplify the problem by noting that, since atoms are more massive than electrons, they also have a much slower dynamics. Therefore, one adopts the Born–Oppenheimer approximation, in which one solves for the

Chapter 1. Phonons

electronic degrees of freedom keeping the ions (atoms) frozen at fixed positions. Within this approximation, the electrons are described by the Hamiltonian:

$$H_{BO}(\mathbf{R}) = -\frac{\hbar^2}{2m} \sum_i \frac{\partial^2}{\partial \mathbf{r}_i^2} + \frac{e^2}{2} \sum_{i \neq j} \frac{1}{|\mathbf{r}_i - \mathbf{r}_j|} + V_{\mathbf{R}}(\mathbf{r}) + E_N(\mathbf{R}), \quad (1.48)$$

where the indexes i, j label the electrons, the indexes I, J label the ions, $V_{\mathbf{R}}$ is the ion-electron electrostatic potential:

$$V_{\mathbf{R}}(\mathbf{r}) = -\sum_{iI} \frac{Z_I e^2}{|\mathbf{r}_i - \mathbf{R}_I|}, \quad (1.49)$$

where $Z_I e$ is the ionic charge and the ion-ion interaction is given by E_N :

$$E_N(\mathbf{R}) = \frac{e^2}{2} \sum_{I \neq J} \frac{Z_I Z_J}{|\mathbf{R}_I - \mathbf{R}_J|}. \quad (1.50)$$

The ground state energy of this Hamiltonian defines a potential energy surface, i.e. an energy as a function of the ionic positions in the sample. The ions instead are subject to the lattice Hamiltonian (Eq. 1.15), where the potential V used throughout the discussion of phonons is nothing else but the potential energy surface.

Therefore, in order to compute the phonon properties, we need to obtain the second derivative of the potential energy surface around an equilibrium configuration of the system where ionic forces are zero. Let us suppose for the moment that we are able to solve the Hamiltonian H_{BO} and see how we can obtain the second derivative. We proceed in steps, realising first that the first derivative, the forces, can be obtained with the Hellman–Feynman theorem:

$$\mathbf{F}_I = -\frac{\partial E(\mathbf{R})}{\partial \mathbf{R}_I} = \left\langle \psi(\mathbf{R}) \left| \frac{\partial H(\mathbf{R})}{\partial \mathbf{R}_I} \right| \psi(\mathbf{R}) \right\rangle \quad (1.51)$$

$$= -\int n_{\mathbf{R}}(\mathbf{r}) \frac{\partial V_{\mathbf{R}}(\mathbf{r})}{\partial \mathbf{R}_I} d\mathbf{r} - \frac{\partial E_N(\mathbf{R})}{\partial \mathbf{R}_I}, \quad (1.52)$$

where $n_{\mathbf{R}}(\mathbf{r})$ is the electronic density of the ground state. The forces are readily computable, since we know the analytical expression of $V_{\mathbf{R}}$ and $E_N(\mathbf{R})$, whereas the electronic density comes by having diagonalised the electronic Hamiltonian. Proceeding to the second derivation, we obtain:

$$\frac{\partial^2 E(\mathbf{R})}{\partial \mathbf{R}_I \partial \mathbf{R}_J} = -\frac{\partial \mathbf{F}_I}{\partial \mathbf{R}_J} = + \int \frac{\partial n_{\mathbf{R}}(\mathbf{r})}{\partial \mathbf{R}_J} \frac{\partial V_{\mathbf{R}}(\mathbf{r})}{\partial \mathbf{R}_I} d\mathbf{r} + \int n_{\mathbf{R}}(\mathbf{r}) \frac{\partial^2 V_{\mathbf{R}}(\mathbf{r})}{\partial \mathbf{R}_I \partial \mathbf{R}_J} d\mathbf{r} + \frac{\partial^2 E_N(\mathbf{R})}{\partial \mathbf{R}_I \partial \mathbf{R}_J}. \quad (1.53)$$

Once again the second derivatives of $V_{\mathbf{R}}$ and E_N are easy to obtain. Here the difficult part consists in the computation of the derivative of the electronic density $\frac{\partial n_{\mathbf{R}}(\mathbf{r})}{\partial \mathbf{R}_I}$, also called the density response to an ionic displacement.

Therefore we need two ingredients: the density functional theory to solve the Hamiltonian H_{BO} and a perturbation theory to get the density response.

Density functional theory

The direct solution to the Schrödinger equation requires the computation of the many-body wave function $\psi(\mathbf{r}_1, \mathbf{r}_2, \dots)$. By far, this is a too complex task to solve for most practical applications in solid state physics. The exact many body wave function in fact depends on the coordinates of all the electrons present in the unit cell of the crystal, and therefore is a function of $3N_e$ variables, too many to be efficiently treated.

Density functional theory is based on two properties that allow a dramatic simplification of the problem. First, the ground state energy is a functional of the charge density [79] and therefore, rather than looking for a wavefunction solution of $3N_e$ variables, we can simply optimize the density, function of 3 variables only. Secondly, it is possible to map the interacting electron system into a system of non-interacting particles, which however have the same density of the original system [87]. The advantage is that the non-interacting Hamiltonian is a much simpler problem than the interacting case and can be solved.

The governing equation of the independent particles is:

$$\left(-\frac{\hbar^2}{2m} \frac{\partial^2}{\partial \mathbf{r}^2} + V_{SCF}(\mathbf{r}) \right) \psi_n(\mathbf{r}) = H_{SCF} \psi_n(\mathbf{r}) = \epsilon_n \psi_n(\mathbf{r}) \quad (1.54)$$

where ϵ_n and ψ_n are n -th eigenvalue and wave function for a particle subject to the potential:

$$V_{SCF}(\mathbf{r}) = V(\mathbf{r}) + e^2 \int \frac{n(\mathbf{r}')}{|\mathbf{r} - \mathbf{r}'|} d\mathbf{r}' + v_{xc}(\mathbf{r}), \quad (1.55)$$

where V is the potential originated by the nuclei and v_{xc} is the exchange-correlation potential.

The difficulties of the description of the many body problem have not disappeared completely, since, although the DFT Hamiltonian is easy to solve, one does not know the exact expression for v_{xc} . Luckily, there are several good approximations for v_{xc} that can be used. In this Thesis we used exclusively the local density approximation [114], which approximates the unknown xc potential at a given position in space with that of a homogeneous electron gas with a density corresponding to the local value of the density at that point and that was found to well describe the phonon properties of 2D materials [59, 75].

With the choice of the functional, all parts of the DFT Hamiltonian are known and it can be diagonalised. The final result for the total energy of the N_e interacting electrons is:

$$E[n] = 2 \sum_{n=1}^{N/2} \epsilon_n - \frac{e^2}{2} \int \frac{n(\mathbf{r})n(\mathbf{r}')}{|\mathbf{r} - \mathbf{r}'|} d\mathbf{r}d\mathbf{r}' + E_{xc}[n] - \int n(\mathbf{r})v_{xc}(\mathbf{r})d\mathbf{r}, \quad (1.56)$$

where for simplicity only a non-spin polarized material is considered. The charge density of the electrons is instead the same density of the independent Kohn–Sham particles:

$$n(\mathbf{r}) = 2 \sum_{n=1}^{N/2} |\psi_n(\mathbf{r})|^2. \quad (1.57)$$

Density functional perturbation theory

Having seen how DFT computes the ground state charge density and energy, it is possible to compute the ionic forces. However, we need the charge density response to compute the dynamical matrix (Eq. 1.53), which can be obtained with perturbation theory [38, 39]. Let's suppose to perturb the potential with the displacement of an atom: $V_{SCF} \rightarrow V_{SCF} + \Delta V_{SCF}$. The extra term gives raise to a change in the wave function with respect to the unperturbed ground state and a perturbation of the energy levels:

$$\begin{aligned}\psi &\rightarrow \psi + \Delta\psi, \\ \Delta\epsilon_n &= \langle \psi_n | \Delta V_{SCF} | \psi_n \rangle.\end{aligned}\tag{1.58}$$

Inserting these modifications into Eq. 1.54, one obtains the Sternheimer equation:

$$(H_{SCF} - \epsilon_n) |\Delta\psi_n\rangle = -(\Delta V_{SCF} - \Delta\epsilon_n) |\psi_n\rangle,\tag{1.59}$$

where the perturbation of the potential is explicetely given by:

$$\Delta V_{SCF}(\mathbf{r}) = \Delta V(\mathbf{r}) + e^2 \int \frac{\Delta n(\mathbf{r}')}{|\mathbf{r} - \mathbf{r}'|} d\mathbf{r}' + \left. \frac{dv_{xc}(n)}{dn} \right|_{n=n(\mathbf{r})} \Delta n(\mathbf{r}),\tag{1.60}$$

and the change in density is obtained directly from $\Delta\psi$:

$$\Delta n(\mathbf{r}) = 4\Re \sum_{n=1}^{N/2} \psi_n^*(\mathbf{r}) \Delta\psi_n(\mathbf{r}).\tag{1.61}$$

The Sternheimer equation can be solved self-consistently and thus obtain the electron-density response.

Density functional perturbation theory has proved to be extremely successful in estimating the phonon dispersion, giving results in excellent agreement with experimental data without the use of any fitting parameter [59]. For example, we report in Figure 1.3 the phonon dispersion of graphene, i.e. the results of the diagonalisation of the dynamical matrix, on the high symmetry lines of the Brillouin zone. In this Thesis, all phonon properties have been computed with density functional perturbation theory. In particular, we used the implementation of the open-source software suite Quantum ESPRESSO [63], which is a DFT solver based on an expansion of the wave function in a plane-wave basis.

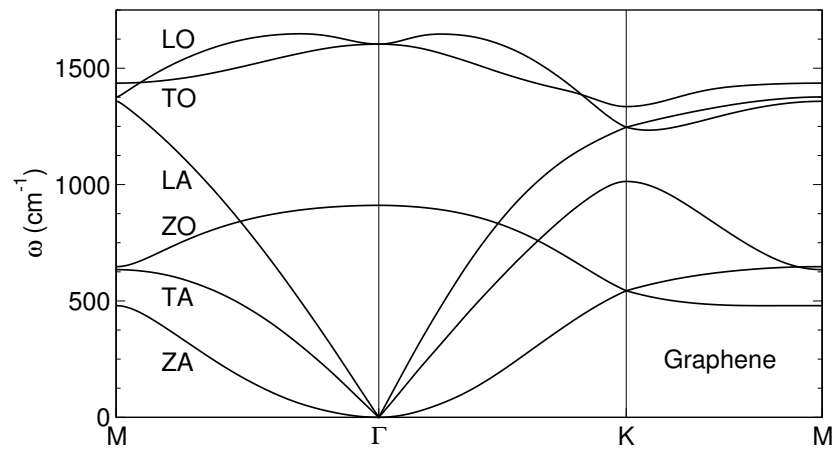


Figure 1.3 – The phonon dispersion of graphene is plotted over a high symmetry path in the Brillouin zone of graphene. The 6 branches are: out-of-plane acoustic (ZA), transverse acoustic (TA), longitudinal acoustic (LA), out-of-plane optic (ZO), transverse optic (TO), longitudinal optic (LO).

2 Phonon scattering

The harmonic approximation is an excellent starting point for the study of atomic vibrations in a crystal. We have seen in the previous chapter that it is possible to obtain a first estimate of equilibrium properties such as the lattice energy or the specific heat. There are however some drawbacks that cannot be addressed if we limit the Taylor expansion of the lattice Hamiltonian to the second order. Most importantly for the aim of this Thesis, the harmonic approximation predicts an infinite thermal conductivity for a perfect crystal (as we will see in Chapter 3). Therefore, since we want to characterise the intrinsic lattice thermal conductivity, anharmonic effects are fundamental to consider, at least to lowest order.

In this chapter, we will present the perturbation theory approach (found in many textbooks, see [132, 123]), in which the harmonic crystal is the reference state and the deviations from the harmonic Hamiltonian are considered a small perturbation. In particular, we will show how to add the 3-phonon interactions, i.e. the third order derivative of the lattice potential, and the phonon-isotope scatterings. The phonon scatterings considered in this work by no means should be considered exhaustive. However, following the procedure outlined in this section, one can add also the effects of different kinds of phonon interactions, for example higher order phonon-phonon interactions, defects, impurities, dislocations and any other deviation from the perfectly harmonic Hamiltonian.

2.1 Phonon-phonon interaction

In the previous chapter, we considered the approximated Hamiltonian defined by the second order term of the Taylor expansion of the lattice potential (see Eq. 1.17). In this section we will retain also the third order term, the lowest order anharmonic term, and we will try to express it in terms of the creation and annihilation operators introduced previously. The Hamiltonian in terms of the atomic displacements in real space is:

$$H = H_{\text{harm}} + \frac{1}{3!} \sum_{lb\alpha l'b'\beta l''b''\gamma} \psi_{\alpha\beta\gamma}(lb, l'b', l''b'') u_{\alpha}(lb) u_{\beta}(l'b') u_{\beta}(l''b''), \quad (2.1)$$

Chapter 2. Phonon scattering

where we adopted for simplicity the short-hand notation:

$$\psi_{\alpha\beta\gamma}(lb, l'b', l''b'') = \left. \frac{\partial^3 V}{\partial u_\alpha(lb) \partial u_\beta(l'b') \partial u_\gamma(l''b'')} \right|_0. \quad (2.2)$$

In complete analogy with the previous chapter - but with some additional algebra - we can operate a Fourier transform and express the position and momentum operators in terms of the collective variables $\mathbf{X}(\mathbf{q}, b)$ and $\mathbf{P}(\mathbf{q}, b)$, finding:

$$H = H_{\text{harm}} + \frac{1}{3!V^{3/2}} \sum_{\mathbf{q}\mathbf{q}'\mathbf{q}''b'b''\alpha\beta\gamma} \psi_{\alpha\beta\gamma}(\mathbf{q}b, \mathbf{q}'b', \mathbf{q}''b'') \delta_{\mathbf{q}+\mathbf{q}'+\mathbf{q}'', \mathbf{G}} X_\alpha(\mathbf{q}b) X_\beta(\mathbf{q}'b') X_\gamma(\mathbf{q}''b''), \quad (2.3)$$

where:

$$\psi_{\alpha\beta\gamma}(\mathbf{q}b, \mathbf{q}'b', \mathbf{q}''b'') = \sum_{l', l''} \psi_{\alpha, \beta, \gamma}(0b, l'b', l''b'') e^{i\mathbf{q}' \cdot \mathbf{R}_{l'}} e^{i\mathbf{q}'' \cdot \mathbf{R}_{l''}}, \quad (2.4)$$

is the Fourier transform of the matrix of third order derivatives. Then, writing \mathbf{X} and \mathbf{P} in terms of the creation and annihilation operators (see Eq. 1.26), we can write:

$$\begin{aligned} H &= H_{\text{harm}} + \frac{1}{3!} \sum_{\mathbf{q}s, \mathbf{q}'s', \mathbf{q}''s''} \psi(\mathbf{q}s, \mathbf{q}'s', \mathbf{q}''s'') \delta_{\mathbf{q}+\mathbf{q}'+\mathbf{q}'', \mathbf{G}} \\ &\quad (a_{\mathbf{q}s}^\dagger - a_{-\mathbf{q}s})(a_{\mathbf{q}'s'}^\dagger - a_{-\mathbf{q}'s'})(a_{\mathbf{q}''s''}^\dagger - a_{-\mathbf{q}''s''}) \\ &= H_{\text{harm}} + \Delta H, \end{aligned} \quad (2.5)$$

where:

$$\psi(\mathbf{q}s, \mathbf{q}'s', \mathbf{q}''s'') = \frac{i\hbar^{3/2}}{\sqrt{V}} \sum_{bb'b''\alpha\beta\gamma} \frac{e_\alpha(b|\mathbf{q}s) e_\beta(b'|\mathbf{q}'s') e_\gamma(b''|\mathbf{q}''s'') \psi_{\alpha\beta\gamma}(\mathbf{q}b, \mathbf{q}'b', \mathbf{q}''b'')}{\sqrt{8m_b m_{b'} m_{b''} \omega_{\mathbf{q}s} \omega_{\mathbf{q}'s'} \omega_{\mathbf{q}''s''}}}. \quad (2.6)$$

Unfortunately, the eigenstates of $a_{\mathbf{q}s}^\dagger, a_{\mathbf{q}s}$ are no longer the eigenstates of the anharmonic Hamiltonian (one can show that the harmonic and anharmonic terms do not commute) and therefore the solution to the anharmonic problem is more complicated to find. It is for this reason that we add the effect of anharmonicity as a perturbation over the harmonic Hamiltonian. Let us therefore start from the harmonic description of the lattice, which is defined by the phonon states:

$$|n_{\mathbf{q}s} n_{\mathbf{q}'s'} \dots\rangle = |n_{\mathbf{q}s}\rangle \otimes |n_{\mathbf{q}'s'}\rangle \otimes \dots \quad (2.7)$$

In the harmonic case, all phonons are perfectly decoupled and are a set of independent oscillators. The anharmonic term instead introduces couplings between the oscillators, so that it is possible that a phonon excitation is transferred from one mode to another. Let us therefore compute the probability to observe a transition from an initial state $|i\rangle$ to a final

state $|f\rangle$ in a unit of time. This scattering rate can be obtained using the Fermi golden rule (see for example Ref. [54] for a formal derivation):

$$P_i^f(3ph) = \frac{2\pi}{\hbar} |\langle f | \Delta H | i \rangle|^2 \delta(E_f - E_i), \quad (2.8)$$

where ΔH is the perturbation to the harmonic Hamiltonian ($H = H_{\text{harm}} + \Delta H$) and $E_{i,f}$ is the energy of the initial / final state.

The number of possible transitions is extremely large in principle, if we are to consider all possible initial and final states. However, the Fermi golden rule is very specific in selecting the combinations of final and initial states that have a non-zero transition rate. To see this, first notice that the perturbation ΔH consists in a summation of terms in the form:

$$(a_{\mathbf{q}s}^\dagger - a_{-\mathbf{q}s})(a_{\mathbf{q}'s'}^\dagger - a_{-\mathbf{q}'s'})(a_{\mathbf{q}''s''}^\dagger - a_{-\mathbf{q}''s''}). \quad (2.9)$$

Writing down this term explicitly we obtain:

$$\begin{aligned} & a_{\mathbf{q}s}^\dagger a_{\mathbf{q}'s'}^\dagger a_{\mathbf{q}''s''}^\dagger - a_{\mathbf{q}s}^\dagger a_{\mathbf{q}'s'}^\dagger a_{-\mathbf{q}''s''} - a_{\mathbf{q}s}^\dagger a_{-\mathbf{q}'s'} a_{\mathbf{q}''s''}^\dagger - a_{-\mathbf{q}s} a_{\mathbf{q}'s'}^\dagger a_{\mathbf{q}''s''}^\dagger \\ & + a_{\mathbf{q}s}^\dagger a_{-\mathbf{q}'s'} a_{-\mathbf{q}''s''} + a_{-\mathbf{q}s} a_{\mathbf{q}'s'}^\dagger a_{-\mathbf{q}''s''} + a_{-\mathbf{q}s} a_{-\mathbf{q}'s'} a_{\mathbf{q}''s''}^\dagger - a_{-\mathbf{q}s} a_{-\mathbf{q}'s'} a_{-\mathbf{q}''s''}. \end{aligned} \quad (2.10)$$

Although this term is no longer local in (\mathbf{q}, s) (as in the harmonic case), it only acts between two states that differ only by three phonons, leaving all the other modes unmodified. Therefore, to compute all the relevant transitions, we don't need to consider all the possible phonon states, but only all possible phonon triplets. Also, as a consequence of the properties of the creation and annihilation operators, the phonon excitation number can only change by three quanta. For example, the first term creates an excitation in each of the three phonon states and gives a non zero scattering rate only for the matrix element $\langle n_{\mathbf{q}s} + 1, n_{\mathbf{q}'s'} + 1, n_{\mathbf{q}''s''} + 1 | a_{\mathbf{q}s}^\dagger a_{\mathbf{q}'s'}^\dagger a_{\mathbf{q}''s''}^\dagger | n_{\mathbf{q}s}, n_{\mathbf{q}'s'}, n_{\mathbf{q}''s''} \rangle$; and so on for the other terms. Enumerating the various cases, there can only be four kinds of processes:

1. creation of 3 phonons;
2. creation of 2 phonons and annihilation of 1 phonon;
3. creation of 1 phonons and annihilation of 2 phonon;
4. annihilation of 3 phonons.

No other kinds of processes are allowed by the lowest order anharmonic term.

As a further simplification, the Fermi golden rule imposes the conservation of energy. Therefore, the transitions of kind 1 and 4 are not allowed as they violate this conservation law. Only the processes of the kind 2, the phonon decay, or 3, the phonon coalescence, are admitted, as shown in Figure 2.1.

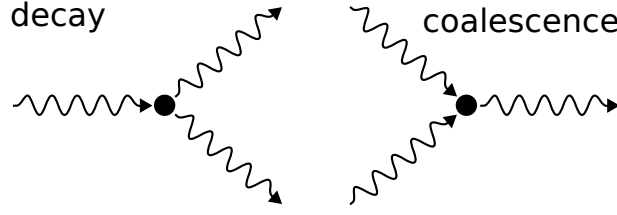


Figure 2.1 – The lowest order phonon-phonon scattering in crystals is described by two kind of interactions: phonon decay, when a phonon is destroyed and two other modes are excited, or the phonon coalescence, in which two phonons are destroyed and a third one is created.

2.2 Normal and Umklapp scattering

Let us analyse the scattering of a phonon in the state $|n_{qs}\rangle$. The scattering processes involve, for both decay and coalescence, two more phonons in the states $(q' s')$ and $(q'' s'')$. We introduced in the previous section the conservation of energy, which imposes a constraint on the phonon frequencies of the three phonons under consideration. Moreover, there is an additional constraint on the momentum of the phonons. The anharmonic term of the Hamiltonian (Eq. 2.5) contains a factor $\delta_{\mathbf{q}+\mathbf{q}'+\mathbf{q}'',\mathbf{G}}$, which appears as a direct consequence of the Fourier transform (see Eq. 1.14) when switching from the real to the reciprocal space description and is a direct consequence of the periodic properties of the Bravais lattice. This relation is the conservation of crystal momentum, stating that the momentum of the three phonons must satisfy a relation of the form:

$$\mathbf{q} + \mathbf{q}' + \mathbf{q}'' = \mathbf{G} . \quad (2.11)$$

This shows that in a three-phonon process, the momentum of a phonon does not need to be conserved exactly. Instead, there can be a mismatch between the initial and final momentum, equal to any reciprocal lattice vector \mathbf{G} .

Summarising, the laws of energy and crystal momentum conservation greatly restrict the possible scattering processes of the phonon (\mathbf{q}, s) . When it undergoes decay, it satisfies the following conservation laws:

$$\begin{aligned} \omega_{qs} &= \omega_{q's'} + \omega_{q''s''} , \\ \mathbf{q} + \mathbf{G} &= \mathbf{q}' + \mathbf{q}'' . \end{aligned} \quad (2.12)$$

For phonon coalescence:

$$\begin{aligned} \omega_{qs} + \omega_{q's'} &= \omega_{q''s''} , \\ \mathbf{q} + \mathbf{q}' &= \mathbf{q}'' + \mathbf{G} . \end{aligned} \quad (2.13)$$

If these laws are not obeyed there is no possible transition between the initial and final states.

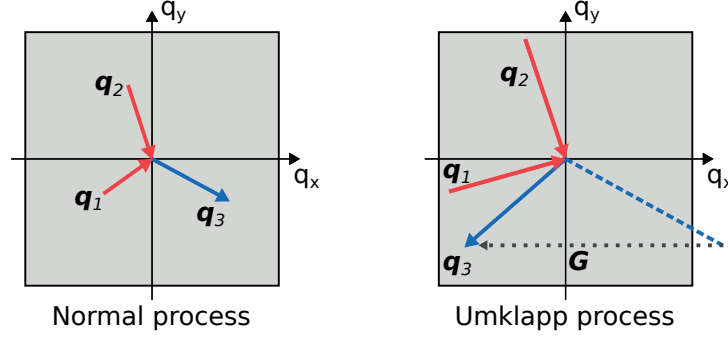


Figure 2.2 – Normal and Umklapp processes in a phonon coalescence process. In a normal process, the sum of the momenta of the two initial phonon modes is a vector lying inside the first Brillouin zone (the grey square). In a Umklapp event, the sum of the two momenta is outside the first Brillouin zone, but there is a reciprocal lattice vector that allows to fold it back inside.

The conservation of crystal momentum imposes a further restriction on the possible number of phonon triplets to consider. Two phonon states suffice to determine the third phonon wavevector. Peierls introduced a further distinction between 3-phonon scattering events. The processes that strictly conserve momentum ($\mathbf{G} = 0$) are called *normal*, whereas if momentum is not conserved ($\mathbf{G} \neq 0$) they are dubbed *Umklapp* which means *turn over* in German, since it can reverse the direction of momentum, see Figure 2.2. To distinguish the normal from the Umklapp processes, one simply needs to compute the third wavevector out of the other two as $\mathbf{q}'' = \mathbf{q} \pm \mathbf{q}'$. If \mathbf{q}'' lies in the Brillouin zone, like the other two points, the process is normal, and Umklapp if instead it needs a certain reciprocal lattice vector \mathbf{G} to be folded back into the Brillouin zone. We will later see that this distinction is extremely important in the context of thermal transport, since a crystal with only normal scattering events has an infinite thermal conductivity, as we will prove in Section 3.2.

2.3 Three-phonon scattering rate

We are finally equipped for computing the transition rates involving a triplet of phonons using the Fermi golden rule. The probability for a phonon mode ($\mathbf{q}s$) to undergo a decay event with two other phonon modes is:

$$\begin{aligned}
 P_{\mathbf{q}s}^{\mathbf{q}'s', \mathbf{q}''s''} &= \frac{2\pi}{\hbar^2} |\langle n_{\mathbf{q}s} - 1, n_{\mathbf{q}'s'} + 1, n_{\mathbf{q}''s''} + 1 | \Delta H | n_{\mathbf{q}s}, n_{\mathbf{q}'s'}, n_{\mathbf{q}''s''} \rangle|^2 \delta(\omega_{\mathbf{q}s} - \omega_{\mathbf{q}'s'} - \omega_{\mathbf{q}''s''}) \\
 &= \frac{2\pi}{\hbar^2 \mathcal{V}} \delta(\omega_{\mathbf{q}s} - \omega_{\mathbf{q}'s'} - \omega_{\mathbf{q}''s''}) \delta_{\mathbf{q} - \mathbf{q}' - \mathbf{q}'', \mathbf{G}} |\psi(\mathbf{q}s, -\mathbf{q}'s', -\mathbf{q}''s'')|^2 \\
 &\quad n_{\mathbf{q}s} (n_{\mathbf{q}'s'} + 1) (n_{\mathbf{q}''s''} + 1) \\
 &= \mathcal{L}_{\mathbf{q}s}^{\mathbf{q}'s', \mathbf{q}''s''} n_{\mathbf{q}s} (n_{\mathbf{q}'s'} + 1) (n_{\mathbf{q}''s''} + 1).
 \end{aligned} \tag{2.14}$$

Similarly, for the coalescence process we obtain:

$$\begin{aligned}
 P_{\mathbf{q}_s, \mathbf{q}'s'}^{\mathbf{q}''s''} &= \frac{2\pi}{\hbar^2} |\langle n_{\mathbf{q}_s} - 1, n_{\mathbf{q}'s'} - 1, n_{\mathbf{q}''s''} + 1 | \Delta H | n_{\mathbf{q}_s}, n_{\mathbf{q}'s'}, n_{\mathbf{q}''s''} \rangle|^2 \delta(\omega_{\mathbf{q}_s} + \omega_{\mathbf{q}'s'} - \omega_{\mathbf{q}''s''}) \\
 &= \frac{2\pi}{\hbar^2 \mathcal{V}} \delta(\omega_{\mathbf{q}_s} + \omega_{\mathbf{q}'s'} - \omega_{\mathbf{q}''s''}) \delta_{\mathbf{q}+\mathbf{q}'-\mathbf{q}'', \mathbf{G}} |\psi(\mathbf{q}_s, \mathbf{q}'s', -\mathbf{q}''s'')|^2 \\
 &\quad n_{\mathbf{q}_s} n_{\mathbf{q}'s'} (n_{\mathbf{q}''s''} + 1) \\
 &= \mathcal{L}_{\mathbf{q}_s, \mathbf{q}'s'}^{\mathbf{q}''s''} n_{\mathbf{q}_s} n_{\mathbf{q}'s'} (n_{\mathbf{q}''s''} + 1). \tag{2.15}
 \end{aligned}$$

In both cases, we extracted an intrinsic rate \mathcal{L} which does not depend on the temperature or the phonon populations and is only determined by the third-order derivatives of the lattice Hamiltonian. Therefore, temperature does not affect the strength of the phonon coupling, it only enters the scattering rates indirectly through the phonon populations, which we know at equilibrium to be equal to the Bose–Einstein distribution function.

2.4 Ab initio evaluation

The computation of the scattering rates for phonon decay and coalescence depends on several quantities. Most of them are simply related to harmonic properties, that is, quantities depending on the dynamical matrix. The additional part that we need to obtain from density functional perturbation theory is the matrix of anharmonic force constants ψ .

We learned in Section 1.4 that it is possible to compute the forces of a system, i.e. the 1-st order energy response to a perturbation, just by the knowledge of the charge density. In our particular case of interest, the perturbation is the displacement of an atom from the equilibrium position. Moreover, we have seen that it is possible to compute also the dynamical matrix, i.e. the energy response to the perturbation at the second order, just by the knowledge of the first order response of the charge density to the perturbation.

It is not by chance that the n^{th} order energy response depends on the charge density response of a smaller order. In fact, there is a general theorem of quantum mechanics, commonly found under the name of the $2n + 1$ theorem [66], which states that the knowledge of the n^{th} order response of the wave-function (or density) is sufficient to compute the $2n + 1$ -th energy response. The implications of this theorem are of great help to our case. Since in Section 1.4 we sketched the technique to obtain the first order charge density response, by means of the $2n + 1$ theorem it is possible to use this information to compute the third order energy derivatives needed for the phonon-phonon coupling. Indeed, it can be shown that the third

derivative with respect to a perturbation λ (the phonon displacement) can be computed as:

$$\begin{aligned}
 \frac{\partial^3 E}{\partial \lambda^3} = & 2 \sum_{n=1}^{N/2} \langle \Delta \psi_n | \Delta V_{SCF} - \Delta \epsilon_n | \Delta \psi_n \rangle \\
 & + 2 \sum_{n=1}^{N/2} \left(\langle \Delta \psi_n | \frac{\partial^2 V}{\partial \lambda^2} | \psi_n \rangle + c.c. \right) \\
 & + 2 \sum_{n=1}^{N/2} \left(\langle \psi_n | \frac{\partial^3 V}{\partial \lambda^3} | \psi_n \rangle + c.c. \right) \\
 & + \frac{1}{6} \int \frac{\delta v_{xc}}{\delta n_1 \delta n_2 \delta n_3} \Delta n(\mathbf{r}_1) \Delta n(\mathbf{r}_2) \Delta n(\mathbf{r}_3) d\mathbf{r}_1 d\mathbf{r}_2 d\mathbf{r}_3 .
 \end{aligned} \tag{2.16}$$

Therefore, knowing the charge density response (Δn), the anharmonic force constants can be computed. The implementation of this equation in the reciprocal space is not straightforward, its formulation has been developed only recently [56] and it later has been implemented in Quantum ESPRESSO [112]. Working with this reciprocal space formulation of density functional perturbation theory, it is possible to obtain the matrix $\psi(\mathbf{q}s, \mathbf{q}'s', \mathbf{q}''s'')$ directly at any arbitrary set of wave vectors.

2.5 Mass disorder scattering

Up to this point we considered only an ideal Hamiltonian in which all atoms have the same mass. However, atoms in a real crystal do not all have the same mass due to the presence of different stable isotopes for each atomic species. The presence of different masses breaks the translational periodicity of the crystal and gives rise to phonon scattering. Assuming the effect of the mass disorder to be small in some sense, we treat this perturbatively on top of the Hamiltonian without mass disorder.

Let us consider as a starting point the harmonic Hamiltonian which takes into account the presence of atoms of different masses in every unit cell of the crystal:

$$H = \frac{1}{2} \sum_{\alpha l b} M_{lb} \dot{u}_\alpha^2(lb) + V^{\text{harm}} , \tag{2.17}$$

where the mass of the atom of basis index b changes its value for different crystal unit cells l . We neglect for simplicity the anharmonic terms of the potential and merely look at the lowest order differences from the harmonic system.

The lattice Hamiltonian above is difficult to solve and we can no longer apply the technique of the Fourier transform learned for the case of the harmonic Hamiltonian, since mass disorder breaks the crystal periodicity. However, the problem can be tackled in perturbation theory. We first introduce the average mass of the atom b :

$$\bar{M}_b = \sum_i f_{ib} M_{ib} \tag{2.18}$$

Chapter 2. Phonon scattering

where f_{ib} is the probability of observing the isotope i in the basis site b . It is worth noting that the introduction of the isotopic distribution f is meant to simplify the problem by subtly reintroducing the lattice periodicity: rather than studying the detailed distribution of isotopes in the lattice sites, we imagine to deal with a system in which each crystal atom has a probability distribution of masses. Most likely this is not a limitation for applications. In fact, we do not expect a natural clustering of isotopes in a material and, if the crystal is large enough, the distribution of isotopes can be considered uniform. The Hamiltonian can be rewritten as:

$$H = H_0 + \Delta H, \quad (2.19)$$

$$H_0 = \frac{1}{2} \sum_{\alpha lb} \bar{M}_b \dot{u}_\alpha^2(lb) + V^{\text{harm}},$$

$$\Delta H = \frac{1}{2} \sum_{\alpha lb} (M_{lb} - \bar{M}_b) \dot{u}_\alpha^2(lb) = \frac{1}{2} \sum_{\alpha lb} \Delta M_{lb} \dot{u}_\alpha^2(lb), \quad (2.20)$$

where the perturbation is determined by the mass difference of the isotope from the average value. To express the Hamiltonian in terms of the creation and annihilation operators, we make use of Eq. 1.33 and express ΔH as:

$$\Delta H = \frac{1}{V} \sum_{\mathbf{q}s, \mathbf{q}'s'} \hbar \sqrt{\omega_{\mathbf{q}s} \omega_{\mathbf{q}'s'}} e_{\mathbf{q}s}^* e_{\mathbf{q}'s'} (a_{\mathbf{q}s}^\dagger - a_{-\mathbf{q}s}) (a_{\mathbf{q}'s'}^\dagger - a_{-\mathbf{q}'s'}) \mathcal{M}_{\mathbf{q}\mathbf{q}'} \quad (2.21)$$

$$= \sum_{\mathbf{q}s, \mathbf{q}'s'} \Delta H_{\mathbf{q}s, \mathbf{q}'s'}, \quad (2.22)$$

where

$$\mathcal{M}_{\mathbf{q}\mathbf{q}'} = \sum_{lb} \Delta M_{lb} e^{i(\mathbf{q}-\mathbf{q}') \cdot \mathbf{x}_{lb}}. \quad (2.23)$$

This last equation reveals a difficulty of studying the isotopic scattering: the coupling term $\mathcal{M}_{\mathbf{q}\mathbf{q}'}$ depends on the detailed distribution of mass differences in the crystal. To simplify the problem, we assume the uniform distribution of the isotopes, so that the mass difference ΔM_{lb} depends only on the basis index and we can simply average over the probability distribution of isotopes f_{ib} .

At variance with the three-phonon interaction, there is no requirement in the conservation of crystal momentum. Therefore, isotopic processes dissipate momentum (and heat flux, for what concerns thermal conductivity). Moreover, this perturbation introduces a coupling between states that differ only by two phonons. We find the transition probabilities by applying the Fermi golden rule:

$$P_{\mathbf{q}s}^{\mathbf{q}'s'} = \frac{2\pi}{\hbar} |\langle f | \Delta H_{\mathbf{q}s, \mathbf{q}'s'} | i \rangle|^2 \delta(E_f - E_i). \quad (2.24)$$

The requirement of energy conservation allows only transitions with the creation of one phonon ($\mathbf{q}s$) and the annihilation of a phonon ($\mathbf{q}'s'$) or viceversa. Therefore, the only relevant

scattering rates for the transitions of a phonon in the state $(\mathbf{q}s)$ are given by the expression:

$$P_{\mathbf{q}s}^{\mathbf{q}'s'} = \frac{\pi\omega_{\mathbf{q}s}\omega_{\mathbf{q}'s'}}{2N_0} \left(n_{\mathbf{q}s}n_{\mathbf{q}'s'} + \frac{n_{\mathbf{q}s} + n_{\mathbf{q}'s'}}{2} \right) \sum_b g_b |\mathbf{e}^*(b|\mathbf{q}s) \cdot \mathbf{e}(b|\mathbf{q}s)|^2 \delta(\omega_{\mathbf{q}s} - \omega_{\mathbf{q}'s'}), \quad (2.25)$$

where we symmetrised the phonon population terms so that $P_{\mathbf{q}s}^{\mathbf{q}'s'} = P_{\mathbf{q}'s'}^{\mathbf{q}s}$, and we introduced a mass disorder parameter:

$$g_b = \sum_i f_{ib} \left(1 - \frac{M_{ib}}{\bar{M}_b} \right). \quad (2.26)$$

Using the results of this chapter, we have at our hands all the necessary ingredients needed for the computation of 3-phonon and phonon-isotope scattering rates. Now it is time to introduce a theory capable of using these scattering rates to predict the lattice thermal conductivity.

3 The phonon Boltzmann transport equation

The application of a temperature gradient brings an energy unbalance in the crystal, felt by all elementary excitations present in the system such as electrons, holes, phonons, magnons and others. In response to the perturbation, the system attempts to reestablish the equilibrium situation where the excess of energy (heat) is spread uniformly over the sample. Therefore, in presence of a temperature gradient, heat tends to be transferred from the hot to the cold side of the material. The quantitative measure of this effect is given by thermal conductivity, defined as the ratio between the heat flux and the temperature gradient. Of all the possible excitations that can carry heat throughout the sample, lattice vibrations give often the largest contribution to heat transfer and this Thesis will focus only on their contribution to the thermal conductivity. In particular, lattice thermal conductivity is often the dominant heat transfer mechanism in insulators, semiconductors and semimetals, and even in metals, where also electrons contribute to the heat transfer, the lattice contribution is not negligible at room temperature.

The microscopic modeling of lattice thermal transport in solids can be tackled using the phonon Boltzmann transport equation. This methodology had been introduced by Peierls almost a century ago (1929) [113] as the main result of his Ph.D. Thesis. Despite being derived long ago, it is still the main theoretical framework to study the microscopic origin of heat transport in crystals. In fact, only the advent of modern computers and reliable ab-initio estimates of microscopic parameters has opened the possibility to solve the equation with a good accuracy and without resorting to oversimplifying assumptions that can miss some relevant features of thermal transport. The Boltzmann equation is not universally applicable to phonon transport and there are known phenomena that cannot be described (or at least require extensions of the formalism), for example the coherent propagation of phonons or high phonon density conditions. Other formalisms, like the Green-Kubo theory [68, 89] have a broader range of applicability but also a considerably increased complexity. However - within its range of applicability - the Boltzmann equation provides an appealingly simple equation (at least, with respect to Green-Kubo methods), and has proved to be a valuable tool for describing accurately the thermal conductivity of most crystals. Therefore, we will proceed and use it for

characterising the thermal conductivity of 2D materials.

In this chapter, we recall the foundations of the Peierls–Boltzmann theory of thermal transport by phonons. The harmonic phonon properties and the scattering rates derived in the previous chapter will be the only ingredients necessary to set up this model of thermal transport. After the derivation of the Boltzmann equation, we will see two important properties associated to the equation. First, we will see that the equation can be casted in a variational formulation, which has close links with the entropy of the phonon gas. Lastly, we will comment on the Matthiessen rule, a law that is very often used to combine the contribution of different scattering processes to thermal conductivity. The theory exposed here can also be found in greater detail in most textbooks about phonons or transport (see for example Refs. [132, 123]). We report here the details necessary to understand the developments of next chapters.

3.1 Formal derivation

The basic idea of Peierls theory is to adapt the Boltzmann equation, originally written for a gas of classical particles, to the case of phonons. The procedure is not directly applicable, since the phonon defined in the previous chapters is actually a wave of lattice displacements. A fundamental assumption of the semiclassical approach is that we can define a wavepacket as a superposition of waves localised both in real and reciprocal space, so that we can represent it as a particle with a well defined position \mathbf{r} and momentum \mathbf{q} . Such wavepacket, built out of a superposition of lattice waves, will be at the center of the discussion for the rest of the Thesis and for simplicity we will call it a phonon (even if the phonon wavepacket is different than the phonon monochromatic wave, the literature has adopted for simplicity the same terminology).

The assumptions of the semiclassical approach presented above are not trivial to justify and there are some conditions upon which the definition of the wavepacket are valid. Being a superposition of waves, the wavepacket is spread in real space over a distance δr . In order to treat the phonon as a particle and assign it a precise position, it is necessary that the average distance L traveled by the phonon (the phonon mean free path) be much larger than the spread δr . Also, the interaction potential that gives raise to the scattering of such wavepacket, should be sufficiently slowly varying in space so that it can be considered to be constant over the extent of the wavepacket. Similarly, in order to have a well defined momentum, it is necessary that the spread δq is such that $\delta q \ll q$. Under these conditions, the phonon can be thought as a classical particle, with a position \mathbf{r} , a momentum \mathbf{q} and a velocity \mathbf{v}_{qs} . Putting the real and reciprocal space conditions together and using the uncertainty principle $\delta r \cdot \delta q \approx 1$, the condition of validity for the semiclassical approach is that the phonon wavevector $\lambda = \frac{2\pi}{q}$ must be much smaller than the mean free path $\lambda \ll \delta r \ll L$.

After having introduced the phonon, we need to understand which is the expectation value for the number of phonons in each state $n_{\nu}(\mathbf{r}, t)$ for every different location inside the crystal at a time t . The index $\nu = (\mathbf{q}, s)$ is a notation for condensing the wavevector and the phonon branch

index, which will substantially simplify the notation for the rest of the Thesis. In the simple case of thermal equilibrium, we saw that Bose–Einstein distribution describes the phonon excitation number. After we apply a gradient of temperature to the sample, the number of phonons changes and we need to write down a procedure to compute it. Let us therefore take a statistical approach and, rather than studying the random walk of each phonon, we examine how every phonon in the state ν evolves on average. The phonon Boltzmann equation describes the average behavior of the phonon and once solved will give us with the steady state phonon distribution $n_\nu(\mathbf{r}, t)$.

Let us then consider the $n_\nu(\mathbf{r}, t)$ phonons occupying a region of the phase space $d\mathbf{r}$. If no scattering has occurred, all phonons at a previous time $t - dt$ must have been in the position $\mathbf{r} - \mathbf{v}_\nu dt$. Therefore:

$$n_\nu(\mathbf{r}, t) = n_\nu(\mathbf{r} - \mathbf{v}_\nu dt, t - dt) \approx n_\nu(\mathbf{r}, t) - \mathbf{v}_\nu dt \frac{\partial n_\nu(\mathbf{r}, t)}{\partial \mathbf{r}} - dt \frac{\partial n_\nu(\mathbf{r}, t)}{\partial t}. \quad (3.1)$$

The mere presence of a phonon velocity thus allows their diffusion. However, not all phonons can move from $\mathbf{r} - \mathbf{v}_\nu dt$ to \mathbf{r} because of scatterings, which might destroy or redistribute them in other states ν' . Therefore, we need to consider an additional change in the phonon distribution with a rate:

$$\left. \frac{\partial n_\nu(\mathbf{r}, t)}{\partial t} \right|_{\text{scatt}}. \quad (3.2)$$

Gathering these mechanisms together, we may write the total rate of change of the distribution function and find the phonon Boltzmann transport equation in its most general form:

$$\frac{\partial n_\nu(\mathbf{r}, t)}{\partial t} + \mathbf{v}_\nu \cdot \frac{\partial n_\nu(\mathbf{r}, t)}{\partial \mathbf{r}} = \left. \frac{\partial n_\nu(\mathbf{r}, t)}{\partial t} \right|_{\text{scatt}}. \quad (3.3)$$

The scattering operator appearing in the equation still needs to be written down explicitly. First of all, we note that at the thermal equilibrium, when n_ν is simply given by the Bose–Einstein distribution \bar{n}_ν and there is no dependence on space and time, the Boltzmann equation requires the collision term to vanish:

$$\left. \frac{\partial \bar{n}_\nu(\mathbf{r}, t)}{\partial t} \right|_{\text{scatt}} = 0. \quad (3.4)$$

Instead, when not at equilibrium, there is an unbalance causing the scattering term to be different from zero. To construct the expression of the scattering operator, let us start for simplicity with the case of the isotopic scattering, which only involves two phonon states. The probability for the transition from a state ν to ν' is given by:

$$P_\nu^{\nu'} = n_\nu(n_{\nu'} + 1) \mathcal{L}_\nu^{\nu'}, \quad (3.5)$$

where we have shown in Section 2.5 that \mathcal{L} is independent both of temperature and details of

Chapter 3. The phonon Boltzmann transport equation

the distribution n_ν , so that the total probability for observing the transition is the intrinsic rate \mathcal{L} times the factors taking into account the populations of the phonons at the initial and final states ν and ν' . By microscopic reversibility $\mathcal{L}_{\nu'}^\nu = \mathcal{L}_\nu^{\nu'}$ (a result that follows from Eqs. 2.14 and 2.15). Therefore the probability for observing the inverse mechanism is:

$$P_{\nu'}^\nu = (n_\nu + 1)n_{\nu'}\mathcal{L}_{\nu'}^\nu. \quad (3.6)$$

Putting together these information, the total change rate of the phonon ν must combine the depopulation due to phonons exiting the state ν with the repopulation coming from other phonons ν' . Therefore, the scattering operator for the isotopic scattering (or more generally for scatterings involving two phonon states) is:

$$\left. \frac{\partial n_\nu(\mathbf{r}, t)}{\partial t} \right|_{2, \text{scatt}} = \sum_{\nu'} [(n_\nu + 1)n_{\nu'} - n_\nu(n_{\nu'} + 1)] \mathcal{L}_\nu^{\nu'}. \quad (3.7)$$

A similar discussion can be made also for the three-phonon processes, finding a scattering operator in the form:

$$\begin{aligned} \left. \frac{\partial n_\nu(\mathbf{r}, t)}{\partial t} \right|_{3, \text{scatt}} &= \sum_{\nu' \nu''} \{ [(n_\nu + 1)(n_{\nu'} + 1)n_{\nu''} - n_\nu n_{\nu'}(n_{\nu''} + 1)] \mathcal{L}_{\nu \nu'}^{\nu''} \\ &\quad + \frac{1}{2} [(n_\nu + 1)n_{\nu'} n_{\nu''} - n_\nu(n_{\nu'} + 1)(n_{\nu''} + 1)] \mathcal{L}_\nu^{\nu' \nu''} \}, \end{aligned} \quad (3.8)$$

where the factor $\frac{1}{2}$ avoids the double counting of the final states in the phonon decay, $\mathcal{L}_{\nu \nu'}^{\nu''}$ is the intrinsic rate for phonon coalescence and $\mathcal{L}_\nu^{\nu' \nu''}$ for the phonon decay. The total scattering operator that describes both 3-phonon processes and isotopic scattering events is just the sum of the two separate scattering operators.

Using these expressions for the scattering operator, the Boltzmann equation is an integro-differential equation of still formidable complexity. To simplify it, we consider only small perturbations of temperature, so that we can always define a local temperature $T(\mathbf{r}, t)$ and so that the out-of-equilibrium distribution $n_\nu(\mathbf{r}, t)$ deviates by a small amount from the local thermal equilibrium $\bar{n}_\nu(\mathbf{r}, t)$. Under these conditions we don't need to consider the full scattering integral, instead it is sufficient to linearise it for small deviations $n_\nu - \bar{n}_\nu$. The linear approximation suggests the introduction of a deviation from equilibrium function h_ν , defined as:

$$n_\nu \equiv \bar{n}_\nu - h_\nu \frac{\partial \bar{n}_\nu}{\partial(\beta \hbar \omega_\nu)} = \bar{n}_\nu + \bar{n}_\nu(\bar{n}_\nu + 1)h_\nu, \quad (3.9)$$

so that the deviation from equilibrium is $\bar{n}_\nu(\bar{n}_\nu + 1)h_\nu$. Luckily, the isotopic scattering operator can be written exactly in terms of the linear deviation from equilibrium:

$$\left. \frac{\partial n_\nu(\mathbf{r}, t)}{\partial t} \right|_{2, \text{scatt}} = \sum_{\nu'} [\bar{n}_{\nu'}(\bar{n}_{\nu'} + 1)h_{\nu'} - \bar{n}_\nu(\bar{n}_\nu + 1)h_\nu] \mathcal{L}_\nu^{\nu'}. \quad (3.10)$$

The expression for the 3-phonon interaction instead cannot be exactly expressed in terms of the deviation from equilibrium of the phonon distribution, and it is necessary to expand it in series and neglect higher order terms. In this way, we obtain the linearised scattering operator:

$$\left. \frac{\partial n_\nu}{\partial t} \right|_{\text{scatt}} = - \sum_{\nu''} [\bar{P}_{\nu\nu''}^{\nu''} (h_\nu + h_{\nu'} - h_{\nu''}) + \frac{1}{2} \bar{P}_\nu^{\nu'\nu''} (h_\nu - h_{\nu'} - h_{\nu''})] - \sum_{\nu'} \bar{P}_\nu^{\nu'} (h_\nu - h_{\nu'}), \quad (3.11)$$

where the scattering rates \bar{P} are:

$$\begin{aligned} \bar{P}_{\nu\nu'}^{\nu''} &= \bar{n}_\nu \bar{n}_{\nu'} (\bar{n}_{\nu''} + 1) \mathcal{L}_{\nu\nu'}^{\nu''}, \\ \bar{P}_\nu^{\nu'\nu''} &= \bar{n}_\nu (\bar{n}_{\nu'} + 1) (\bar{n}_{\nu''} + 1) \mathcal{L}_\nu^{\nu'\nu''}, \\ \bar{P}_\nu^{\nu'} &= \bar{n}_\nu (\bar{n}_{\nu'} + 1) \mathcal{L}_\nu^{\nu'}. \end{aligned} \quad (3.12)$$

As a consequence of the linearisation, the action of the scattering operator on the distribution function can be represented with a matrix - vector multiplication:

$$\left. \frac{\partial n_\nu}{\partial t} \right|_{\text{scatt}} = - \sum_{\nu'} A_{\nu\nu'} h_{\nu'} = - \sum_{\nu'} \Omega_{\nu\nu'} n_{\nu'} = -Ah = -\Omega n, \quad (3.13)$$

where the two scattering matrices A and Ω are related as $\Omega_{\nu\nu'} \bar{n}_{\nu'} (\bar{n}_{\nu'} + 1) = A_{\nu\nu'}$ and the scattering matrix A is defined by [61]:

$$A_{\nu\nu'} = - \left[\sum_{\nu'',\nu'''} (\bar{P}_{\nu\nu''}^{\nu''} + \frac{1}{2} \bar{P}_{\nu\nu''}^{\nu'''} + \sum_{\nu'''} P_{\nu\nu''}^{\nu''}) \right] \delta_{\nu,\nu'} + \sum_{\nu''} (\bar{P}_{\nu\nu''}^{\nu'} - \bar{P}_{\nu\nu''}^{\nu''} + \bar{P}_{\nu\nu''}^{\nu'}) + \bar{P}_\nu^{\nu'}. \quad (3.14)$$

In writing this expression we made use of the detailed balance condition $P_{\nu,\nu'}^{\nu''} = P_{\nu''}^{\nu,\nu'}$ to reorder the indexes appropriately. The usage of a matrix notation will prove extremely convenient for studying the Boltzmann equation, in particular we will use the matrix A to discuss iterative solutions of the Boltzmann equation and Ω when we will diagonalise the scattering matrix. Again for later convenience, let us mention that the scattering matrix is often separated into two components, the diagonal A^{out} and the off-diagonal part A^{in} :

$$A_{\nu\nu'}^{\text{out}} = - \frac{\bar{n}_\nu (\bar{n}_\nu + 1)}{\tau_\nu} \delta_{\nu,\nu'}, \quad (3.15)$$

$$A_{\nu\nu'}^{\text{in}} = \sum_{\nu''} (\bar{P}_{\nu,\nu''}^{\nu'} - \bar{P}_{\nu\nu''}^{\nu''} + \bar{P}_{\nu\nu''}^{\nu'}) + \bar{P}_\nu^{\nu'}. \quad (3.16)$$

The meaning of the name of the two matrices [61] will be clearer with the introduction of the relaxation time approximation in Section 4.1, and they refer to the fact that $A_{\nu\nu}^{\text{out}}$ is the rate of depopulation of the phonon ν , while $A_{\nu\nu'}^{\text{in}}$ is the repopulation of the mode ν due to the scattering of other phonons.

The steady state problem

In a large number of cases we are simply interested at solving the time independent problem, in which a constant gradient of temperature is applied to the crystal. In this case, the time derivative appearing in the Boltzmann equation can be set to zero. The remaining part of the drifting operator can be further simplified:

$$\mathbf{v}_\nu \cdot \frac{\partial n_\nu(\mathbf{r}, t)}{\partial \mathbf{r}} = \mathbf{v}_\nu \cdot \nabla T \frac{\partial n_\nu(\mathbf{r}, t)}{\partial T} \approx \mathbf{v}_\nu \cdot \nabla T \frac{\partial \bar{n}_\nu(\mathbf{r}, t)}{\partial T}. \quad (3.17)$$

The first equality takes advantage that the system is homogeneous in space and the distribution differs in real space only due to the presence of a different temperature. The approximation instead holds for a small deviation from thermal equilibrium, where in fact also the linearisation of the scattering operator holds, so that the change of the out-of-equilibrium distribution due to temperature is approximately the same of the Bose–Einstein distribution. Therefore, the steady state homogeneous Boltzmann equation is greatly simplified and becomes:

$$\mathbf{v}_\nu \cdot \nabla T \frac{\partial \bar{n}_\nu(\mathbf{r}, t)}{\partial T} = - \sum_{\nu'} A_{\nu\nu'} h_{\nu'}. \quad (3.18)$$

We look for solution to this equation that are linear in the temperature gradient:

$$\begin{aligned} h_\nu &\approx f_\nu \nabla T, \\ n_\nu &\approx \bar{n}_\nu + \bar{n}_\nu (\bar{n}_\nu + 1) \nabla T f_\nu. \end{aligned} \quad (3.19)$$

so that the Boltzmann equation is reduced to:

$$v_\nu \frac{\partial \bar{n}_\nu(\mathbf{r}, t)}{\partial T} = - \sum_{\nu'} A_{\nu\nu'} f_{\nu'} \quad (3.20)$$

where v_ν is the component of \mathbf{v}_ν parallel to ∇T . The advantage of the matrix notation is to make explicit the mathematical structure of the equation, which is simply a linear algebra problem:

$$A f = b, \quad (3.21)$$

where we introduced a vector $b_\nu = -v_\nu \frac{\partial \bar{n}_\nu}{\partial T} = -v_\nu \bar{n}_\nu (\bar{n}_\nu + 1) \frac{\hbar \omega_\nu}{k_B T^2}$.

The solution to this equation could be obtained directly by inversion of the scattering matrix: $f = A^{-1} b$. Let us suppose for the time being that this equation can be solved; with the knowledge of the deviation function f_ν the most difficult part of the transport problem is solved. The lattice heat flux can be evaluated, to lowest order, as [72]:

$$Q = \frac{1}{V} \sum_\nu \hbar \omega_\nu v_\nu n_\nu = \frac{1}{V k_B T^2} \sum_\nu \bar{n}_\nu (\bar{n}_\nu + 1) \hbar \omega_\nu v_\nu f_\nu \nabla T. \quad (3.22)$$

Comparing this equation to the definition of the thermal conductivity k :

$$Q = -k\nabla T, \quad (3.23)$$

we can finally compute the lattice thermal conductivity of the Boltzmann–Peierls theory:

$$k = -\frac{1}{V k_B T^2} \sum_{\nu} \bar{n}_{\nu} (\bar{n}_{\nu} + 1) \hbar \omega_{\nu} v_{\nu} f_{\nu}. \quad (3.24)$$

As we can see, the thermal conductivity can be easily obtained if the phonon deviation distribution f_{ν} is known. However, obtaining the solution to the problem is an extremely computationally expensive operation, given that the matrix is extremely large, and the entire Chapter 4 will be dedicated to methods for finding the solution. Before venturing into these methods, we introduce additional properties of the Boltzmann equation that will be useful for the discussion of this Thesis.

3.2 Conductivity without scattering

At this point, we are equipped to understand the distinction between normal and Umklapp processes introduced before and show that the thermal conductivity of a crystal with only normal processes is infinite. First of all, it is not true that every single normal process conserves the heat flux [132]. In fact, let us consider an initial phonon ν , carrying a heat flux $\hbar \omega_{\nu} v_{\nu}$. After a normal scattering process, for example a decay event, the heat flux is $\hbar(\omega_{\nu'} v_{\nu'} + \omega_{\nu''} v_{\nu''})$. While the energy is conserved by the scattering process, the velocity does not need to and thus the heat flux may not be conserved in an isolated normal scattering event. Only in the special case of acoustic phonons with the same linear dispersion, the velocity is simply proportional to momentum and heat fluxes are exactly conserved.

To properly interpret normal events, we need instead to study what is the statistical (or collective) behavior of phonons. Let us consider a system in which only normal scattering events take place. We proved in Section 1.3 that, in a system where momentum is conserved, the stable distribution of the system is the drifting distribution:

$$n_{\nu}^{\text{drift}} = \frac{1}{e^{\beta(\hbar \omega_{\nu} - \mathbf{v}^{\text{drift}} \cdot \mathbf{q})} - 1}. \quad (3.25)$$

This distribution carries a non-zero heat flux. Since n_{ν}^{drift} must be a solution of the Boltzmann equation in absence of Umklapp scatterings, it follows that it is a stationary distribution of the normal scattering operator [69]:

$$\left. \frac{\partial n_{\nu}^{\text{drift}}}{\partial t} \right|_{\text{normal scatt}} = 0 \quad (3.26)$$

This result also implies that the drifting distribution is an eigenvector of the normal scattering matrix with zero eigenvalue.

Chapter 3. The phonon Boltzmann transport equation

Let us also recall Eq. 3.4, where we've shown that the Bose–Einstein distribution is a stationary solution to the problem, that is, the Bose–Einstein distribution is an eigenvector of the scattering matrix with a zero eigenvalue, independently of the conservation of momentum. If we try to compute the heat flux or the total momentum due to the Bose–Einstein distribution, we obtain a zero heat flux and total momentum, which follows from the parity of the functions involved. Thus, the Bose–Einstein distribution is a stationary solution for the phonon gas, which does not contribute to heat transfer.

If instead we set the system of phonons into a condition with non zero momentum, normal processes alone will not be able to bring the system into full thermal equilibrium, even if no temperature gradient is applied. At most, normal processes relax the system into the drifting distribution, with the drifting velocity determined by the amount of momentum present in the system. Since the drifting distribution supports a non-zero heat flux and since this distribution persists even in absence of a temperature gradient, it follows that a system with only normal scattering events has infinite thermal conductivity. One should not, however, think that normal processes could be neglected: these still enter the Boltzmann equation and redistribute the phonon population across modes, as we will discuss later in this Thesis.

Using the same arguments, a harmonic crystal without phonon scattering conserves momentum, and therefore it also has an infinite thermal conductivity. The inclusion of anharmonicity is therefore necessary to characterise thermal conductivity.

3.3 Variational principle

Boltzmann, after having written his equation for a gas of particles, derived in 1872 the H-theorem, proving the existence of a quantity that represents the entropy of the system. Using the properties of the scattering operator, it is possible to show that the entropy can only increase over the course of time (a result that Boltzmann claimed to be a ‘proof’ of the second law of thermodynamics). It was noted in the 50s [85, 86, 132] that the same ideas developed by Boltzmann for the classical system can be transferred to the phonon system. Although we do not intend to study directly the entropy associated to the Boltzmann equation, these ideas are at the base for a variational formulation of the phonon Boltzmann equation, which is of great utility for finding solutions to the problem.

To proceed, it is convenient to adopt a bra-ket notation for the algebraic operations, so that the scalar product between two distribution functions is defined by:

$$\langle f | g \rangle = \sum_{\mathbf{v}} f_{\mathbf{v}} g_{\mathbf{v}}. \quad (3.27)$$

The scattering matrix A is characterised by a number of mathematical properties:

1. A is real, i.e. $A_{\mathbf{v}\mathbf{v}'} \in \mathbb{R}, \forall \mathbf{v}, \mathbf{v}'$;

2. A is symmetric, i.e. $A_{v'v} = A_{vv'}$;
3. A is semi-positive definite on the ensemble of solutions, i.e. $\langle f|A|f \rangle \geq 0, \forall f$.

The first property is trivial, since by construction the probabilities entering the matrix are real numbers. The second follows from the detailed balance condition. The last property can be demonstrated (see for example the appendix of Ref. [61] for a proof) and it derives from the non-negativity of the scattering probabilities.

There are several physical implications of the properties mentioned above (see also Section 4.5). The one we'll be dealing with in this section is the variational principle [132]:

Theorem: The solution of the Boltzmann equation gives the functional $\mathcal{F}[f] = \langle f|A|f \rangle$ its maximum value.

Proof. Let ϕ be the solution to the Boltzmann equation. Choose any other function ψ , not necessarily a solution of the Boltzmann equation, but that satisfies:

$$\langle \psi|A|\psi \rangle = \langle \psi|b \rangle .$$

Then:

$$\begin{aligned} 0 &\leq \langle (\phi - \psi)|A|(\phi - \psi) \rangle && \text{by matrix property 3} \\ &= \langle \phi|A|\phi \rangle + \langle \psi|A|\psi \rangle - \langle \phi|A|\psi \rangle - \langle \psi|A|\phi \rangle \\ &= \langle \phi|A|\phi \rangle + \langle \psi|A|\psi \rangle - 2 \langle \psi|A|\phi \rangle \\ &= \langle \phi|A|\phi \rangle + \langle \psi|A|\psi \rangle - 2 \langle \psi|b \rangle && \text{using the Boltzmann equation} \\ &= \langle \phi|A|\phi \rangle - \langle \psi|A|\psi \rangle && \text{by definition of } \psi . \end{aligned}$$

Therefore:

$$\langle \phi|A|\phi \rangle \geq \langle \psi|A|\psi \rangle .$$

□

The functional $\langle f|A|f \rangle$ is practical for proving the theorem, but it can be reformulated in other more physically convenient ways [132]. Using Eq. 3.24, let us note that $k = \frac{1}{\mathcal{V}} \langle b|f \rangle$ when f is the solution of the Boltzmann equation and for such f we also have $\langle f|A|f \rangle = \langle b|f \rangle$. Therefore, we can state the variational principle as a problem of minimisation of the thermal resistivity functional ($\rho = \frac{1}{k}$) [132]:

$$\rho[f] = \mathcal{V} \frac{\langle f|A|f \rangle}{(\langle b|f \rangle)^2} . \tag{3.28}$$

Chapter 3. The phonon Boltzmann transport equation

Similarly, we can define a variational thermal conductivity functional:

$$k[f] = \frac{1}{V} (2 \langle b|f \rangle - \langle f|A|f \rangle). \quad (3.29)$$

Note that, although we are calling it a thermal conductivity (resistivity) functional, it assumes a physical meaning only when computed at the solution of the Boltzmann equation. The existence of this functional is particularly important for deriving a variational method for finding the solution of the Boltzmann equation.

3.4 Matthiessen rule

We learned that various phonon scattering events, in particular three-phonon and isotopic processes, are the microscopic origin of thermal resistance. It would be interesting however to quantify how much of the total thermal resistance is attributed to each kind of scattering. For example, we may consider a crystal in which only the 3-phonon scatterings (process 1) take place and another in which only isotopic scatterings are observed (process 2). For both crystal we are able to compute the thermal resistivity ρ_1 and ρ_2 , how do they relate to the thermal resistivity ρ of a crystal that has both kinds of scattering?

The Matthiessen rule states that the total thermal resistivity is the sum of resistivities due to a single source of scattering:

$$\rho = \rho_1 + \rho_2. \quad (3.30)$$

This empirical rule aims at simplifying the problem and often works, but strictly speaking is not correct and we will see indeed that has limited applicability in 2D materials. Using the variational principle, we can prove that the correct general relation is [132]:

$$\rho \geq \rho_1 + \rho_2. \quad (3.31)$$

To demonstrate it, let's consider the variational thermal resistivity of Eq. 3.28 (we set the volume to one in the following for simplicity). Now, let's suppose to separate the scattering matrix into the two different components 1 and 2 (for example separate 3-phonon from isotopic scatterings):

$$A = A_1 + A_2. \quad (3.32)$$

The total resistivity is:

$$\rho = \frac{\langle f|A_1|f \rangle + \langle f|A_2|f \rangle}{(\langle f|b \rangle)^2}. \quad (3.33)$$

The function f is the solution that minimises the total resistivity functional defined by A , and does not need to be identical to the function that minimises the functionals ρ_1 and ρ_2 defined

by A_1 or A_2 only. Let us instead denote with f_1 and f_2 the solutions for the thermal resistivity functionals ρ_1 and ρ_2 . By the variational principle:

$$\begin{aligned} \rho &= \frac{\langle f|A_1|f \rangle}{(\langle f|b \rangle)^2} + \frac{\langle f|A_2|f \rangle}{(\langle f|b \rangle)^2} \\ &\geq \frac{\langle f_1|A_1|f_1 \rangle}{(\langle f_1|b \rangle)^2} + \frac{\langle f_2|A_2|f_2 \rangle}{(\langle f_2|b \rangle)^2} \\ &= \rho_1 + \rho_2 . \end{aligned} \tag{3.34}$$

Therefore, the Matthiessen law overestimates the exact thermal conductivity:

$$\frac{1}{k} \leq \frac{1}{k_1} + \frac{1}{k_2} . \tag{3.35}$$

It's always impossible to rigorously separate the contribution to the total thermal conductivity of different scattering processes and the Matthiessen rule is an approximation with varying range of applicability. At most, we can compute the total thermal conductivities for every given system and compare differences to quantify how important is the inclusion of one scattering process. In Chapter 8 we will study the range of applicability of this rule and also comment it in relation to phonon lifetimes.

4 Solutions of the Boltzmann transport equation

As we have seen in the previous chapter, the Boltzmann equation is a linear algebra problem, whose solution is formally obtained by inverting the scattering matrix. This simple minded picture for finding the solution is of little help in practice. In fact, the matrix inversion is an extremely expensive operation to be performed and therefore it is convenient to think at alternative methods. Moreover, after inverting the matrix and computing the value of the thermal conductivity, there is no obvious physical way of interpreting the results obtained in terms of microscopic quantities.

In this chapter, we will focus on methods for solving the linearised Boltzmann equation to find the out-of-equilibrium distribution function and thus the steady state thermal conductivity of a crystal. The first two methods that we will discuss, the single-mode relaxation time approximation (SMA) and the Callaway method, are two theories that give an approximate solution to our problem. Historically, the SMA has been the first way of solving the transport problem, a tool that was introduced by Boltzmann himself in the study of a classical gas. The Callaway approximation is instead a method originally developed for the study of phonons at low temperature conditions. The nice feature of these two methods is an appealingly simple closed-form solution that allows a physical interpretation. However, they rely on some assumptions on the scattering operator, whose validity will be discussed down below, that do not always apply and are sometimes insufficient to describe 2D materials.

The following three methods instead are capable of solving the linear Boltzmann equation exactly, without any assumption on the form of the scattering operator. The iterative method has been the first algorithm that successfully managed to solve a phonon Boltzmann equation, developed about 20 years ago [110, 109, 108] and now probably the most commonly used method. It has successfully been applied to crystals using phonon properties from first principles. For example, the first exactly solved ab-initio Boltzmann equation has been studied by Mingo et al. [44] for silicon, for alloys it has been solved by Garg et al. [62] and since then it has later been used in several studies. However, this method has only a limited domain of convergence in 2D materials and is not capable of describing the thermal conductivity of graphene (we will see this in Section 8.3). In addition to the iterative method, we will

see a recent method that takes advantage of the variational interpretation of the Boltzmann equation to find efficiently the exact solution [61]. This will be the method of choice for the results of Chapters 6, 7 and its robustness is particularly important for the study of 2D materials and addresses some deficiencies of the iterative method.

Lastly, we will also show how to tackle the problem using a direct diagonalisation of the scattering matrix. This method has a much worse efficiency than the variational method and in fact very few people studied the theory behind this method and even fewer attempted the diagonalisation. However it provides a closed-form solution of the Boltzmann equation and, as an original result of this Thesis, we found that it is capable to provide a rigorous physical interpretation of the Boltzmann equation.

4.1 Single mode relaxation time approximation

As a first attempt in finding the solution to the Boltzmann equation, we start in this section with the single-mode relaxation time approximation (SMA). Since the complete problem is a challenging task, we simplify the scattering operator by using only its diagonal elements

$$A \approx A_{v,v'}^{\text{out}} = \frac{\bar{n}_v(\bar{n}_v + 1)}{\tau_v} \delta_{v,v'}, \quad (4.1)$$

where τ_v is the phonon lifetime or phonon relaxation time. Historically, the first solution has been the single relaxation time approximation, an even simpler version of what we will see in which there is only one relaxation time for all modes, i.e. the matrix is replaced essentially by a single scalar.

To understand why τ_v is called a relaxation time, it is necessary to consider the time-dependent Boltzmann transport equation. Using the SMA, it becomes:

$$\frac{\partial n_v(\mathbf{r}, t)}{\partial t} + \mathbf{v}_v \cdot \nabla n_v(\mathbf{r}, t) = - \frac{n_v(\mathbf{r}, t) - \bar{n}_v}{\tau_v^{\text{SMA}}}. \quad (4.2)$$

Suppose now to study a homogeneous system at thermal equilibrium, so that the space dependence can be dropped. At time t_0 we excite a phonon mode homogeneously across the sample and take it to an excitation number n_v . The governing equation for larger times is simply:

$$\frac{\partial n_v(\mathbf{r}, t)}{\partial t} = - \frac{n_v(\mathbf{r}, t) - \bar{n}_v}{\tau_v^{\text{SMA}}}. \quad (4.3)$$

The solution of this equation is $n_v(t) = \bar{n}_v + (n_v(t_0) - \bar{n}_v)e^{-t/\tau_v}$. This shows that the phonon relaxes back to the Bose–Einstein equilibrium with a characteristic time τ_v . More precisely, the time it takes for the phonon to decay by a factor $1/e$ defines the relaxation time τ_v . Therefore, the diagonal elements of the scattering matrix are those describing the depopulation of the phonon mode v .

4.1. Single mode relaxation time approximation

Let us now return to the steady state problem and find the expression for the SMA thermal conductivity from the SMA Boltzmann equation:

$$v_v \frac{\partial \bar{n}_v}{\partial T} = - \frac{\bar{n}_v(\bar{n}_v + 1)}{\tau_v^{\text{SMA}}} f_v. \quad (4.4)$$

The equation is diagonal in the phonon index v , which allows for a trivial solution:

$$f_v = - \frac{\hbar \omega_v v_v \tau_v^{\text{SMA}}}{k_B T^2}. \quad (4.5)$$

In a matrix notation, the SMA solution to the Boltzmann transport equation is:

$$f = (A^{\text{out}})^{-1} b. \quad (4.6)$$

Inserting the SMA phonon deviation distribution into the expression of thermal conductivity (Eq. 3.24), we find:

$$\begin{aligned} k^{\text{SMA}} &= \frac{1}{V} \sum_v \bar{n}_v(\bar{n}_v + 1) \hbar \omega_v v_v f_v \\ &= \frac{1}{V k_B T^2} \sum_v \bar{n}_v(\bar{n}_v + 1) (\hbar \omega_v)^2 v_v^2 \tau_v^{\text{SMA}} \\ &= \frac{1}{V} \sum_v C_v v_v^2 \tau_v^{\text{SMA}}, \\ &= \frac{1}{V} \sum_v C_v v_v \Lambda_v^{\text{SMA}}, \end{aligned} \quad (4.7)$$

where in the last equality we introduced the phonon mean free path Λ_v^{SMA} :

$$\Lambda_v^{\text{SMA}} = \tau_v^{\text{SMA}} v_v. \quad (4.8)$$

Since the phonon propagates at velocity v_v for a characteristic time τ_v before decaying, it follows that Λ_v is the average distance the phonon can travel before its excitation has decayed by a factor $\frac{1}{e}$, i.e. the phonon mean free path. Therefore, Λ represents the characteristic distance at which the phonon scattering can reestablish thermal equilibrium.

The result is completely analogous to the classical kinetic theory of gases, that introduced the notion of relaxation times (the first documented use of the word 'relaxation time' dates back to Maxwell, in a seminal work [102] in which a modern version of the kinetic theory of a particle gas was formulated). Although we do not report here the theory in full detail, the kinetic thermal conductivity is given as well by the expression $k = C v \Lambda$, where C is the specific heat of the gas, v is the average particle velocity and Λ is the average mean free path. In the kinetic theory, the particles are identical and thus there is no index on the particle states. Beside this difference on the allowed particle states, the phonon Boltzmann equation has a striking analogy with the kinetic gas theory within the relaxation time approximation and for this reason we can interpret the phonon transport problem as that of a gas of quasiparticles

Chapter 4. Solutions of the Boltzmann transport equation

randomly colliding with each other with a characteristic time τ_v^{SMA} and drifting in one direction due to the presence of a gradient of temperature at a velocity v_v by carrying a thermal energy C_v .

What are we neglecting using the SMA? First of all, it cannot be a complete explanation since we set the out-of-diagonal matrix elements to zero. The analysis on the decay of the phonon ν can also be extended to the other phonon modes $\nu' \neq \nu$. Equation 4.2 describes that the phonons ν' at time $t > t_0$ are never excited and are always left at the Bose–Einstein equilibrium. However, this cannot be the correct description: when the phonon ν scatters, it necessarily has to change the excitation number of other phonon modes ν' . The out-of-diagonal elements describe the coupling between the various phonon modes that arise from the scattering and thus describes the repopulation of the phonon mode ν by the scattering that occurs at other phonon modes ν' . For this reason, we indicated the out-of-diagonal part of the matrix as A^{in} . The diagonal term A^{out} describes only the depopulation of the phonon mode.

Closely related to this point, the out-of-diagonal elements are also necessary to describe correctly normal scattering events. Think for example at the problem of Section 3.2, where we were considering a crystal in which only normal scattering events take place, which should have an infinite thermal conductivity. Even if we limit all scattering to normal events, it is still possible to compute the relaxation time for each phonon mode. Yet, each phonon mode will have a finite relaxation time, i.e. a finite probability for decaying into another state, and therefore the thermal conductivity would be finite. As Ziman well described in his book [132], this happens because the length Λ_v^{SMA} describes the characteristic length at which the phonon mode is scattering (in fact, τ_v is also the phonon lifetime, i.e. the average time between phonon collisions). This does not necessarily have an obvious connection to the length at which the excess of heat is dissipated. In fact, heat flux does not need to be completely dissipated at every phonon scattering and the SMA is not capable of describing how the heat flux is shuttled through the various modes. Instead, the SMA describes more properly the length at which heat is transferred from one phonon to another and therefore it only gives an approximate treatment of the heat transport theory.

4.2 Callaway approximation

When a crystal is cooled to cryogenic temperatures, the Umklapp processes tend to freeze [34] and the normal scattering events become dominant. As explained in the previous section, the shortcomings of the SMA prevent it to be capable of describing the phonon transport in these conditions. In an attempt to study the thermal conductivity of Germanium at temperatures smaller than 20K, Callaway [47] put forward an improvement on the SMA description of normal processes.

Following his derivation, we separate the contribution to the scattering matrix due to normal

(\mathcal{N}) scattering events from all the other resistive (\mathcal{R}) mechanisms:

$$\Omega \cdot n = \Omega_{\mathcal{R}} \cdot n + \Omega_{\mathcal{N}} \cdot n. \quad (4.9)$$

For simplicity, we retain the SMA approach of neglecting the off-diagonal elements of the matrix and we let the resistive part decay, as before, to the thermal equilibrium distribution (note that the term $\bar{n}_v(\bar{n}_v + 1)f_v$ appearing in Eq. 4.4 is equal to $(n_v - \bar{n}_v)/\nabla T$). At variance with the SMA, we try to insert the knowledge that the most probable phonon distribution that conserves momentum is the drifting distribution n_v^{drift} (see Section 1.3). Therefore, we let the phonon distribution decay towards n_v^{drift} when driven by the normal processes:

$$\begin{aligned} \sum_{v'} (\Omega_{\mathcal{R}})_{vv'} n_v &= \frac{n_v - \bar{n}_v}{\tau_v^{\mathcal{R}}} \\ \sum_{v'} (\Omega_{\mathcal{N}})_{vv'} n_v &= \frac{n_v - n_v^{\text{drift}}}{\tau_v^{\mathcal{N}}}. \end{aligned} \quad (4.10)$$

The Boltzmann equation within the Callaway approximation becomes:

$$\mathbf{v}_v \cdot \nabla T \frac{\partial \bar{n}_v}{\partial T} = -\frac{n_v - \bar{n}_v}{\tau_v^{\mathcal{R}}} - \frac{n_v - n_v^{\text{drift}}}{\tau_v^{\mathcal{N}}} \quad (4.11)$$

To further simplify the equations, we expand the drifting distribution in Taylor series:

$$n_v^{\text{drift}} = \frac{1}{e^{\beta(\hbar\omega_v - \mathbf{q} \cdot \mathbf{V})} - 1} \approx \bar{n}_v + \bar{n}_v(\bar{n}_v + 1) \frac{\mathbf{q} \cdot \mathbf{V}^{\text{drift}}}{k_B T}. \quad (4.12)$$

Inserting it back into the Boltzmann equation we find:

$$v_v \bar{n}_v(\bar{n}_v + 1) \frac{\hbar\omega_v}{k_B T^2} = -\frac{\bar{n}_v(\bar{n}_v + 1)}{\tau_v} f_v + \frac{\mathbf{q} \cdot \mathbf{V}^{\text{drift}}}{\nabla T k_B T} \frac{\bar{n}_v(\bar{n}_v + 1)}{\tau_v^{\mathcal{N}}}, \quad (4.13)$$

where we used the relation $\frac{1}{\tau_v} = \frac{1}{\tau_v^{\mathcal{N}}} + \frac{1}{\tau_v^{\mathcal{R}}}$. The equation has a closed-form solution for the out-of-equilibrium phonon deviation:

$$f_v = -\frac{v_v \hbar\omega_v \tau_v}{k_B T^2} + \frac{\mathbf{q} \cdot \mathbf{V}^{\text{drift}}}{\nabla T k_B T} \frac{\tau_v}{\tau_v^{\mathcal{N}}}. \quad (4.14)$$

The Boltzmann equation alone does not provide a way to fix the drift velocity, therefore we need another way to impose an auxiliary condition. Callaway proposed that the total momentum carried by the phonon gas should not be changed by normal collisions (alternatives have been

Chapter 4. Solutions of the Boltzmann transport equation

explored in Ref. [31]). This statement reads as:

$$0 = \frac{\partial \mathbf{P}}{\partial t} \Big|_{\mathcal{N}} \quad (4.15)$$

$$0 = \sum_{\mathbf{v}} \mathbf{q} \frac{\partial n_{\mathbf{v}}}{\partial t} \Big|_{\mathcal{N}}$$

$$0 = \sum_{\mathbf{v}} \mathbf{q} \frac{\bar{n}_{\mathbf{v}}(\bar{n}_{\mathbf{v}} + 1)}{\tau_{\mathbf{v}}^{\mathcal{N}}} \left(f_{\mathbf{v}} - \frac{\mathbf{q} \cdot \mathbf{V}^{\text{drift}}}{\nabla T k_B T} \right)$$

$$0 = \sum_{\mathbf{v}} \mathbf{q} \frac{\bar{n}_{\mathbf{v}}(\bar{n}_{\mathbf{v}} + 1)}{\tau_{\mathbf{v}}^{\mathcal{N}}} \left(\frac{\hbar \omega_{\mathbf{v}} v_{\mathbf{v}} \tau_{\mathbf{v}}}{T} + \frac{\mathbf{q} \cdot \mathbf{V}^{\text{drift}}}{\nabla T} \left(1 - \frac{\tau_{\mathbf{v}}}{\tau_{\mathbf{v}}^{\mathcal{N}}} \right) \right). \quad (4.16)$$

Rearranging terms, we can extract the value of the drift velocity:

$$\mathbf{V}^{\text{drift}} = -\mu \nabla T \quad (4.17)$$

$$\mu = \frac{1}{T} \frac{\sum_{\mathbf{v}} \bar{n}_{\mathbf{v}}(\bar{n}_{\mathbf{v}} + 1) q_{\parallel} v_{\mathbf{v}} \hbar \omega_{\mathbf{v}} \frac{\tau_{\mathbf{v}}}{\tau_{\mathbf{v}}^{\mathcal{N}}}}{\sum_{\mathbf{v}} \bar{n}_{\mathbf{v}}(\bar{n}_{\mathbf{v}} + 1) q_{\parallel}^2 \frac{1}{\tau_{\mathbf{v}}^{\mathcal{N}}} \left(1 - \frac{\tau_{\mathbf{v}}}{\tau_{\mathbf{v}}^{\mathcal{N}}} \right)},$$

where q_{\parallel} is the component of the phonon wavevector (remember that $\mathbf{v} = (\mathbf{q}, s)$) parallel to the gradient of temperature, and μ is a phonon mobility giving the constant of proportionality between the drifting velocity and the temperature gradient.

The Boltzmann-Callaway equation is therefore solved and using f and V^{drift} in the expression for thermal conductivity we find:

$$k = \frac{1}{k_B T^2 \mathcal{V}} \sum_{\mathbf{v}} \bar{n}_{\mathbf{v}}(\bar{n}_{\mathbf{v}} + 1) (\hbar \omega_{\mathbf{v}})^2 v_{\mathbf{v}}^2 \tau_{\mathbf{v}} \quad (4.18)$$

$$+ \frac{1}{k_B T^2 \mathcal{V}} \left(\sum_{\mathbf{v}} \bar{n}_{\mathbf{v}}(\bar{n}_{\mathbf{v}} + 1) \hbar \omega_{\mathbf{v}} v_{\mathbf{v}} q_{\parallel} \frac{\tau_{\mathbf{v}}}{\tau_{\mathbf{v}}^{\mathcal{N}}} \right)^2 \Big/ \left(\sum_{\mathbf{v}} \bar{n}_{\mathbf{v}}(\bar{n}_{\mathbf{v}} + 1) (q_{\parallel})^2 \frac{\tau_{\mathbf{v}}}{\tau_{\mathbf{v}}^{\mathcal{N}} \tau_{\mathbf{v}}^{\mathcal{R}}} \right).$$

The Callaway expression for the thermal conductivity contains in the first term the SMA approximation. In addition to it, the new treatment of normal processes introduces a correcting term. In the chapters of applications on 2D materials, we will verify how much this expression improves the SMA and how it compares with exact solutions of the Boltzmann equation.

A number of ideas that are present in the Callaway model led us to find some of the original results of this Thesis. The Callaway approximation improves the SMA, which describes a single relaxation model of the phonon gas towards equilibrium, and essentially replaces it with a two-fluid model in which the phonon gas can relax either to the drifting or to the Bose-Einstein distributions. The time scale of the two relaxations is given by the two relaxation times $\tau^{\mathcal{N}}$ and $\tau^{\mathcal{R}}$. Although the Callaway model is not exact, as it still relies on approximations to the scattering operator, it is actually suggesting that a single relaxation time per phonon mode is not enough to describe the exact transport. This idea is actually what led us to suppose that, in materials where the Callaway approximation gives a huge improvement over the SMA, second sound might exist. In fact second sound, especially in the original formulation for superfluid

Helium, is intimately related with the presence of a two fluid system [90]: for the case of liquid Helium, second sound is the oscillation between the normal and superfluid component of the excitations; in our case, we saw an analogy with the normal and Umklapp component of the phonon gas. Therefore, we will investigate in greater detail the issue of second sound in 2D materials in Chapter 7. Moreover, the idea of interpreting the relaxation of a phonon with two different relaxation times goes in the right direction for describing thermal transport exactly. In Section 4.5 we will show that rather than using 2 relaxation times, the exact solution can be interpreted in terms of N different relaxation times for each phonons.

4.3 Iterative method

The iterative method has been the first to exactly solve the linear Boltzmann equation, pioneered by Omini and Sparavigna [108, 109, 110] in the context of a Lennard–Jones crystal and later applied for the first time with ab-initio scattering rates by Broido et al. [44]. At the moment, the method is the most common exact solver of the phonon Boltzmann equation.

Using the matrix notation, the iterative method can be formulated in a very intuitive way. We start with an initial guess of the phonon deviation distribution, typically this is the SMA solution $f_0 = (A^{\text{out}})^{-1}b$. Next, we iteratively improve the solution, computing the solution at the i -th step of the iteration procedure as:

$$f_i = \sum_{j=0}^i \left(- (A^{\text{out}})^{-1} A^{\text{in}} \right)^j (A^{\text{out}})^{-1} b. \quad (4.19)$$

The method therefore is a geometric series of the matrix $(- (A^{\text{out}})^{-1} A^{\text{in}})$. Using the properties of a geometric series it is easy to prove that - within its domain of convergence - the series tends to the correct solution of the Boltzmann equation. Note that in this method we make use of the complete scattering operator, both diagonal and off-diagonal terms, and therefore it can solve the complete linear Boltzmann equation exactly.

The algorithm has the great merit of being the first method applied to find the exact solution of the Boltzmann equation. However, it should be pointed out that it only converges as a geometric series, i.e. if and only if all the eigenvalues of the matrix $(- (A^{\text{out}})^{-1} A^{\text{in}})$ are smaller than one in absolute value. Quite generally we can state that if the out-of-diagonal elements of the matrix are not sufficiently small, the eigenvalues of the iterative matrix will not be small and the method will not converge. The domain of convergence of this equation has not been studied in great detail. In preliminary tests on 2D materials, we found that the algorithm was not able to reach a converged value after several hundreds of iterations, so that the exploration of other methods was necessary. In fact, we will show in Section 8.3 by diagonalising the iterative matrix that this method diverges for graphene at room temperature. Additionally, since we will see that in many 2D materials the out-of-diagonal scattering matrix elements are non-negligible, the applicability of the iterative method should be verified case-by-case.

4.4 Variational method

In Section 3.3 we introduced a variational thermal conductivity functional:

$$k[f] = \frac{1}{\mathcal{V}} (2 \langle b|f \rangle - \langle f|A|f \rangle). \quad (4.20)$$

The thermal conductivity can be found as the maximal value of such functional:

$$k = \max_{\{f\}} \frac{1}{\mathcal{V}} (2 \langle b|f \rangle - \langle f|A|f \rangle). \quad (4.21)$$

Therefore, there exists an entire family of methods that try to find the optimal value of the phonon deviation f , that maximises the thermal conductivity functional.

In the past (for example the approach of Ref. [71]) the problem of functional optimization was most often approached by writing the distribution function f with a trial function dependent on some variational parameters. The solution was then obtained tuning the variational parameters to optimize the thermal conductivity. This approach greatly improves the results of the SMA, but is not guaranteed to obtain the exact solution of the Boltzmann equation, and the accuracy of the final result greatly depends on the choice of the trial function. Moreover, it is not desirable to use a trial function too complex, as the computational efficiency is penalised by the addition of more variational parameters.

Very recently Fugallo and coworkers [61] applied a conjugate gradient method that maximises the thermal conductivity functional. Since the matrix A is semi-positive definite (see Section 3.3) it can be shown that there exists a maximum of the thermal conductivity functional and that it is unique. Therefore, the conjugate gradient algorithm is capable of improving the thermal conductivity in a systematic way, reaching the only global maximum of the functional and therefore finding the correct distribution function f , without the usage of any variational parameter. Moreover, the conjugate gradient always converges to the correct solution without limitations on the values of the matrix and therefore does not have convergence issues like the previous iterative method.

The conjugate gradient algorithm is a standard method that can be found in several books (for example Ref. [119]). The pseudo-code for the conjugate gradient algorithm is shown in Alg. 1: The cost of the algorithm is comparable to the iterative method, as each step of the conjugate gradient method requires the multiplication of the scattering matrix A with a vector, the most computationally expensive part.

In its pure form, the algorithm converges slowly to the solution [61]. For this reason, it is convenient to take advantage of the diagonally dominant character of the scattering matrix and precondition the functional. The terms of the Boltzmann equation are scaled by the vector

Algorithm 1 Conjugate gradient

initialise

$$f_0 = (A^{\text{out}})^{-1} b = f^{\text{SMA}}$$

$$r_0 = b - A f_0$$

$$p_0 = r_0$$

$$i = 0$$

loop

$$\alpha_i = \frac{r_i r_i}{p_i A p_i}$$

$$f_{i+1} = f_i + \alpha_i p_i$$

if $k[f_{i+1}] \approx k[f_i]$ **then return**

$$r_{i+1} = r_i - \alpha_i A p_i$$

$$\beta_i = \frac{r_{i+1} r_{i+1}}{r_i r_i}$$

$$p_{i+1} = r_{i+1} + \beta_i p_i$$

$$i = i + 1$$

of the diagonal part of the scattering matrix A^{out} in the following way:

$$\tilde{f} = \sqrt{A^{\text{out}}} f \tag{4.22}$$

$$\tilde{b} = \frac{1}{\sqrt{A^{\text{out}}}} b$$

$$\tilde{A} = \frac{1}{\sqrt{A^{\text{out}}}} A \frac{1}{\sqrt{A^{\text{out}}}}$$

$$\tilde{\mathcal{F}}[\tilde{f}] = \frac{1}{2} \tilde{f} \tilde{A} \tilde{f} - \tilde{b} \tilde{f} = \mathcal{F}[f].$$

Typically, we found that the preconditioned conjugate gradient method is able to converge in about 20 iterations for the 2D materials studied in this Thesis.

In summary, the preconditioned conjugate gradient is an efficient tool for finding the solution of the Boltzmann equation. It does not have limitations on its convergence properties, it always obtains the exact solution and converges in few iterations. In our opinion, there is one drawback this method shares with the iterative method: neither of them is capable of interpreting the transport in terms of microscopic relaxation times or mean free paths. Both tools (within their convergence domain) are capable of obtaining the exact phonon deviation distribution f and they both give a total value of thermal conductivity, but we did not find a simple way to derive relaxation times or mean free paths from the distribution f . This is in contrast with many other works (see for example Ref. [94]), which claim the opposite. The argument is that the thermal conductivity (Eq. 3.24) can be cast in a kinetic gas expression like Eq. 4.7 if one defines a relaxation time $\tau_v = \frac{f_v}{v_v \hbar \omega_v}$ or a mean free path $\Lambda_v = \frac{f_v}{\hbar \omega_v}$. However, the definition of such quantities by the simple argument of analogy leaves space for objections. For example, it is not evident how such τ_v can be associated with a decay by a factor $1/e$ of the phonon excitation. Also, the relaxation time can diverge when the phonon v has zero velocity, yet it can travel for a finite mean free path. Eventually, the mean free path can have both negative and positive sign, so that it cannot be interpreted as an average distance between

scattering events. As a novel result of this Thesis, we will overcome these limitations in the next section providing a rigorous definition of exact relaxation times and mean free paths.

4.5 Relaxons

In a last attempt of finding the solution of the Boltzmann equation, we will study in this section the diagonalisation of the scattering operator. The method has been used by very few authors in the past. As far as we know, Guyer and Krumhansl [69] have tried for the first time to write the solution of the Boltzmann equation in terms of the eigenvectors of the normal scattering operator. Hardy [74] extended this idea diagonalising the complete scattering matrix during a study of second sound. These works only wrote the theory but did not attempt an explicit diagonalisation of the matrix and only more recently Chaput computed the eigenvalue spectrum for studying the thermal response to a time dependent temperature perturbation [52]. Beside these authors and their coworkers, we couldn't find other works who diagonalised the scattering matrix. In fact, the method is seemingly unappealing if one simply desires to get the static thermal conductivity: for this purpose, the iterative or the variational methods are much more computationally feasible than an explicit diagonalisation.

Despite the computational cost associated to this method, we will see, as a novel result of this Thesis [51], that the diagonalisation provides an interpretation of thermal transport, which is formally similar to the SMA, but takes correctly into account all the phonon correlations due to scattering.

Let us start by reconsidering the linear Boltzmann equation:

$$\frac{\partial n_{\mathbf{v}}(\mathbf{r}, t)}{\partial t} + \mathbf{v}_{\mathbf{v}} \cdot \nabla n_{\mathbf{v}}(\mathbf{r}, t) = - \sum_{\mathbf{v}'} \Omega_{\mathbf{v}\mathbf{v}'} n_{\mathbf{v}'}(\mathbf{r}, t). \quad (4.23)$$

We first note that it is not possible to define a phonon relaxation time. In analogy with the procedure outlined for the explanation of the SMA relaxation time, we study a homogeneous system at thermal equilibrium, in which we excite a phonon at time t_0 . The system is governed by the equation:

$$\frac{\partial n_{\mathbf{v}}(\mathbf{r}, t)}{\partial t} = - \sum_{\mathbf{v}'} \Omega_{\mathbf{v}\mathbf{v}'} n_{\mathbf{v}'}(\mathbf{r}, t). \quad (4.24)$$

In this more general situation, the solution for the phonon relaxation does not have anymore a simple exponential form $e^{-t/\tau}$. The out-of-diagonal matrix elements are responsible for a coupling between phonons that prevents the definition of a phonon relaxation time.

It is still possible to define a relaxation time. To proceed, we first note that the drifting operator, i.e. the left side of Eq. 4.23 is diagonal in \mathbf{v} but the scattering operator is not. Since the information about the time scale of the relaxation is contained in the latter, we extract it by diagonalising the scattering operator. First, we symmetrise the Boltzmann transport equation

[73, 88, 74, 52] with the transformations:

$$\tilde{\Omega}_{\nu\nu'} = \Omega_{\nu\nu'} \sqrt{\frac{\tilde{n}_{\nu'}(\tilde{n}_{\nu'} + 1)}{\tilde{n}_{\nu}(\tilde{n}_{\nu} + 1)}}, \quad (4.25)$$

$$\tilde{n}_{\nu} = (\tilde{n}_{\nu}(\tilde{n}_{\nu} + 1))^{-\frac{1}{2}} n_{\nu}, \quad (4.26)$$

so that $\tilde{\Omega}_{\nu,\nu'} = \tilde{\Omega}_{\nu',\nu}$. The transformation leaves the Boltzmann equation untouched, but now $\tilde{\Omega}$ posses the same properties of the matrix A : it is real, symmetric and semi-positive definite [73, 74]. Now, we diagonalise the scattering matrix $\tilde{\Omega}$:

$$\sum_{\nu'} \tilde{\Omega}_{\nu\nu'} \theta_{\nu'}^{\alpha} = \frac{1}{\tau_{\alpha}} \theta_{\nu}^{\alpha}. \quad (4.27)$$

The scalar product between two eigenvectors is defined by $(\theta^{\alpha}, \theta^{\beta}) = \sum_{\nu} \theta_{\nu}^{\alpha} \theta_{\nu}^{\beta}$. Since the matrix is semi-positive definite, it follows that $\frac{1}{\tau_{\alpha}} \geq 0, \forall \alpha$. Moreover, its eigenvalues have a well defined parity and they can be either even or odd: $\theta_{\nu}^{\alpha} = \pm \theta_{-\nu}^{\alpha}$, where $-\nu = (-\mathbf{q}, s)$ [74]. We know very little about the eigenvalue spectrum *a-priori*, however we know that the Bose–Einstein distribution is an eigenvector with zero eigenvalue:

$$\theta_{\nu}^0 = \frac{\sqrt{\tilde{n}_{\nu}(\tilde{n}_{\nu} + 1)} \hbar \omega_{\nu}}{\sqrt{k_B T^2 C}}, \quad (4.28)$$

where $C = \frac{1}{V} \sum_{\nu} C_{\nu}$. The eigenvectors form a complete basis for any phonon distribution [74] and therefore we can write the phonon distribution n_{ν} as a linear combination of eigenvectors:

$$\tilde{n}_{\nu}(\mathbf{x}, t) = \sum_{\alpha} f_{\alpha}(\mathbf{x}, t) \theta_{\nu}^{\alpha}. \quad (4.29)$$

In the basis of the eigenvectors, the Boltzmann equation becomes:

$$\frac{\partial f_{\alpha}(\mathbf{x}, t)}{\partial t} + \sum_{\beta} \mathbf{V}_{\alpha\beta} \cdot \nabla f_{\beta}(\mathbf{x}, t) = -\frac{1}{\tau_{\alpha}} f_{\alpha}(\mathbf{x}, t), \quad (4.30)$$

where $\mathbf{V}_{\alpha\beta} = \sum_{\nu} \theta_{\nu}^{\alpha} \mathbf{v}_{\nu} \theta_{\nu}^{\beta}$. In contrast with the standard formulation of the Boltzmann equation, here the scattering operator is diagonal whereas the non-diagonal term now is the diffusion operator. It is also worth noting that the formalism is equivalent to the SMA in the special case of diagonal $\tilde{\Omega}$: α coincides with ν , $\tau = \tau^{\text{SMA}}$ and $\theta_{\nu'}^{\alpha} = \delta_{\nu,\nu'}$.

In this Thesis, we interpret the eigenvectors θ^{α} as a set of collective excitations which we call *relaxons*, and whose occupation numbers are given by f_{α} . We assigned this name due to the relaxation properties of this collective excitation. If we consider an homogeneous system ($\nabla f^{\beta} = 0$) in which only one relaxon is excited at an initial time, the system relaxes back to equilibrium as $f_{\alpha}(t) = f_{\alpha}(t_0) e^{-t/\tau_{\alpha}}$. Therefore, relaxons are characterised by a well defined relaxation time τ_{α} . The fact that all lifetimes are positive guarantees that thermal equilibrium

Chapter 4. Solutions of the Boltzmann transport equation

is reached at infinite time. Only the Bose–Einstein state that has a zero lifetime is stationary, i.e. it does not evolve in time and is the only surviving state at infinite times. Since we solved the time evolution of the system analytically, we can use Eq. 4.29 to prove that phonons do not have a relaxation time. Upon excitation, the phonon ν relaxes back to equilibrium as a linear combination of relaxon relaxations: $n_\nu(t) = \sum_\alpha f_\alpha(t_0) \theta_\nu^\alpha e^{-t/\tau_\alpha}$. Therefore, the phonon relaxes back to equilibrium according to N different relaxation times, where N is the number of phonons present in the system (i.e. the size of the scattering matrix).

The velocities appear in Eq. 4.30 as a matrix $V_{\alpha\beta}$ coupling different relaxons. This was to be expected to some extent since the diffusion operator is diagonal in the phonon basis and the change of representation introduces off-diagonal elements. Therefore we cannot unambiguously identify a relaxon velocity in all circumstances. However, the equations are substantially simplified in an homogeneous system where we can approximate $\nabla n_\nu \approx \frac{\partial \bar{n}_\nu}{\partial T} \nabla T$ for small temperature gradients (see Eq. 3.17). In this case, the homogeneous Boltzmann equation in the relaxon basis writes as:

$$\frac{\partial f_\alpha(t)}{\partial t} + \sqrt{\frac{C}{k_B T^2}} \nabla T(t) \cdot \mathbf{V}_\alpha = -\frac{f_\alpha(t)}{\tau_\alpha}, \quad (4.31)$$

where $\mathbf{V}_\alpha = V_{\alpha,\beta=0}$. Both the drifting and the collision operator are diagonal and this time we can identify a relaxon velocity \mathbf{V}_α . Therefore, only if the system is not homogeneous, as when surfaces are present (Ch. 5), it is not straightforward to define a relaxon velocity.

Let's simplify further and consider the steady state in presence of a temperature gradient $\nabla T(t) = \nabla T$. Now we can set $\frac{\partial f_\alpha}{\partial t} = 0$ in Eq. 4.31. We look for solutions that are linear in the gradient of temperature $f_\alpha = \sum_i f_\alpha^i \nabla_i T$, where i is a cartesian direction. The relaxon Boltzmann equation reduces to:

$$\sqrt{\frac{C}{k_B T^2}} V_\alpha^i = -\frac{f_\alpha^i}{\tau_\alpha}, \quad (4.32)$$

which can easily be inverted to obtain f . Using the relation between phonons and relaxon occupation numbers $n_\nu = \sqrt{\bar{n}_\nu(\bar{n}_\nu + 1)} \sum_{i\alpha} \nabla_i T f_\alpha^i \theta_\nu^\alpha$, we can compute the thermal conductivity:

$$\begin{aligned} k^{ij} &= \frac{1}{\nabla_i T} \sum_\nu \hbar \omega_\nu v_\nu^j n_\nu = \sum_\alpha f_\alpha^i \sqrt{k_B T^2 C} V_\alpha^j \\ &= \sum_\alpha C V_\alpha^i V_\alpha^j \tau_\alpha = \sum_\alpha C V_\alpha^i \Lambda_\alpha^j, \end{aligned} \quad (4.33)$$

where we introduced the relaxon mean free path Λ_α^j , and the summation is done only over odd relaxons (for even relaxons $V_\alpha^i = 0$). This is perhaps the key result of this method. The thermal transport without any approximation on the scattering operator can be interpreted with the kinetic theory of gases. The exact thermal conductivity is described by a kinetic theory of the relaxon gas, where each relaxon has a lifetime τ_α travels at an average velocity V_α and carries the thermal energy C for an average distance Λ_α before thermalisation lets the relaxon

population decay by a factor $1/e$. Therefore we can determine the time, velocity and length scale of thermal transport. No other work has given, to our knowledge, a similar interpretation of thermal conductivity and we will apply it for the first time to graphene in Chapter 8 with interesting findings.

4.6 Technical details

The numerical solutions of most theoretical models need to resort to some approximations, and the methods for the Boltzmann equation make no exception.

First of all, the summation on the Brillouin-zone wavevectors \mathbf{q} for an infinite crystal should actually be a continuous integration. Since infinite summations are not possible on computers, the \mathbf{q} -points summations need to be limited to a uniformly distributed Monkhorst-Pack mesh. One should therefore choose a sufficiently dense grid of points and increase it until the error has decreased to a sufficiently small value.

The \mathbf{q} -points are not the only computational parameter appearing in the Boltzmann equation. The scattering rates contain Dirac- δ expressions that ensure the conservation of energy and crystal momentum. The conservation of momentum can be exactly enforced if the grid of \mathbf{q} -points is centered on the Γ point of the Brillouin zone (in this case every summation of \mathbf{q} points is another point of the grid). The conservation of energy instead needs an approximation. In this Thesis, we opted for a simple gaussian approximation of the Dirac- δ :

$$\delta(\hbar\omega) = \frac{1}{\sqrt{\pi}\sigma} e^{-\left(\frac{\hbar\omega}{\sigma}\right)^2}. \quad (4.34)$$

The smearing parameter σ has to be optimized at the same time of the \mathbf{q} -point mesh. The converged value is the one as close as possible to the limit for $\sigma \rightarrow 0$ and $k \rightarrow \infty$.

5 Surface scattering

In the previous chapters we limited the study of the Boltzmann equation to the case of infinite crystals. In this idealised picture we have shown how to compute the intrinsic value of the crystal thermal conductivity. However, all measurements are performed on crystals of finite size and we have to adapt the theory in order to describe these conditions.

Even without diving into a detailed explanation, we can guess empirically how the presence of a surface can impact the thermal conductivity. Within the SMA, the thermal conductivity is roughly proportional to the mean free paths Λ of the phonons:

$$k = \frac{1}{\mathcal{V}} \sum_{\nu} C_{\nu} v_{\nu} \Lambda_{\nu}. \quad (5.1)$$

In an infinite crystal, Λ is exclusively determined by the distance between intrinsic phonon scattering events, like, as we have seen, the 3-phonon interaction and the phonon-isotope scattering. When the sample has a finite size, let's say a characteristic size L , we can expect that the phonon cannot travel for a distance larger than L without hitting the surface. As a first guess, we can think at the surface as a region where the phonon scatters and is brought back to thermal equilibrium. We can therefore expect that the correct value to use for Λ_{ν} is either L or the intrinsic scattering length, whichever of the two scatterings is the most likely to occur.

From this simple analysis, that will soon be corroborated by more quantitative evaluations, we can already guess that the crystal can be approximated as infinite when the characteristic size of the sample is much larger than the mean free path for heat carriers. The surface scattering is therefore of great relevance in some cases. First, at low temperatures when the Umklapp scattering freeze out (or whenever the resistive scatterings are small), the mean free paths grow dramatically. In fact, in the limit of $T \rightarrow 0$, the probability for a phonon-phonon scattering event tends to zero and the mean free paths tend to diverge. The presence of the surface is preventing a divergence of thermal conductivity, since it will limit the largest distance the phonons can travel. Second, also at room temperature the thermal conductivity can be mostly determined by the surface, if the sample is much smaller than the length scale of the mean free path. This in particular is a very important area of contemporary research, since several

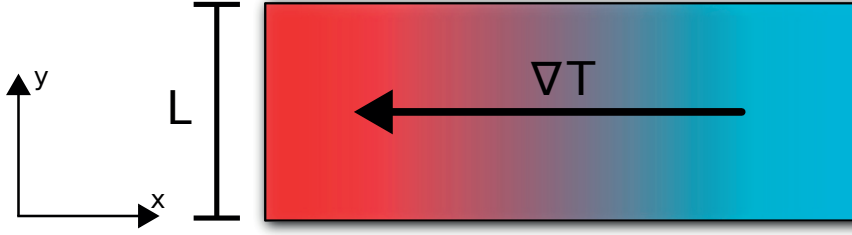


Figure 5.1 – Sketch of the ribbon of a 2D material that will be analysed in this chapter. Note that the direction in which the temperature gradient is applied is infinite. The surface effect will instead be introduced by a finite width of the sample.

applications can take advantage or rely on materials whose size reaches the microscopic (or nano) scale. For example, one of the various strategies to improve the performance of thermoelectrics is to nanostructure the material, so that heat carriers are scattered more efficiently by surfaces and the thermal conductivity is reduced. Also in semiconductor technology, where the size of CPUs keeps shrinking, it is crucial to understand how heat is dissipated through the material.

In this chapter, we will study the heat flow of a two-dimensional ribbon, as shown in Figure 5.1. The direction in which the temperature gradient is applied, labeled as x , is approximated as infinite. There is also a perpendicular direction, indicated by y , in which the ribbon has instead a finite width L . We will study the steady state thermal conductivity of this ribbon and, for simplicity of the discussion, we will use the single-mode relaxation time approximation [77, 48]. In addition, we will investigate the ballistic regime [49, 48], sometimes also called Casimir limit, in which the intrinsic phonon scattering can be neglected and only the surface scattering is considered.

5.1 Definition of the problem

Even when the crystal has a finite size, we can still suppose that in all interior points of the sample there exists a distribution function $n_\nu(\mathbf{r})$, which describes the most probable number of phonon excitations in the state ν at position \mathbf{r} . We can still write the Boltzmann equation as before:

$$\mathbf{v}_\nu \nabla n_\nu(\mathbf{r}) + \sum_{\nu'} \Omega_{\nu\nu'} n_\nu(\mathbf{r}) = 0. \quad (5.2)$$

By using the Boltzmann equation in a crystal of finite size we are making some additional assumptions with respect to the bulk case. As a first hypothesis, we are assuming that the Bloch theorem is a good approximation for the quantum numbers of the lattice vibrations. Strictly speaking, the Bloch theorem does not hold anymore, since we are breaking the perfect periodicity of the crystal with a surface. However, this becomes a concern only when the ribbon is extremely narrow (for example, a few unit cells). In this limiting scenario, the

wavevectors allowed in the direction of finite size will be much less than those possible in the bulk. However, we are interested in a ribbon which has a width of some microns, as this is the size most relevant for applications and in this case the limitation on the wavevector is not a big issue. For example, for the materials studied in this work, we found converged conductivities by sampling the Brillouin zone with about 100×100 points. The largest wavelength that is sampled with this choice of \mathbf{q} -points corresponds to about 25nm, meaning that all wavelengths considered are still allowed in a ribbon of width $\approx 1 \mu\text{m}$. Longer wavelengths have a negligible contribution and we can use the Bloch theorem for our study. Note that if we were to study a much narrower ribbon, one can still study the system accurately by treating it as 1-dimensional. The additional assumption we make, is that the phonon force constants, used to compute velocities and scattering operator, do not depend on the position inside the sample, i.e. the surface does not deform the lattice. To take into account how the phonon properties change as the surface is approached is a formidable task. Therefore, we approximate the scattering properties as constant throughout the interior of the space, and we will parametrise the surface properties by imposing appropriate boundary conditions. This approach can be considered a good approximation for sufficiently large systems, where the surface transport is small compared to the bulk.

The characteristic feature of boundary scattering that makes it so different from other intrinsic events, is that it does not occur uniformly throughout the sample. Therefore, we cannot simply add another rate to the scattering operator. The phonon distribution function in this case depends on the position inside the crystal, mostly affecting the phonons close to the surface than others. For this reason, at variance with the infinite system, we cannot approximate anymore $\nabla n_{\nu}(\mathbf{r}) \approx \frac{\partial n_{\nu}}{\partial T} \nabla T$ and the Boltzmann equation needs to be considered in its more generic form. In order to proceed, let us separate, without loss of generality, the out-of-equilibrium function in two terms:

$$n_{\nu} = \bar{n}_{\nu} + g_{\nu} , \quad (5.3)$$

so that the difference from the equilibrium case is given by g . To make the diffusion term treatable analytically, we suppose that the temperature is constant along the y direction, i.e. temperature changes only along the x direction according to ∇T . In this approximation, the Boltzmann equation becomes:

$$\nabla_x T v_{\nu}^x \frac{\partial \bar{n}_{\nu}}{\partial T} + v_{\nu}^y \cdot \nabla_y g_{\nu}(y) + \sum_{\nu'} \Omega_{\nu\nu'} g_{\nu}(y) = 0 . \quad (5.4)$$

On mathematical ground, Eq. 5.4 is a non-homogeneous linear order differential equation, whose unknown is the vector (with index ν) of functions $g_{\nu}(y)$ as a function of the position along the width of the ribbon y .

The equation can be integrated to obtain $g_{\nu}(y)$, however, to fix the integration constants, we need to impose suitable boundary conditions. Let us consider, for example, a phonon ν which is travelling with a velocity exactly parallel to x , i.e. $v_{\nu}^y=0$ so that the second term

of Eq. 5.4 disappears. Since this phonon will never be able to bounce on the surfaces, the Boltzmann equation simplifies to the bulk case, and the surface does not alter the diffusion of the phonon. Let's instead consider a phonon ν such that its velocity is $v_\nu^y > 0$. This phonon is leaving the surface located at $y = 0$, where it emerged as the result of a previous scattering event. For this phonon mode, the solution $g_\nu(y)$ is different from the bulk case and has a y dependence, thus it needs a boundary condition. The simplest and only boundary condition that we will use in this Thesis, is the so-called Casimir limit. In this approximation, we suppose that the surface is able to absorb phonons and locally thermalise the system. Hence, the phonon ν was at thermal equilibrium when it was emitted by the surface at $y = 0$ that it is leaving. In mathematical terms, we have to impose that $n_\nu(y = 0) = \bar{n}_\nu$ or, in other terms, that $g_\nu(y = 0) = 0$. Conversely, a phonon ν leaving the surface at $y = L$ with a velocity $v_\nu^y < 0$, must have been at thermal equilibrium when it was located at the surface, i.e. $g_\nu(y = L) = 0$.

In a more general case, the surface does not necessarily have to establish the local thermal equilibrium. For example, we can imagine the presence of surface modes that will conduct some heat and cause the phonons to be thermally excited also at the surface. Therefore, the boundary condition should be generalised to $g_\nu(0) = g_\nu(L) = \delta_\nu$. However, the computation of such boundary condition δ_ν is not a trivial task and, since it depends on the microscopic details of the surface, it varies in principles for every sample. As is customary in literature, we simplify the discussion by fixing a value of this boundary condition and we proceed for the rest of this Thesis only with the Casimir limit.

5.2 SMA surface scattering

To proceed and extract a solution to the surface scattering problem, we now restrict the generality of the discussion and adopt the SMA. The Boltzmann equation (Eq. 5.4) is simplified to

$$v_\nu^x \nabla_x T \frac{\partial \bar{n}_\nu}{\partial T} + v_\nu^y \frac{\partial g_\nu(y)}{\partial y} + \frac{g_\nu(y)}{\tau_\nu} = 0. \quad (5.5)$$

The first term is constant in y , so, to outline this we substitute it with a y -independent quantity:

$$R_\nu = -v_\nu^x \nabla_x T \frac{\partial \bar{n}_\nu}{\partial T}. \quad (5.6)$$

In this way, it is more visible that the problem is just a linear order differential equation in y :

$$v_\nu^y \frac{\partial g_\nu(y)}{\partial y} + \frac{g_\nu(y)}{\tau_\nu} = R_\nu. \quad (5.7)$$

If $v_\nu^y = 0$, the problem is analogous to the already known infinite system as mentioned above. Let's then focus on the case $v_\nu^y > 0$ (the results for the case $v_\nu^y < 0$ will be identical, besides a sign). One can verify that the solution of the differential equation, compatible with Casimir's

boundary condition $g_v(0) = 0$, is:

$$g_v(y) = \tau_v R_v [1 - e^{-y/\tau_v v_v^y}]. \quad (5.8)$$

Very often, this result is written as an effective correction to the intrinsic phonon lifetimes. To do this, we note that the Boltzmann equation can be written in a form similar to the homogeneous case:

$$v_v^x \nabla_x T \frac{\partial \bar{n}_v}{\partial T} + \frac{\langle g_v \rangle}{\tau_v^{\text{eff}}} = 0, \quad (5.9)$$

where we averaged the y -dependency of g by integrating over the ribbon's cross section:

$$\langle g_v \rangle = \frac{1}{L} \int g_v(y) dy, \quad (5.10)$$

and we defined an effective phonon lifetime as:

$$\frac{1}{\tau_v^{\text{eff}}} = \frac{1}{\tau_v} + \frac{1}{\tau_v^b}, \quad (5.11)$$

$$\frac{1}{\tau_v^b} = \frac{\int v_v^y \frac{\partial n_v(x, y)}{\partial y} dy}{\int n_v(x, y) dy}, \quad (5.12)$$

For the ribbon geometry we integrate this expression between 0 and L and obtain the boundary correction to the phonon relaxation time:

$$\frac{1}{\tau_v^b} = \frac{v_v^y}{L} \frac{(1 - e^{-\frac{L}{\tau_v v_v^y}})}{1 - \frac{\tau_v v_v^y}{L} (1 - e^{-\frac{L}{\tau_v v_v^y}})}. \quad (5.13)$$

To better understand this result, it is convenient to study the two limits in which the phonon lifetime τ is negligible or dominant with respect to τ^b . In the first case, the resulting effective relaxation time is:

$$\lim_{\tau \rightarrow \infty} \frac{1}{\tau_v^b} = \frac{2v_v^y}{L}. \quad (5.14)$$

In other words, the phonon with velocity v_v^y is only able to travel for a distance $L/2$, the average distance between the walls of the ribbon. This result is also called the ballistic limit: in the limit of no internal scattering events, this is the only scattering event seen by the phonon. In the second case, if the intrinsic phonon scattering is very frequent, we have:

$$\lim_{\tau \rightarrow 0} \frac{1}{\tau_v^b} = \frac{v_v^y}{L}, \quad (5.15)$$

so that the effective size of the ribbon felt by the phonon is twice as much as before. Away from

Chapter 5. Surface scattering

these two limits, the effective length of the ribbon falls at values in between the two extreme situations. The effective phonon mean free path can therefore be found as:

$$\frac{1}{\lambda_v^{\text{eff}}} = \frac{1}{v_v^x} \left(\frac{1}{\tau_v} + \frac{1}{\tau_v^b} \right) = \frac{1}{\lambda_v} + \frac{1}{\lambda_v^b}. \quad (5.16)$$

The complete expression for τ^b gives some overhead in the calculations. However, it is typically found that this result does not differ too much from the simple use of the ballistic relaxation time of Eq. 5.14 in place of τ_v^b [132]. The difference between the two expressions is that with this approximations, one scales down also the relaxation time of phonons with $v_v^y = 0$. If we make this final assumption, the surface scattering can be treated approximately as if there was an additional scattering rate in the Boltzmann equation, of the form:

$$P_{vv'}^{\text{size}} = \frac{\bar{n}_v(\bar{n}_v + 1)v_v^y}{L} \delta_{vv'}. \quad (5.17)$$

This term can be easily added to the intrinsic scattering matrix and the Boltzmann equation can then be solved using the same techniques explained in the previous section.

6 Transport in 2D materials

In this chapter we will present our numerical results on thermal transport of 2D materials, developed using the theory exposed in the first part of this Thesis. First, we will review the failure of the single-mode relaxation time approximation in 2D materials. This fact was first pointed out by Lindsay et al. [97] in a study for graphene and subsequently for boron nitride [96]. We extended the analysis to the intrinsic crystal, since their work always made use of a relaxation time for surface scattering [60]. Moreover, we extended the analysis to a broader range of 2D materials, showing that the failure of the relaxation time approximation is very common for this family of crystals, and is robust to variations in the isotopic scattering and to isotropic strain.

To understand the deficiency of this approximation, we will point out in the course of this chapter some effects that hint at the existence of collective phonon excitations, that will be formalised in Chapter 8 with the analysis on relaxons. In particular, we will note that 2D transport is characterised by unusually high rates of normal scattering events [50]. Since normal scatterings act mainly reshuffling phonon distributions without contributing to thermal resistivity, correlations between phonons arise. As a consequence, thermal transport does not fall into common conditions of ballistic or kinetic-diffusive regimes. Instead, the hydrodynamic regimes of Poiseuille and Ziman, hitherto observed only at cryogenic temperatures, take place at room temperature and above. Due to the similarity of the room temperature transport in 2D with the low temperature conditions of 3D crystals, the Callaway model, originally invented for describing thermal conductivity at cryogenic temperatures, provides a good estimate of thermal conductivity.

To compute the results labeled as *exact* of this and the following chapter, we used the variational approach to the Boltzmann transport equation. The list of the computational parameters used in the simulations for all the various materials is reported in appendix A. For all the results of this chapter, we used isotopic scattering at natural abundances.

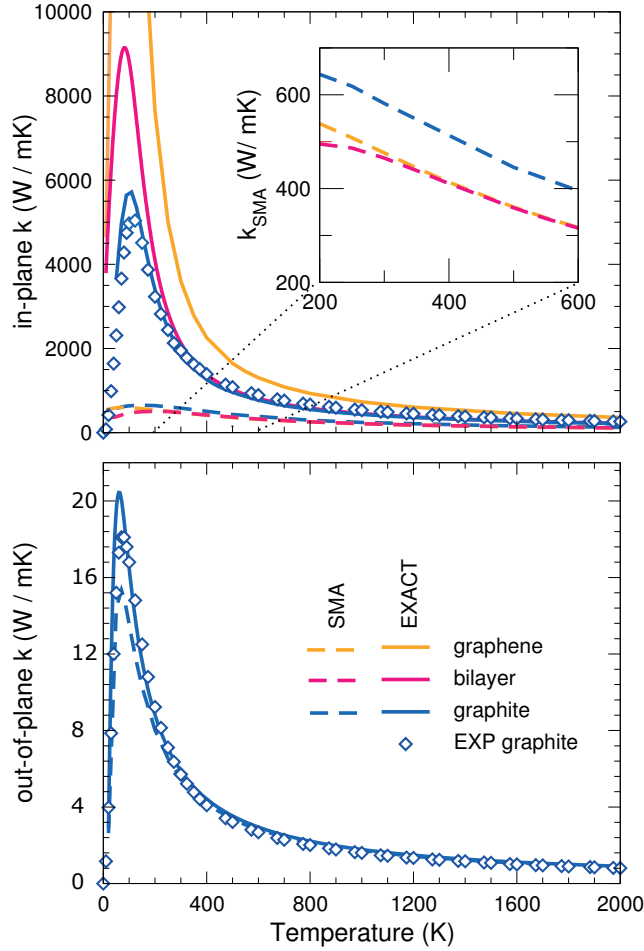


Figure 6.1 – (Top panel) In-plane lattice thermal conductivity in bulk graphite, single- and bilayer graphene of crystalline-domain sizes (see text) $L = 1$ mm and (bottom panel) out-of-plane thermal conductivity of graphite with $L = 0.3$ μm . The data (EXP) of graphite are taken from Ref. [78], which were obtained by a compilation and analysis of several research papers with a widely accepted extrapolation above 300 K, a posteriori shown to be accurate by the present calculations. This extrapolation regime is highlighted by the use of filled diamonds. Solid lines are used for the exact solutions while dashed lines for the single-mode approximation (SMA) solutions. (Inset) Zoomed SMA results for the range $T = 200$ – 600 K, in which in-plane thermal conductivity is qualitatively wrong; graphite conductivity is found to be higher than single- and bilayer graphene.

6.1 Failure of the relaxation time approximation

Thermal conductivity of 2D materials has been object of investigations only since a few years and there are many debatable results. For example, there is no consensus on the thermal conductivity of graphene (see Ref. [36] for a collection of different estimates, spanning from 600 to 4000 $\text{Wm}^{-1}\text{K}^{-1}$). For this reason, it is convenient to start our investigation with graphite, the 3D counterpart of graphene, which is instead a better characterised material. In order to compare measurements with our simulation estimates, it is necessary to include the presence of grain boundaries. It can be shown that, within the SMA, the scattering of phonons on grain boundaries [83] is described in the same way of the effective scattering rate for surfaces presented in Chapter 5.2. In this case however, the length L entering the relaxation time is not anymore the width of the sample perpendicular to the temperature gradient; instead L now is the average grain size. The presence of this scattering term is necessary in particular to describe the low temperature thermal conductivity: in absence of surface scattering the phonon-phonon scatterings freeze out and the thermal conductivity diverges, instead the extrinsic scattering (a surface or a grain) renormalizes the thermal conductivity to finite values. For graphite, we chose a value of $L = 1\text{mm}$ for in-plane transport and $L = 0.3\ \mu\text{m}$ for transport in the out-of-plane direction, chosen as a characteristic distance between stacking faults in carbon planes [60].

In Figure 6.1 we report our estimates of graphite thermal conductivity and compare it with high-precision measurements on perfect crystals of large sizes [78]. The comparison shows a remarkable agreement between measurements and the results of our simulations. However, if the SMA is used, we find a severe underestimation by an order of magnitude for the in-plane conductivity, while keeping a good agreement with experiments for the out-of-plane conductivity. The proper agreement with experiments is realised only when considering the exact solution of the Boltzmann equation. As mentioned above, the inadequacy of the SMA was found also in a recent first-principles work on graphene [99] and in single and multilayer graphene described with an empirical potential [97, 98, 122, 121]. In addition, we have shown [60] that such limitation is not restricted to 2D materials and can be found also at room temperature in 3D layered systems.

Graphene has a much higher thermal conductivity with respect to graphite (top panel of Figure 6.1), as the experimental evidence suggests [36], and the bilayer is intermediate between the two extreme cases. We note also that the increase in thermal conductivity upon reduction of the material thickness cannot be reproduced by the SMA. In fact, as seen for graphite, the values of thermal conductivity are underestimated for the 2D materials. Moreover, the qualitative trends are incorrectly reproduced by the SMA, as it would predict the smallest values for graphene and the highest for graphite, quite the opposite of the exact result.

In the recent years there has been an active debate about the possible divergence of thermal conductivity in two dimensional materials ([107, 93, 131, 57, 97, 104, 41] to name a few), and recently also in an experimental study of graphene [130]. Although we report indeed very high

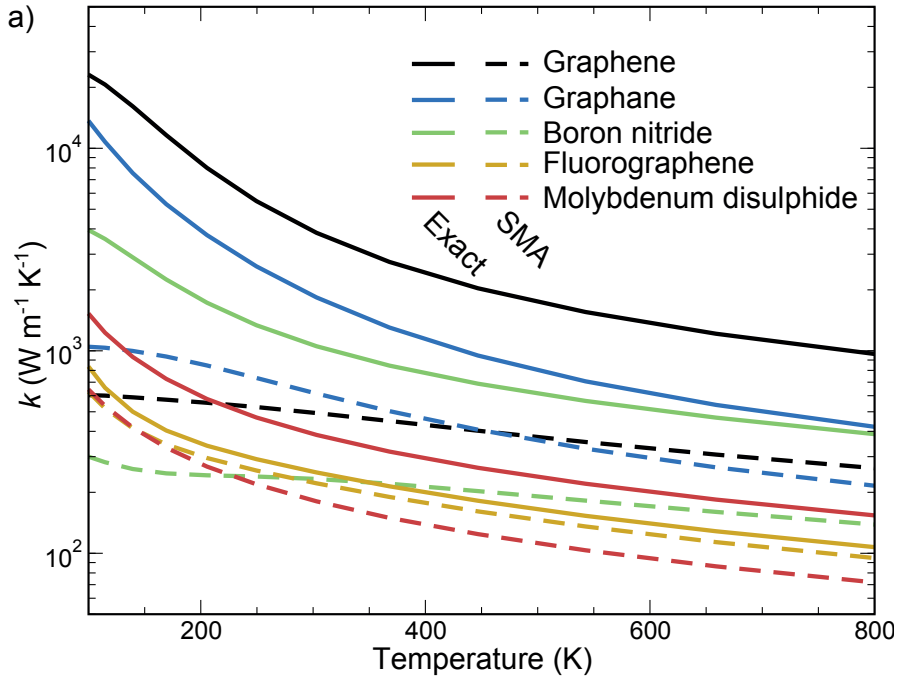


Figure 6.2 – Ab-initio estimates of the thermal conductivity k as a function of temperature for infinite suspended sheets, at natural isotopic abundances. The single-mode relaxation time approximation (SMA) is tested against the exact solution of the first-principles Boltzmann equation.

values of thermal conductivity (and we will find very large mean free paths in Section 7.1), we did not find such divergence and instead the thermal conductivity of an infinite sample at finite temperature converges to a finite value. We can thus provide the highest theoretical limit of the lattice thermal conductivity of graphene, that would be reached in a perfect infinite crystal where no grains or surfaces limit the mean free path. At room temperature the highest predicted thermal conductivity has the value of $3600 \text{ W m}^{-1} \text{ K}^{-1}$ for naturally-occurring graphene and $4300 \text{ W m}^{-1} \text{ K}^{-1}$ for the isotopically pure case. For comparison, these values are of 2200 and $2500 \text{ W m}^{-1} \text{ K}^{-1}$ for a bilayer, and 2000 and $2200 \text{ W m}^{-1} \text{ K}^{-1}$ for graphite.

The failure of the relaxation time approximation is not limited to carbon-based crystals. In Figure 6.2 we extend the study to a larger set of 2D materials, including graphane, boron nitride, fluorographene and molybdenum disulphide, and in Figure 6.3 we test it for some common 2D transition metal dichalcogenides: MoS_2 , MoSe_2 , WS_2 and WSe_2 . For both pictures, we show the intrinsic thermal conductivity, i.e. without including surface scattering. In all cases, the differences between the SMA and exact solutions cannot be neglected, and sometimes, like for example graphene and graphane, the SMA underestimates the thermal conductivity by an order of magnitude at room temperature, the difference growing larger at lower temperatures. Similarly with graphitic materials, the SMA changes even qualitative trends of thermal conductivity, for example predicting incorrectly the thermal conductivity of MoS_2 to be smaller than fluorographene. Therefore, the SMA is not capable of describing

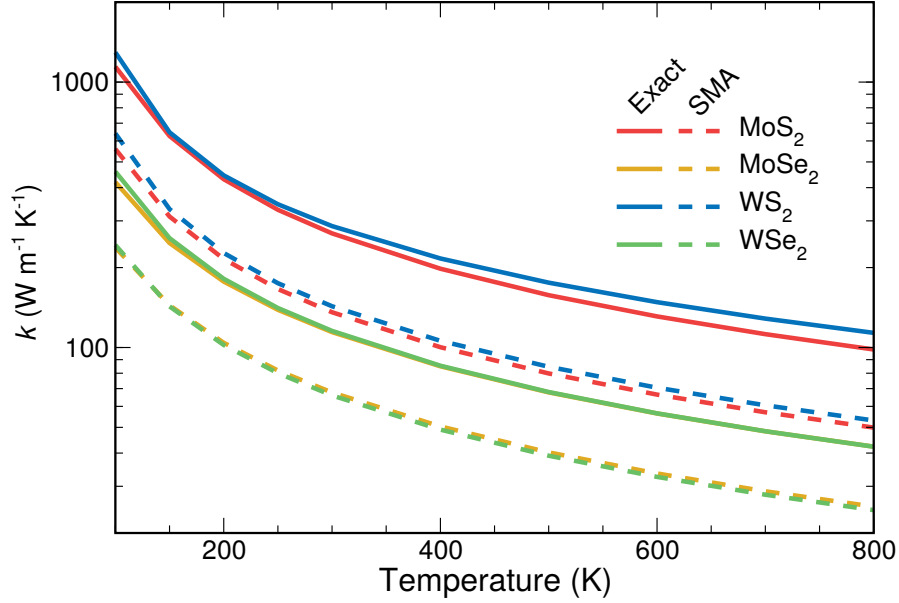


Figure 6.3 – Ab-initio estimates of the thermal conductivity k as a function of temperature for infinite suspended sheets of some transition metal dichalcogenides, at natural isotopic abundances. The single-mode relaxation time approximation (SMA) is tested against the exact solution of the first-principles Boltzmann equation.

neither quantitatively nor qualitatively the thermal conductivity of 2D materials and, as seen for graphite, this can be extended to layered materials as well.

It is also interesting to note that the SMA also alters the effect of strain on thermal conductivity. This topic has been object of debate, due to the presence of contradictory results. Some have predicted a divergence of thermal conductivity in presence of strain that casts doubts on the definition of thermal conductivity itself [43, 32], while others found a finite and sometimes even decreasing thermal conductivity [100, 33, 95, 99]. In Figure 6.4, we see that the exact values of thermal conductivity predict a weak change with applied isotropic in-plane strain. Also, this change does not show a strong size dependence and for three particular cases studied in detail ($L=5\ \mu\text{m}$, $100\ \mu\text{m}$, ∞) the ratio between the strained and unstrained sample is always close to 1 for all the temperatures considered here, changes being typically within 10%. Instead, the SMA provides once again a qualitatively different description and predicts a large increase of thermal conductivity with respect to strain, even diverging for infinite sizes in the limit of zero temperature. In the SMA, the response to strain is strongly dependent on size and temperature, and a strain of 4% leads to a change in k typically larger than 200%. We notice also that the discrepancy between the SMA and the exact solutions increases with L , and persists even in the limit of high temperatures, where the SMA would typically be considered reliable. Therefore, our simulation of an infinite sample contradicts the divergences claimed by Ref. [43] and the simulation at large strains is in contrast with the divergence found in Ref. [32], indicating instead a small effect.

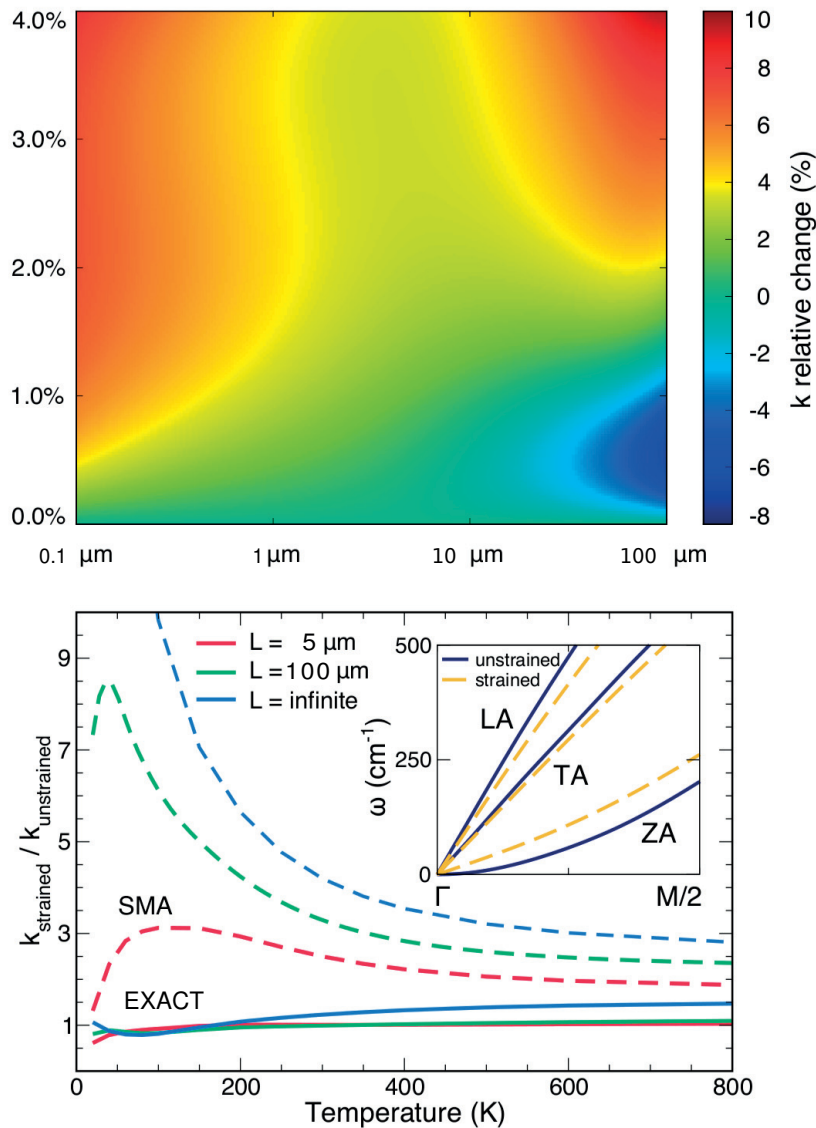


Figure 6.4 – (Top panel) Thermal conductivity percentage variation (%) as a function of strain distribution and grain-size length for the exact solution of the Boltzmann equation. The reference value is the unstrained value of thermal conductivity at various sizes, which are, for example, 356, 646, 831, and 1037 W/mK for sizes L of 0.1, 1, 10, and 100 μm , respectively. (Bottom panel) Ratio between strained (4%) and unstrained cases in the exact solution of the Boltzmann equation and in the SMA for three different crystalline-domain sizes $L = 5 \mu\text{m}$, 100 μm , and ∞ . (Inset) Acoustic phonon dispersion between Γ and $M/2$ for the two different strain limits.

When introducing the SMA in Section 4.1, we pointed out that the SMA neglects the out-of-diagonal elements of the scattering matrix, which are responsible for (1) introducing couplings between phonon modes and (2) describing the repopulation of phonons due to scattering. The SMA, which uses only the diagonal terms, neglects the couplings between phonons and neglects completely the repopulation of phonons. Therefore, collective aspects of the thermal excitations are completely neglected, for the sake of having a simple solution of the Boltzmann equation. The deficiency of the SMA in 2D materials highlights how the description of thermal transport in terms of single-phonon properties is not sufficient, and it is necessary to take into account also the collective aspects of the thermal excitations.

6.2 Phonon transport regimes

In order to make further progress and gain insights on the collective nature of the phonon excitations, it is instructive to inspect the scattering rates for the different processes involved: 3-phonon processes - divided into normal (\mathcal{N}) and Umklapp (\mathcal{U}) events - and isotopic scattering (\mathcal{I}). We show in Figure 6.5 the average linewidths for these processes, defined as

$$\langle \Gamma^i \rangle = \left\langle \frac{2\pi}{\tau^i} \right\rangle = \frac{\sum_{\nu} C_{\nu} 2\pi / \tau_{\nu}^i}{\sum_{\nu} C_{\nu}}, \quad (6.1)$$

where i labels either \mathcal{N} , \mathcal{U} or \mathcal{I} processes and $C_{\nu} = \bar{n}_{\nu}(\bar{n}_{\nu} + 1) \frac{(\hbar\omega_{\nu})^2}{k_B T^2}$ is the specific heat of the phonon mode ν . Conventionally, it is expected that \mathcal{N} events become dominant only at very low temperatures, when \mathcal{U} processes freeze out [132], and even then only provided that \mathcal{I} rates or other extrinsic sources of scattering are negligible. Quite surprisingly, it is seen here that not only \mathcal{N} processes are very relevant, as argued in Ref. [97, 112], but that they represent the dominant scattering mechanisms in these 2D materials at any temperature (with the exception of natural-abundance molybdenum disulphide and boron nitride, where \mathcal{I} is comparable to \mathcal{N} due to the large isotopic disorder of molybdenum and boron). Therefore, the phonon gas in graphene and 2D materials has analogies with an ideal gas of molecules, which conserves both energy and momentum in collisions: for this reason, phonons under these particular regimes are said to be in hydrodynamic regimes.

The predominance of normal scattering processes identifies the regime(s) under which the SMA does not hold anymore and the collective aspects of the phonon dynamics must be considered. In fact, we discussed in Chapter 4 that normal scattering events, which alone would give an infinite thermal conductivity, are poorly described by the SMA, that overestimates their contribution to thermal resistivity. We nevertheless underscore that, even if the momentum-conserving \mathcal{N} processes tend not to dissipate heat-currents, they still affect the total thermal conductivity by altering the out-of-equilibrium phonon distribution. Last, we highlight that the failure of the SMA in these conditions is a rather conceptual one, since it's the assumption that heat-flux is dissipated at every scattering event that becomes invalid. Instead, given that most processes are normal, heat-flux is just being shuttled between phonon modes.

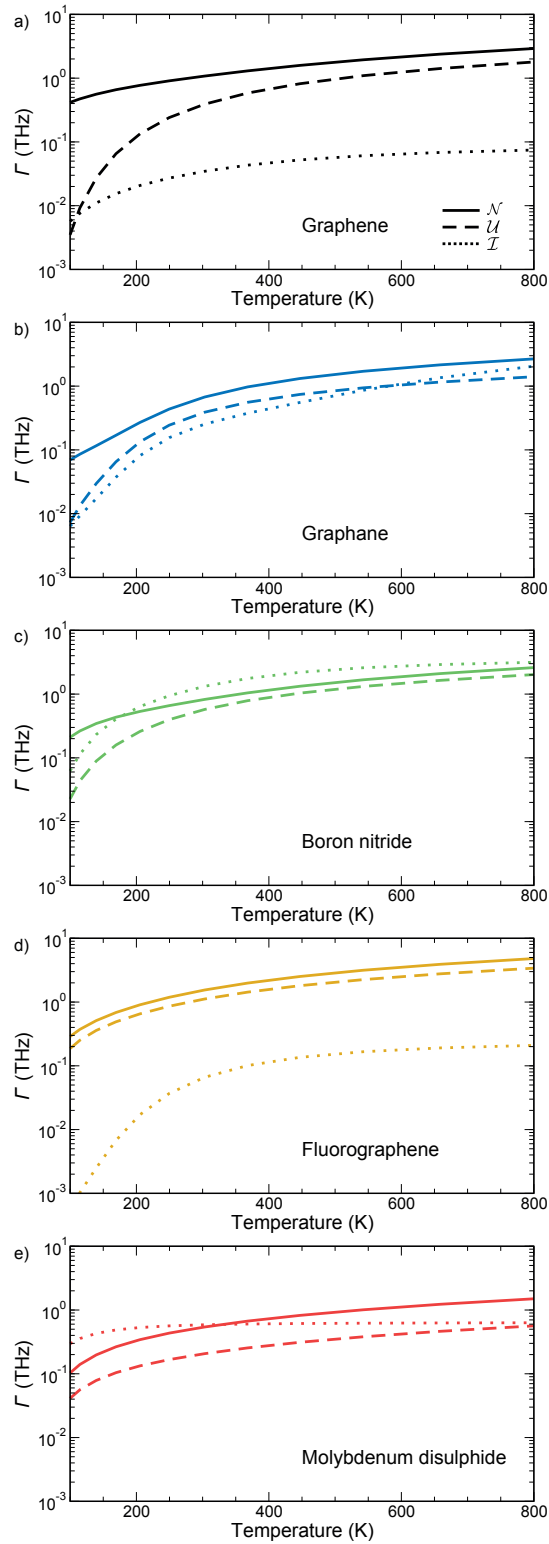


Figure 6.5 – Average linewidths of Normal (\mathcal{N}), Umklapp (\mathcal{U}) and Isotopic (\mathcal{I}) scattering processes in infinite suspended sheets; \mathcal{I} processes are calculated at natural isotopic abundances. \mathcal{N} scattering in all these 2D materials is clearly dominant.

Ballistic	$\mathcal{E} \gg \mathcal{N}$ and $\mathcal{E} \gg \mathcal{R}$
Poiseuille	$\mathcal{N} \gg \mathcal{E} \gg \mathcal{R}$
Ziman	$\mathcal{N} \gg \mathcal{R} \gg \mathcal{E}$
Kinetic	$\mathcal{R} \gg \mathcal{N}$ and $\mathcal{R} \gg \mathcal{E}$

Table 6.1 – Classification of different regimes of thermal conductivity as a function of the linewidths of different scattering events: normal (\mathcal{N}), resistive (\mathcal{R} - combining both Umklapp and isotopic), and extrinsic (\mathcal{E}). Poiseuille and Ziman hydrodynamics are characterized by dominant \mathcal{N} scattering against all other mechanisms.

In order to compare these 2D materials with conventional solids, we summarize in Table 6.1 the different regimes of phonon transport according to the nomenclature of Guyer [70]. In the ballistic regime the dominant scattering events are extrinsic (\mathcal{E}), and are typically due to the finite size of the sample (line defects, surfaces, grain boundaries); in the Poiseuille regime normal (\mathcal{N}) processes dominate, and the heat-flux is dissipated by \mathcal{E} events (this is the first hydrodynamic regime where the gas of phonons is “normal” but it feels the “walls” of the container). In the Ziman regime \mathcal{N} events still dominate, but the heat flux is now dissipated by resistive \mathcal{R} scattering (either Umklapp (\mathcal{U}) or isotopic (\mathcal{I})) - in this regime the “walls” have become irrelevant for the normal gas. Finally, in the kinetic regime intrinsic resistive processes \mathcal{R} (again, typically \mathcal{U} or \mathcal{I}) have the highest linewidth, the sample size is much larger than all typical mean free paths and \mathcal{N} events have become negligible.

It becomes instructive then to compare graphene, taken as reference, with a typical three-dimensional solid, like silicon or germanium. We show in Figure 6.6 the thermal conductivity of graphene both in the case in which we have an infinite sample (k_∞) or a finite ribbon (here of width $L=100\mu\text{m}$, k_L), considering this also in the ballistic limit $k_L^{\text{ballistic}}$ obtained by removing all the internal sources of scattering \mathcal{N} , \mathcal{U} and \mathcal{I} , but preserving the extrinsic scattering \mathcal{E} . The comparison of $k_L^{\text{ballistic}}$ with the exact thermal conductivity k_L in a ribbon of width L shows that the ballistic regime is not a good approximation to k_L . In fact, the introduction of \mathcal{N} scattering events enhances the thermal conductivity well above the ballistic limit. As the thermal conductivity grows with temperature, graphene is in the Poiseuille regime, where \mathcal{N} events facilitate the heat flux, and extrinsic sources of scattering dissipate it (the term Poiseuille comes from an analogy [70] between the flow of phonons in a material with the flow of a fluid in a pipe). The thermal conductivity does not grow indefinitely with temperature, due to the limit imposed by the intrinsic thermal conductivity of an infinite sheet k_∞ . Thus, there is a thermal conductivity peak, and for higher temperatures the heat-flux is mostly dissipated by intrinsic sources ($\mathcal{U} + \mathcal{I}$). Since the \mathcal{N} processes have the largest linewidth at any temperature, the regime at temperatures higher than the peak shifts to Ziman, where the intrinsic resistive processes \mathcal{R} set the typical length scales, and the boundaries become irrelevant. Last, if the intrinsic events \mathcal{R} ($\mathcal{U} + \mathcal{I}$) had the largest linewidth the thermal conductivity would be in the kinetic regime: this is the regime of conventional materials at ordinary temperatures, but it is never reached in these two-dimensional cases.

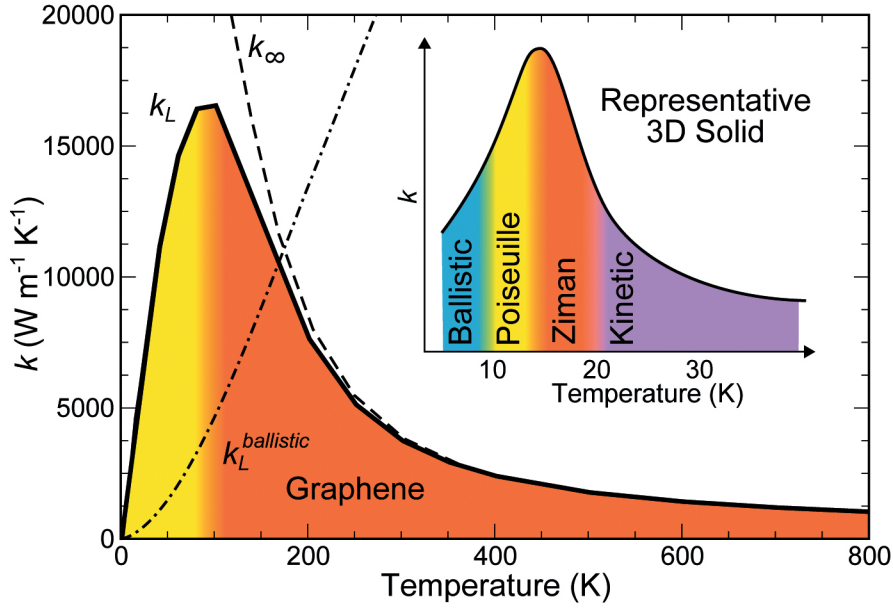


Figure 6.6 – Thermal conductivity of a graphene ribbon of width $L=100\mu\text{m}$ (k_L , solid line) together with its ballistic limit (see text; $k_L^{\text{ballistic}}$, dashed), and of an infinite graphene sheet (k_∞ , dashed line). Inset: thermal conductivity regimes in a standard three-dimensional solid (e.g. silicon or germanium), where peak conductivity is obtained at cryogenic temperatures and the hydrodynamic conditions, if present, are confined around those temperatures.

In conclusion, the two major differences between 2D materials and a conventional solid are i) in the temperature scales involved (the non-kinetic regimes in a conventional solid are all condensed in a narrow energy window around cryogenic conditions, and hydrodynamic regimes may not be present at all), and ii) in the fact that even at the highest temperatures normal processes remain dominant, restricting conductivities to just the hydrodynamic regimes of Poiseuille and Ziman.

6.3 Testing the Callaway approximation

As we explained in Section 4.2, Callaway’s model is an attempt to improve the description of the normal scattering events while keeping a simplified form of the scattering operator. Originally it was developed to describe the thermal conductivity of Germanium at low temperatures (20 K or so) [47], where normal scattering dominates. In these conditions, the phonons behave as a two-component system: first the distribution decays mostly into the drifting distribution, the state compatible with momentum conservation, and from this state it relaxes towards the static equilibrium given by the Bose–Einstein distribution. Having shown that \mathcal{N} processes are very frequent in 2D materials also at room temperature and above, it is worth checking the performance of Callaway’s approximation.

The results are shown in Figures 6.7 and 6.8, compared again with the exact thermal conduc-

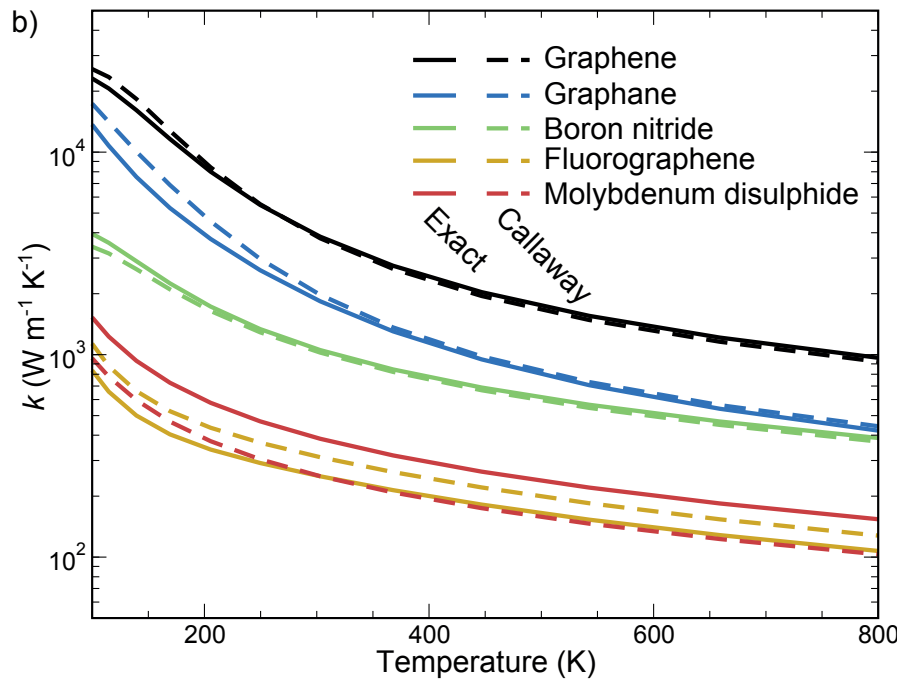


Figure 6.7 – Test of the Callaway model against the exact solution of the Boltzmann equation for some infinite suspended 2D materials. The model greatly improves over the SMA and is able to reproduce the exact conductivity.

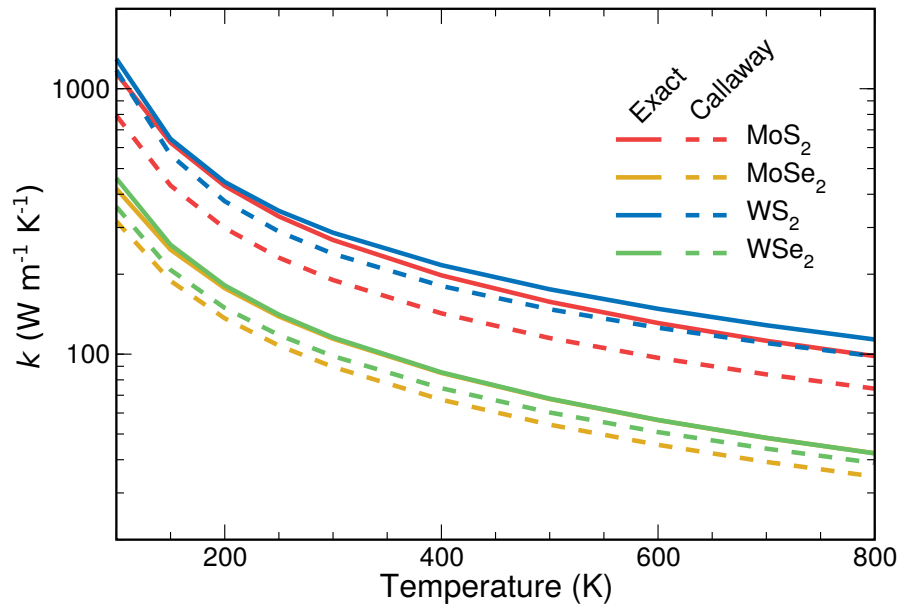


Figure 6.8 – Test of the Callaway model against the exact solution of the Boltzmann equation for some infinite suspended 2D transition metal dichalcogenides. The model improves over the SMA, but the differences with the exact solutions are more pronounced than for graphene and other materials.

tivities. The model broadly reproduces the exact solutions, even if e.g. in fluorographene it overestimates the exact results, or in transition metal dichalcogenides underestimates them. So, even more than providing simple but fairly accurate estimates of the phonon distribution without the need of solving exactly the Boltzmann equation, the value of the model is in the clear physical insight it offers on the microscopic nature of heat transport, allowing us to conclude not only that the dominant presence of \mathcal{N} processes at all temperatures characterizes heat transport in these materials, but also that the distribution function can be broadly described as a drifting distribution according to the prescriptions of Callaway and Klemens [47, 84]. In the dichalcogenides however the model has a reduced effectiveness, suggesting that for those materials it is not possible to describe the system only using a two-component relaxation.

Even though the model has sometimes a limited applicability, it has a great merit in suggesting a possible way of improving the interpretation of thermal conductivity. The introduction of two different relaxation processes has improved the estimates of thermal conductivity over the SMA. This suggested the interpretation of thermal transport in terms of relaxons that we presented in Section 4.5, where we have shown that the introduction of N different decay channels of the phonon distribution allows for an exact description of thermal transport.

7 Fourier's law failures

Fourier's law states that the local heat flux \mathbf{Q} of a material is proportional to the local gradient of temperature, through the thermal conductivity k , a constant property of the material. In its differential form, Fourier's law is written as

$$\mathbf{Q}(\mathbf{r}, t) = -k\nabla T(\mathbf{r}, t). \quad (7.1)$$

Very often, this equation is used in connection with the energy balance equation:

$$C \frac{\partial T(\mathbf{r}, t)}{\partial t} + \nabla \cdot \mathbf{Q}(\mathbf{r}, t) = 0. \quad (7.2)$$

These two equations have great relevance in the context of applied physics. In particular, they can be used to give a continuum description of heat flow, and the unknown heat flow and the temperature profile inside a material can be computed by applying some boundary conditions to the temperature. The information about the microscopic nature of the materials enters the equation only by means of the thermal conductivity. Therefore, knowing k , it is possible to study the heat transport in macroscopic systems of complicated geometries, relevant for many industrial applications but too complicated to be modeled with microscopic theories. The Boltzmann equation is thus a tool that links microscopic scattering rates to the thermal conductivity, which can then be transferred to continuum models. However, Fourier's law is an empirical law that is not derived from a fundamental theory. There are many conditions for which the equation does not hold and cannot be used to describe thermal transport.

In this chapter we will study in detail two circumstances in which Fourier's law does not hold in 2D materials. Firstly, it can occur that the thermal conductivity is not a constant property of the crystal, but is instead determined by the surface [132, 60]. Secondly, Fourier's law is not capable of describing the response to temperature pulses [53] and in some circumstances the material can exhibit a response in the form of heat waves (second sound) [50]. For both cases, we will see that these effects, often negligible for bulk crystals, are very important in 2D materials at the microscale.

7.1 Size dependent conductivity

The thermal conductivity is often assumed to be a constant property of the material. However, with the discussion of Chapter 5, we noticed how surfaces can reduce the effective value of thermal conductivity. When the mean free path of heat carriers is larger than the width of the 2D material, its value is renormalised by the presence of a surface. Therefore, the sharp value of thermal conductivity depends in general on the surface properties of the material and Fourier's law holds, strictly speaking, only in the thermodynamic limit of an infinitely large crystal. It is therefore crucial to characterize the average mean free path at which heat is dissipated, since this determines the material size above which Fourier's law holds. Below this length scale, the details of the temperature profile cannot be reconstructed with Fourier's law, and it is necessary to solve a purely microscopic model.

The analysis of mean free paths in the SMA is a well established methodology: it is sufficient to study the quantity $\lambda_\nu = v_\nu \tau_\nu$ for each phonon mode ν . It is less clear instead what is the correct quantity to study when going beyond the relaxation time approximation. As we discussed in Section 4.4, the knowledge of the phonon distribution does not grant us immediate access to the values of heat mean free paths, since we cannot interpret heat transport in terms of single-phonon properties. In fact, we have seen in the previous chapter that collective phonon excitations are responsible for heat transport in 2D materials, therefore we should look for a alternative ways of estimating the heat mean free path.

One way to characterise the mean free path of collective excitations can be achieved by studying the thermal conductivity as a function of the sample size. In fact, a characteristic sample size L prevents heat to travel for a distance larger than L itself, because it undergoes a scattering event at the boundary (and in Casimir's limit it is assumed to redistribute the carriers isothermally). To model extrinsic scattering, we use the rate of the form v_ν/L , as introduced in Chapter 5.2. With this procedure, we avoid the analysis of mean free paths in terms of phonon modes that cannot describe exactly the surface effect: since thermal conductivity is a collective property, the change of extrinsic sources of scattering does not merely scale down the largest mean free paths of a phonon mode but affects all the modes at once. As reported in Figure 7.1, one moves from a region in which the conductivity rises for increasing values of L (i.e. ballistic-like regime) to a plateau area (diffusive regime) above a length L_{diff} , where the thermal conductivity has reached the thermodynamic limit of intrinsic thermal conductivity. The length L_{diff} , at which the diffusive regime is reached, represents the longest mean free path of heat carriers.

The study of the heat carrier mean free paths at room temperature for graphene, bilayer graphene, in-plane and out-of-plane graphite is reported in Figure 7.1. Since the SMA uses only individual phonon excitations, the L_{diff} observed within the SMA is determined by the phonon mean free paths (in particular, the longest mean free path of the heat carrying phonons). For graphene, L_{diff} falls then in a range of values between 1 μm and 10 μm , in agreement with what is commonly accepted in the literature [43, 112]. Crucially, the exact solution of the Boltzmann

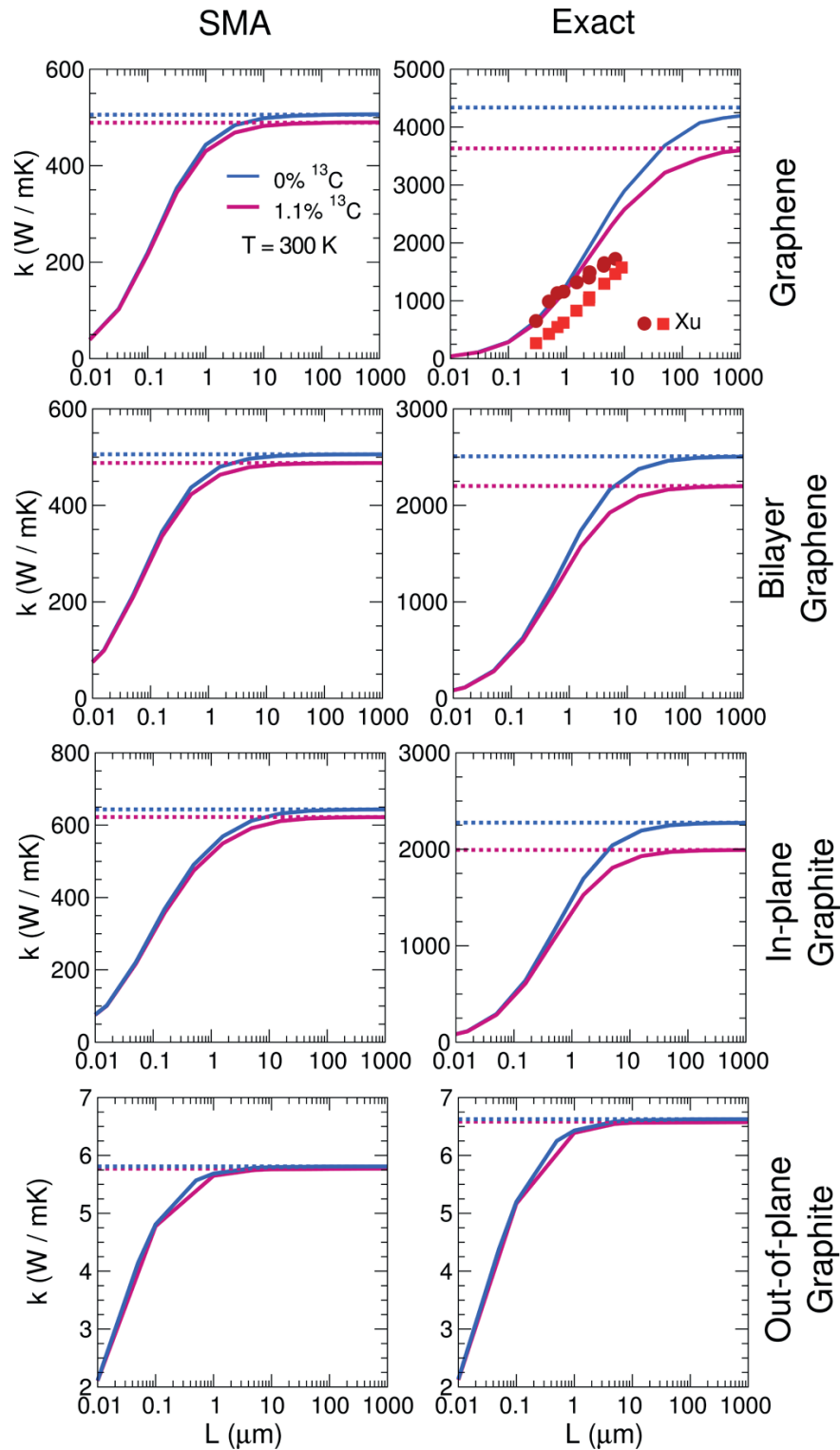


Figure 7.1 – Lattice thermal conductivity of naturally occurring (magenta line) and isotopically pure (blue line) graphene, bilayer graphene, in-plane graphite, and out-of-plane graphite, at 300 K as a function of the crystalline-domain sizes L , in the SMA (left panel) and in the exact solution (right panel). Experimental points from the left panel of Figure 3 in ref [130]. Dotted lines report the values of the thermodynamic limit.

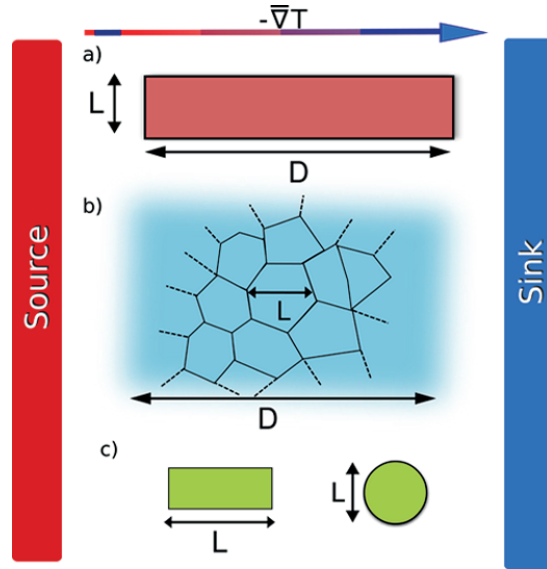


Figure 7.2 – Schematic representation of the different uses of the scattering rate term ν_v/L in the presence of a gradient of temperature between the source and the sink at distance D . (a) Ribbon of width L with $D \gg L$. (b) Polycrystalline sample of domain size L with $D \gg L$. (c) Ribbon of length L or circular sample of diameter L : the theory of surface scattering presented in Chapter 5 does not apply using L in the scattering rate.

equation reaches a diffusive limit for lengths that are two orders of magnitude larger, setting L_{diff} in a range of values between $100 \mu\text{m}$ and 1mm . On the basis of our results, we infer that the logarithmic divergence claimed for graphene in Ref. [130] is only originated by the experimental complexity of extending the study to larger samples. We remark that while other works [98, 99] have performed numerical simulations of the Boltzmann equation on graphene, such studies were limited to lengths up to $50 \mu\text{m}$, and were then not able to access or discuss the effects presented here. As shown in Figure 7.1 the diffusive limit is reached at lower values in going from 2D to 3D, indicating that mean free paths are decreasing. In the out-of-plane direction the difference between SMA and the exact solution is reduced, so that the difference between the mean free paths of phonons isn't too different from the heat carrier mean free paths. Eventually, the reduction of thermal conductivity with respect to the in-plane direction is also reflected in a corresponding reduction of the mean free paths.

Unfortunately, the results of the simulations are not directly comparable with experimental measurements of graphene. In fact, the theory of surface scattering that we introduced is valid only when the distance D between the source and the sink is infinite, or at least much larger than the heat carrier mean free path ($D \gg \lambda$). In case of a ribbon geometry, the mean free path λ is limited by the finite lateral dimension L (Figure 7.2, panel (a)), and it is crucial that the distance D is much larger than L , in such a way that the relation $D \gg \lambda$ holds. Similarly, the distance D is sufficiently large in a polycrystalline material (Figure 7.2, panel (b)) when it is larger than the average size L of the crystal grain. In contrast, experimental setups (Figure

7.2, panel (c)) have a different geometry than that considered in our description of surface scattering and their description requires a different set of boundary conditions to be applied on the material, which we do not cover in this Thesis.

The extremely large values of the heat carriers mean free paths in graphene have some important consequences, given that Fourier's law is valid only for systems large enough to accommodate at least a few mean free paths. Current measurements of thermal conductivity in graphene (see Figure 7.2c) have been performed in samples whose lateral size covered a range from 1 μm up to some tens of μm , which is smaller than the mean free path for the collective phonon excitations. Thus, the use of Fourier's law for interpreting the measurements performed in these systems becomes questionable. Since the sample is small, the conditions in which thermal conductivity is defined from a macroscopic and statistical point of view, i.e. as a diffusion coefficient, are no longer met. We can still use the ratio between the heat flux and the difference of temperature, namely the "thermal conductance", defined also in absence of a diffusion equation. Finally, the proper theoretical procedure to evaluate an effective thermal conductivity comparable to experiments requires the solution of the Boltzmann transport equation with appropriate boundary conditions.

7.2 Second sound

There are well known limitation in the capability of Fourier's law to describe the thermal response to a temperature pulse. Following the phenomenological approach of Chester [53], it is easy to see that combining the Fourier equation with the conservation of energy (Eqs. 7.1 and 7.2), we obtain the equation:

$$\frac{C}{k} \frac{\partial T}{\partial t} - \nabla^2 T = 0, \quad (7.3)$$

which is the typical diffusion equation used to describe the temperature profile in a material with a thermal conductivity k . This equation cannot describe the response to a perturbation in the form of a wave such as $T = T_0 + \delta T e^{i\omega t}$: since this is not a valid solution of the equation at any time, the thermal response should transform the temperature pulse into a valid solution at an infinitely fast rate. This unphysical consideration can be solved by introducing an additional term to Fourier's law in the form:

$$\tau_{\text{ss}} \frac{\partial \mathbf{Q}}{\partial t} + \mathbf{Q} = -k \nabla T. \quad (7.4)$$

This equation includes an additional friction term (actually, a result that dates back to Maxwell), that allows for a finite time to build the response to the initial temperature pulse. Only in the long time limit ($t \gg \tau_{\text{ss}}$) one recovers again the standard Fourier's law. In presence of such a friction term, the temperature profile is described by:

$$\frac{\partial^2 T}{\partial t^2} + \frac{1}{\tau_{\text{ss}}} \frac{\partial T}{\partial t} - v_{\text{ss}}^2 \nabla^2 T = 0, \quad (7.5)$$

Chapter 7. Fourier's law failures

where we introduced a velocity $v_{\text{ss}}^2 = \frac{k}{C\tau_{\text{ss}}}$. When this equation is valid, it is said that a material sustains thermal waves, a phenomenon called second sound.

Second sound is a rare phenomenon that has been observed in a few selected materials at cryogenic temperatures [81, 118, 106, 30, 76]. In most cases, the time τ_{ss} is so small that second sound cannot be observed and the standard non wave-like description of the temperature profile applies. The few materials that host second sound are actually characterised by hydrodynamic thermal transport, when normal processes are dominating the heat dynamics. It is therefore interesting to discuss its existence or characteristics in two dimensions.

In principle more than one microscopic mechanism could lead to the formation of second sound [74]; the common requirement is that a mechanism exists which is causing a slow decay of the heat flux (i.e. a long τ_{ss}). This can indeed happen in case of a large presence of \mathcal{N} events. As mentioned in the discussion of Callaway's model, the conservation of momentum drives n_v towards n_v^{drift} , and once this drifting distribution n_v^{drift} has accumulated, heat propagates as a wave that is eventually damped on longer timescales by the resistive processes that relax the phonons to the equilibrium Bose–Einstein distribution. Thus, at longer distances or larger times, second sound disappears and the solution of Eq. 7.5 becomes indistinguishable from that of Eq. 7.3, describing the usual diffusive heat transport.

Theory of second sound

In this section, we show that if the out-of-equilibrium distribution function n_v is approximately equal to n_v^{drift} , then the Boltzmann equation describes the second sound temperature profile. Hardy derived this result in the constant relaxation time approximation [74] and we extend his argument using the Callaway approximation. In fact, Boltzmann equation can be viewed as a microscopic and more complete formulation of Fourier's law. With this procedure, we will derive the expression for the second sound relaxation time and velocity. We start from the time dependent Boltzmann equation in the Callaway approximation:

$$\frac{\partial n_v(\mathbf{r}, t)}{\partial t} + \mathbf{v}_v \cdot \nabla n_v(\mathbf{r}, t) \approx -\frac{n_v(\mathbf{r}, t) - \bar{n}_v(T(\mathbf{r}, t))}{\tau_v^{\mathcal{R}}} - \frac{n_v(\mathbf{r}, t) - n_v^{\text{drift}}(\mathbf{r}, t)}{\tau_v^{\mathcal{N}}}, \quad (7.6)$$

where we wrote explicitly that the Bose–Einstein distribution depends on space and time only through the temperature:

$$\bar{n}_v(T(\mathbf{r}, t)) = \frac{1}{e^{\hbar\omega_v/k_B T(\mathbf{r}, t)} - 1}. \quad (7.7)$$

We want to analyse the temperature profile in a medium that is kept at an average temperature T_0 to which a time and space dependent temperature perturbation is applied. Let's suppose that the drifting distribution (Eq. 1.47) is a good approximation for the out-of-equilibrium

distribution:

$$n_{\nu}(\mathbf{r}, t) \approx n_{\nu}^{\text{drift}}(\mathbf{r}, t) \approx \bar{n}_{\nu}(T(\mathbf{r}, t)) + \bar{n}_{\nu}(T_0)(\bar{n}_{\nu}(T_0) + 1) \frac{\mathbf{q} \cdot V(\mathbf{r}, t)}{k_B T_0}. \quad (7.8)$$

This assumption is justified if the normal processes dominate the thermal dynamics of phonons and momentum is approximately conserved. Using this approximations, we take the energy flux of the Boltzmann equation multiplying Eq. 7.6 by $\hbar\omega_{\nu}v_{\nu}^i$ and sum over all modes ν (i identifies a generic cartesian direction):

$$\begin{aligned} \frac{\partial}{\partial t} \left(\sum_{\nu} \hbar\omega_{\nu}v_{\nu}^i n_{\nu}^{\text{drift}}(\mathbf{r}, t) \right) + \sum_{\nu} \hbar\omega_{\nu}v_{\nu}^i \mathbf{v}_{\nu} \cdot \frac{d\bar{n}_{\nu}}{dT} \Big|_{T_0} \nabla T(\mathbf{r}, t) &= - \sum_{\nu} \frac{\hbar\omega_{\nu}v_{\nu}^i n_{\nu}^{\text{drift}}(\mathbf{r}, t)}{\tau_{\nu}^{\mathcal{R}}} - 0 \\ &= - \sum_{\nu} \hbar\omega_{\nu}v_{\nu}^i \bar{n}_{\nu}(T_0)(\bar{n}_{\nu}(T_0) + 1) \frac{\mathbf{q} \cdot V(\mathbf{r}, t)}{k_B T \tau_{\nu}^{\mathcal{R}}}. \end{aligned} \quad (7.9)$$

Let us now recall the definition of the heat (energy) flux of phonons:

$$\mathbf{Q}(\mathbf{r}, t) = \frac{1}{\mathcal{V}} \sum_{\nu} \hbar\omega_{\nu} \mathbf{v}_{\nu} n_{\nu}(\mathbf{r}, t), \quad (7.10)$$

and note that only the odd component of the out-of-equilibrium distribution ($n_{\nu} + n_{-\nu}$, where $-\nu = (-\mathbf{q}, s)$) contributes to the heat flux, so that the Bose–Einstein component of the drifting distribution has zero contribution to \mathbf{Q} . To make \mathbf{Q} explicitly appear on the right side of equation 7.9, we define an average resistive lifetime as:

$$\left\langle \frac{1}{\tau^{\mathcal{R}}} \right\rangle_i = \frac{\sum_{\nu, j} \bar{n}_{\nu}(T_0)(\bar{n}_{\nu}(T_0) + 1) \hbar\omega_{\nu} v_{\nu}^i q^j V^j(\mathbf{r}, t) / \tau_{\nu}^{\mathcal{R}}}{\sum_{\nu, j} \bar{n}_{\nu}(T_0)(\bar{n}_{\nu}(T_0) + 1) \hbar\omega_{\nu} v_{\nu}^i q^j V^j(\mathbf{r}, t)}. \quad (7.11)$$

The Boltzmann equation can then be rewritten as an equation for the heat flux:

$$\left\langle \frac{1}{\tau^{\mathcal{R}}} \right\rangle_i^{-1} \frac{\partial Q^i(\mathbf{r}, t)}{\partial t} + \sum_j K^{ij} \nabla_j T(\mathbf{r}, t) + Q^i(\mathbf{r}, t) = 0, \quad (7.12)$$

where we defined a thermal conductivity tensor as:

$$K^{ij} = \frac{1}{\mathcal{V}} \left\langle \frac{1}{\tau^{\mathcal{R}}} \right\rangle_i^{-1} \sum_{\nu} \frac{d\bar{n}_{\nu}}{dT} \Big|_{T_0} \hbar\omega_{\nu} v_{\nu}^i v_{\nu}^j. \quad (7.13)$$

At this point, equation 7.12 is formally equivalent to Eq. 3.9 of Ref. [74], but with an explicit way of constructing the average relaxation time in the Callaway approximation. Our derivation differs from Ref. [74] in that we extend the single relaxation time approximation (constant $\tau_{\nu} = \tau$) to the Callaway approximation retaining a mode dependency, and in that we explicitly use the drifting distribution rather than a generic odd function in order to obtain a closed expression for the average relaxation time. Following the same arguments of Hardy, we now restrict ourselves to the case of an isotropic two dimensional material, where $K^{ij} = K\delta_{i,j}$, $\left\langle \frac{1}{\tau^{\mathcal{R}}} \right\rangle_i = \left\langle \frac{1}{\tau^{\mathcal{R}}} \right\rangle$ and the drift velocity is parallel to ∇T (so that it is possible to take only $j = i$ and the drift velocity V disappears from the equations). To recast equation 7.12 in terms of

temperature, we first need to consider the lattice energy density $U(\mathbf{r}, t)$, where:

$$U(\mathbf{r}, t) = U_0 + u(\mathbf{r}, t), \quad (7.14)$$

$$U_0 = \frac{1}{\mathcal{V}} \sum_{\nu} \hbar \omega_{\nu} \bar{n}_{\nu}(T_0), \quad (7.15)$$

$$u(\mathbf{r}, t) = \frac{1}{NV} \sum_{\nu} \hbar \omega_{\nu} (n_{\nu}(\mathbf{r}, t) - \bar{n}_{\nu}(T_0)). \quad (7.16)$$

For small temperature differences, the energy density is proportional to the temperature difference, as in

$$U(\mathbf{r}, t) = U_0 + C(T(\mathbf{r}, t) - T_0), \quad (7.17)$$

where

$$C = \frac{1}{\mathcal{V}} \sum_{\nu} \left. \frac{d\bar{n}_{\nu}}{dT} \right|_{T_0} \hbar \omega_{\nu} = \frac{1}{\mathcal{V} k_B T^2} \sum_{\nu} \bar{n}_{\nu}(T_0) (\bar{n}_{\nu}(T_0) + 1) (\hbar \omega_{\nu})^2. \quad (7.18)$$

Therefore, the local deviation $u(\mathbf{r}, t)$ from the base energy density U_0 is equal to $u(\mathbf{r}, t) = C(T(\mathbf{r}, t) - T_0)$. We also note that $u(\mathbf{r}, t)$ follows a balance equation:

$$\frac{\partial u(\mathbf{r}, t)}{\partial t} + \nabla \cdot \mathbf{Q}(\mathbf{r}, t) = 0, \quad (7.19)$$

which can be obtained from the Boltzmann Equation by multiplying it by $\hbar \omega_{\nu}$ and summing over all modes [74]. Using equations 7.19, 7.12 and the proportionality between u and T , we obtain the second sound equation:

$$\frac{\partial^2 T(\mathbf{r}, t)}{\partial t^2} + \frac{1}{\tau_{ss}} \frac{\partial T(\mathbf{r}, t)}{\partial t} - (v_{ss})^2 \nabla^2 T(\mathbf{r}, t) = 0, \quad (7.20)$$

with second sound velocity and relaxation time equal to:

$$(v_{ss})^2 = \frac{\sum_{\nu} \frac{\mathbf{v}_{\nu} \cdot \mathbf{v}_{\nu}}{2} \bar{n}_{\nu}(T_0) (\bar{n}_{\nu}(T_0) + 1) (\hbar \omega_{\nu})^2}{\sum_{\nu} \bar{n}_{\nu}(T_0) (\bar{n}_{\nu}(T_0) + 1) (\hbar \omega_{\nu})^2} = \frac{\sum_{\nu} C_{\nu} \frac{\mathbf{v}_{\nu} \cdot \mathbf{v}_{\nu}}{2}}{\sum_{\nu} C_{\nu}}, \quad (7.21)$$

$$\frac{1}{\tau_{ss}} = \left\langle \frac{1}{\tau} \right\rangle = \frac{\sum_{\nu} \bar{n}_{\nu}(T_0) (\bar{n}_{\nu}(T_0) + 1) \hbar \omega_{\nu} v_{\nu}^i q^i / \tau_{\nu}^{\mathcal{R}}}{\sum_{\nu} \bar{n}_{\nu}(T_0) (\bar{n}_{\nu}(T_0) + 1) \hbar \omega_{\nu} v_{\nu}^i q^i}. \quad (7.22)$$

These equations are going to be used in the characterisation of second sound in 2D materials.

Before continuing, it's worth commenting briefly the drifting approximation for second sound, that is, the interpretation of the Boltzmann equation as an equation for momentum fluxes. A similar procedure applies as before, however we multiply the Boltzmann equation by the

momentum $\hbar q^i$, obtaining

$$\frac{\partial J^i(\mathbf{r}, t)}{\partial t} + \sum_j \frac{\partial T^{ij}(\mathbf{r}, t)}{\partial x^j} = -\left\langle \frac{1}{\tau^{\mathcal{R}}} \right\rangle_i J^i(\mathbf{r}, t), \quad (7.23)$$

$$J^i(\mathbf{r}, t) = \frac{1}{\mathcal{V}} \sum_{\mathbf{v}} n_{\mathbf{v}}(\mathbf{r}, t) \hbar q^i, \quad (7.24)$$

$$T^{ij}(\mathbf{r}, t) = \frac{1}{\mathcal{V}} \sum_{\mathbf{v}} n_{\mathbf{v}}(\mathbf{r}, t) \hbar q^i v_{\mathbf{v}}^j, \quad (7.25)$$

$$\left\langle \frac{1}{\tau^{\mathcal{R}}} \right\rangle_i = \frac{\sum_{\mathbf{v}} \bar{n}_{\mathbf{v}}(T_0) (\bar{n}_{\mathbf{v}}(T_0) + 1) (q^i)^2 / \tau_{\mathbf{v}}^{\mathcal{R}}}{\sum_{\mathbf{v}} \bar{n}_{\mathbf{v}}(T_0) (\bar{n}_{\mathbf{v}}(T_0) + 1) (q^i)^2}, \quad (7.26)$$

where J is the crystal-momentum flux and T is the crystal-momentum density. Using Eq. 7.19, the proportionality between u and T and restricting to the symmetries of graphene, it is possible to obtain a damped-wave equation for the temperature [74], with a velocity of second sound equal to:

$$(v_{ss})^2 = \frac{(\sum_{\mathbf{v}} \bar{n}_{\mathbf{v}}(T_0) (\bar{n}_{\mathbf{v}}(T_0) + 1) \omega_{\mathbf{v}} \mathbf{q} \cdot \mathbf{v}_{\mathbf{v}})^2}{2 \sum_{\mathbf{v}} \bar{n}_{\mathbf{v}}(T_0) (\bar{n}_{\mathbf{v}}(T_0) + 1) \omega_{\mathbf{v}}^2 \times \sum_{\mathbf{v}} \bar{n}_{\mathbf{v}}(T_0) (\bar{n}_{\mathbf{v}}(T_0) + 1) \mathbf{q} \cdot \mathbf{q}}. \quad (7.27)$$

However, if one considers a two dimensional Brillouin zone and a phonon with quadratic dispersion (e.g. the out-of-plane ZA mode), one can readily see that the crystal-momentum flux J and the length $v_{ss} \cdot \left\langle \frac{1}{\tau^{\mathcal{R}}} \right\rangle^{-1}$ are both infinite, due to a divergence for small wavevectors ($\int \bar{n}_{\mathbf{v}} (\bar{n}_{\mathbf{v}} + 1) q^2 d\mathbf{q} \propto \int \frac{1}{q^2} \frac{1}{q^2} q^2 q d\mathbf{q} = \int \frac{1}{q} d\mathbf{q}$ diverges when integrating around the Brillouin zone center), whereas the velocity v_{ss} goes to zero and the crystal-momentum density t is finite. Due to the infinite momentum-flux, the drifting approximation for second sound cannot be applied. Similarly, also the theory developed in Ref. [74], which deals with the exact expression of the Boltzmann equation, suffers from the same divergence problem (see equation 4.25, 4.26 and 4.28 of Ref. [74]) and does not hold for 2D materials with quadratic phonon dispersion. These divergences are not present if we consider energy fluxes, and are not present in case of phonons with linear dispersion close to the Brillouin Zone center (as Ref. [74] implicitly assumed).

Second sound in 2D materials

Let us now apply the second sound theory to 2D materials. There are several hints that validate the approximation $n_{\mathbf{v}} \approx n_{\mathbf{v}}^{\text{drift}}$ necessary to the existence of second sound. First, we observed that Callaway's model, that takes into account the decay of the phonon population in such a state, is capable of describing the thermal conductivity in good agreement with exact solutions of the Boltzmann equation. Moreover, we can inspect and compare the deviation from equilibrium functions of the two distributions, that is, we study $f_{\mathbf{v}}$ (see Eq. 3.19) instead of $n_{\mathbf{v}}$, and qV instead of $n_{\mathbf{v}}^{\text{drift}}$ (the linear term in the Taylor expansion of $n_{\mathbf{v}}^{\text{drift}}$ around the Bose-Einstein distribution) [50, 92]. The two distributions are approximately equal if $f_{\mathbf{v}}$ is well

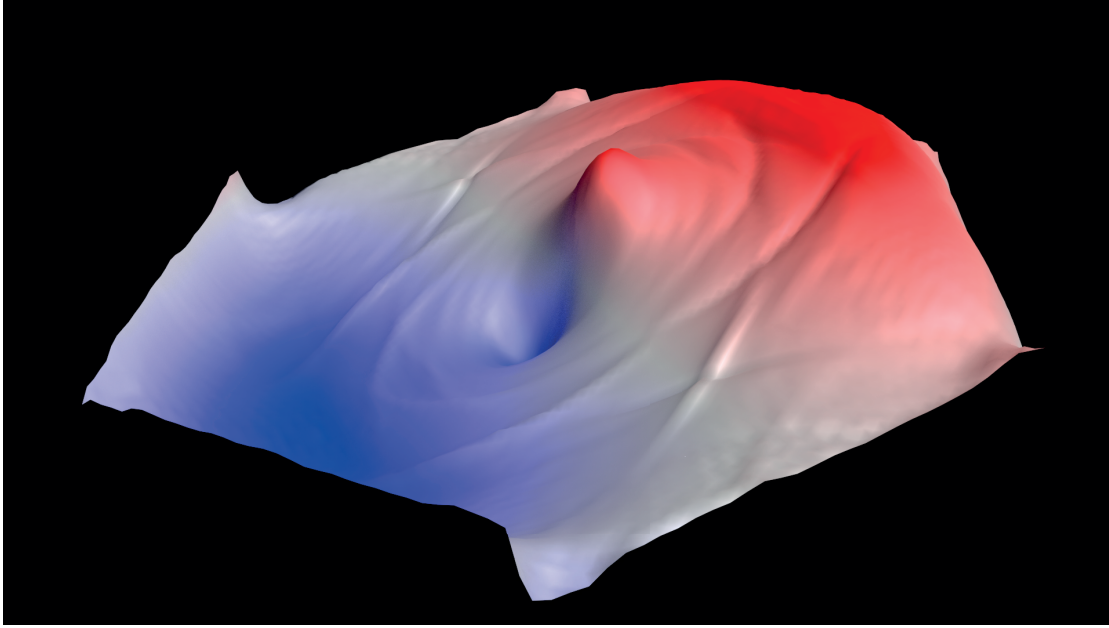


Figure 7.3 – Graphical representation of the out-of-equilibrium deviation function f for the ZA mode of graphene at 300K, as computed by the Boltzmann equation. The linearity of the function throughout large sections of the Brillouin zone suggests that it is well approximated by the drifting distribution.

described by a plane over the Brillouin zone. For example, in Figure 7.3 we graphically inspect the deviation function for graphene at room temperature for the out-of-plane ZA mode. It is evident in the picture that the function is approximately linear in momentum over a large part of the Brillouin zone. In other materials, such as molybdenum disulphide, one could do the same plot and observe that at room temperature the similarity with a linear function is less striking.

In order to be more quantitative and avoid visual inspection, we define the drifting component as:

$$\frac{\sum_{\nu} C_{\nu} f_{\nu} q_{\parallel}}{\sqrt{\sum_{\nu} C_{\nu} f_{\nu}^2} \sqrt{\sum_{\nu} C_{\nu} q_{\parallel}^2}}, \quad (7.28)$$

which is equal to one if the out-of-equilibrium distribution is equal to the drifting distribution. We plot this quantity for all materials considered in Figure 7.4 (as a percentage), and we observe that more than 40% of the phonon distribution of graphene at room temperature is determined by the drifting distribution, and that this ratio grows at lower temperatures. The ratio is slightly smaller in all other materials, falling below 30% for fluorographene and 10% molybdenum disulphide. Therefore, in graphene, graphane and boron nitride a large fraction of the heat flux is carried by the drifting distribution (which is a good approximation of n_{ν} for the study of the heat flux propagation), while in fluorographene and molybdenum disulphide

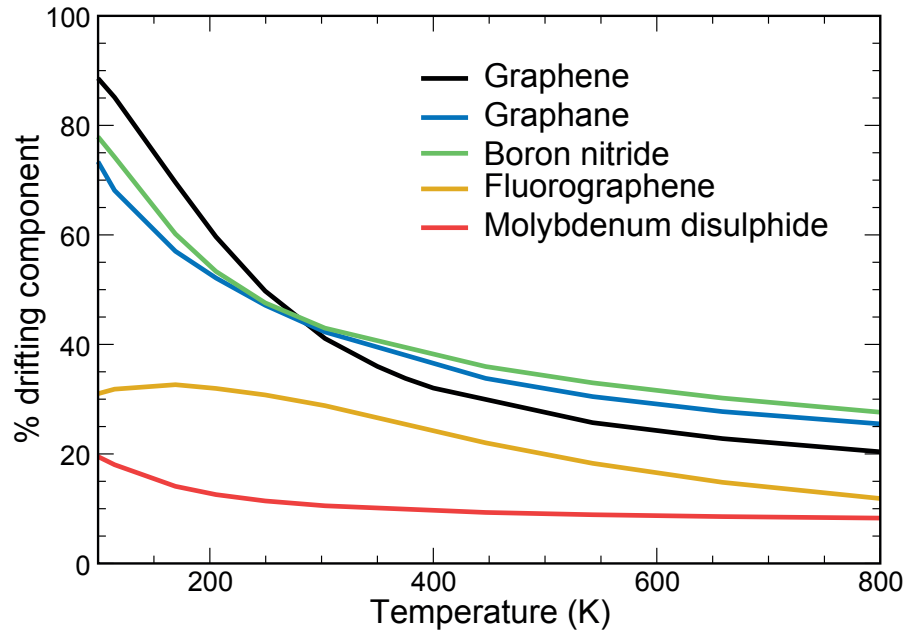


Figure 7.4 – Projection of the out-of-equilibrium phonon distribution onto the drifting distribution (percentage values).

the drifting distribution is not a good descriptor of the out-of-equilibrium distribution, as also hinted by the reduced effectiveness of the Callaway model.

When the drifting distribution is a good approximation to the out-of-equilibrium distribution, the material will display second sound. The second-sound heat wave is characterized by a velocity v_{ss} and a relaxation time τ_{ss} that define a second-sound length $\lambda_{ss} = v_{ss}\tau_{ss}$, i.e. the characteristic distance over which the heat wave propagates before decaying.

The second sound relaxation times in Figure 7.5 indicate that the energy flux dissipation decays on a time scale of the order of hundred picoseconds at room temperature for the three materials of higher conductivity. The second-sound velocities depend only on harmonic properties, and can be easily computed - they are reported in the Figure 7.6 as a function of temperature, and compared with the average velocity of acoustic phonons. In particular, the phonon group velocities of the three acoustic branches (transverse (TA), longitudinal (LA) and out-of-plane (ZA)) are averaged as $\bar{v}^2 = (\sum_v C_v \frac{v_v \cdot v_v}{2}) / \sum_v C_v$. We find that values of v_{ss} lay typically in between the larger average velocities of the longitudinal (LA) and transverse (TA) acoustic branches, and the much lower average velocity of the out-of-plane acoustic mode (ZA).

The propagation lengths $\lambda_{ss} = \tau_{ss} v_{ss}$ for the second-sound wave in graphene and graphane reach the micron scale, even at room temperature, while boron nitride is characterized by second sound lengths of a fraction of a micron (the values of λ_{ss} for molybdenum disulphide and fluorographene are shown in Figure 7.7 for completeness, even if those materials do not

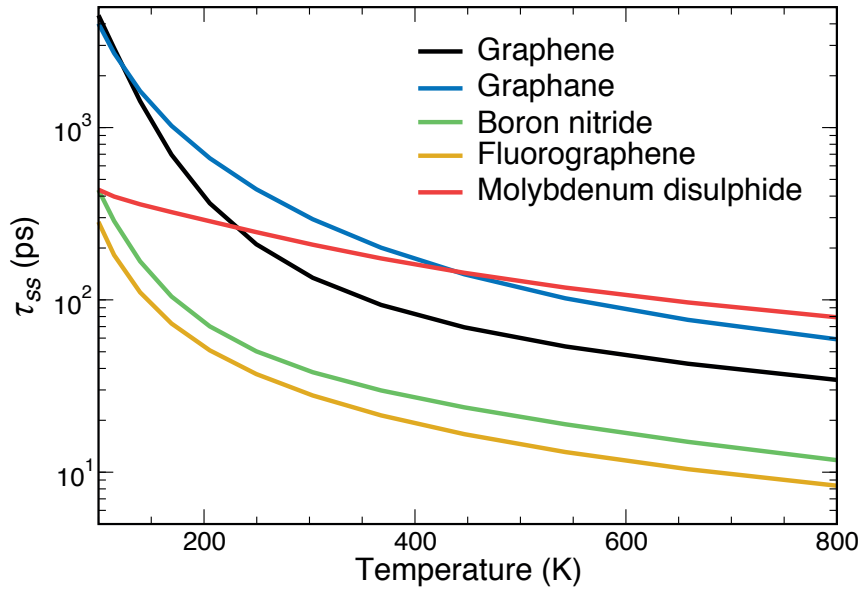


Figure 7.5 – Second sound relaxation times for the different materials considered.

host second sound). At lower temperatures, where \mathcal{U} processes tend to freeze and only \mathcal{S} are present, damping of the second sound becomes less effective and the heat wave propagates over longer distances.

As mentioned, the presence of second sound has been verified experimentally in the past [81, 118, 106, 30, 76] in 3D materials at cryogenic temperatures, and it is conveniently studied as the response of a material to a temperature pulse. One should then be able to observe at a distance standard pulses due to the diffusive propagation by the LA, TA and ZA modes; in addition, the second sound signature will appear as a further peak due to the formation of the drifting distribution. One should also always consider the size of the experimental setup, since this will affect phonons which travel ballistically, i.e. without scattering between the heat source and the detector, and that would diminish the component of heat travelling in the other modes. Their effect on second sound should be negligible as long as the distance between pump and probe is larger than λ_{ss} . Finally, let us note that the estimate of λ_{ss} is obtained here as a statistical average, and thus we cannot exclude the existence of tails of the second sound mode propagating at much longer distances.

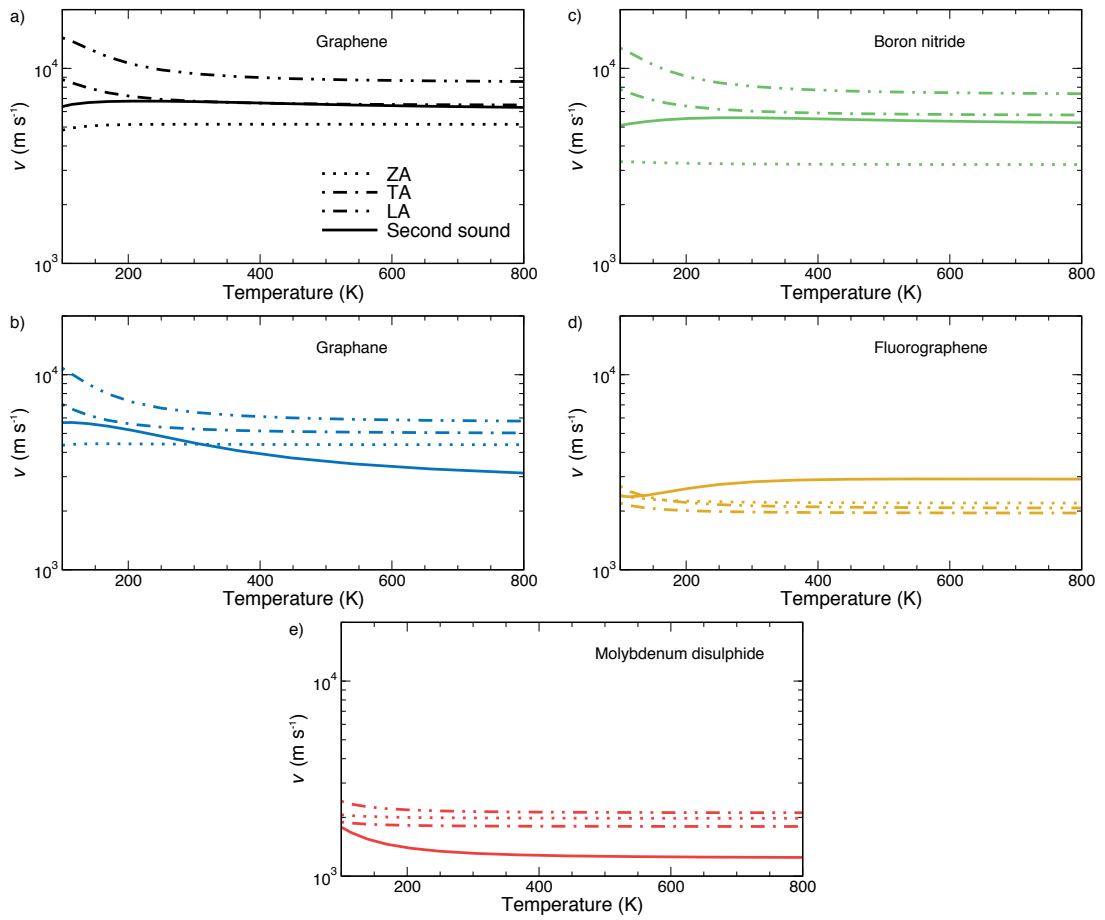


Figure 7.6 – Velocities for the acoustic-phonon branches, compared with the velocities of drifting second sound.

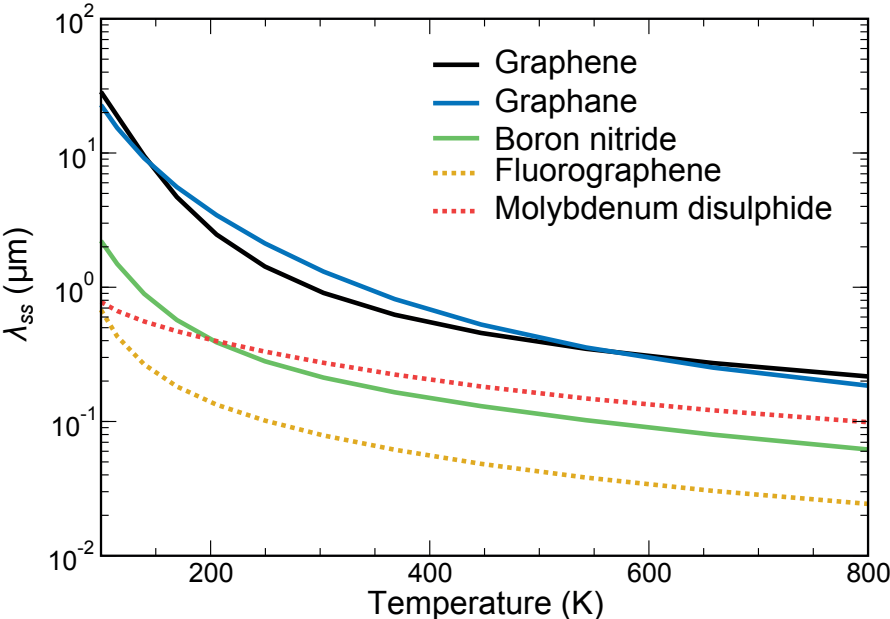


Figure 7.7 – Characteristic propagation length of second sound, describing the wave-like propagation of heat. Dotted lines are used for the materials where second sound has a low probability of being observed. We note that for graphene and graphane at room temperature the typical decay length of second sound is of the order of microns.

8 Relaxons in graphene

In the previous chapters, we have shown that thermal transport in 2D materials is driven by collective excitations of phonons. The large presence of normal processes plays a key role in redistributing the phonon populations across modes and introducing correlations between phonons. Moreover, we have seen that the phonon mean free paths are much smaller than the dissipation length for heat, and we predicted that second sound, i.e. the formation of a phonon wavepacket in the form of a drifting distribution, could be observed in graphene and other 2D materials.

However, a proper definition of these collective excitations can only be achieved by diagonalising the dynamical matrix and using the concept of relaxon that we introduced in Section 4.5. Although there exist few works that diagonalised the scattering matrix to obtain the thermal conductivity (as for example Refs. [52, 124]), we are not aware of studies that interpreted thermal transport in terms of relaxons. In this chapter we apply this interpretation of thermal transport to graphene. In particular we will compare relaxation times, velocities and mean free paths in the two main pictures of thermal transport: as a gas of phonons (i.e. within the SMA) and as a gas of relaxons. Finally, we will show that Matthiessen's rule, a property often assumed to hold, is violated in graphene and that the iterative method for solving the Boltzmann equation has a limited domain of convergence, insufficient for graphene at room temperature.

To simplify the discussion, we limit the study to relaxons in an infinite sample of graphene at room temperature (300K). In order to have a direct comparison with the results of the variational methods presented in the previous chapters, we kept the same computational parameters, so that the scattering matrix is identical within numerical error and includes the effect of 3-phonon interactions and isotopic scattering at natural carbon abundances [128]. The resulting matrix has 98304 rows and as many columns, which can be diagonalised only using massively parallel software libraries. In particular, we diagonalised it exactly using the routine PDSYEV of the ScaLAPACK library [42]. The results of the diagonalisation have been validated against the variational method, by finding a thermal conductivity of $3.9 \cdot 10^3$ W/(mK) which well compares with the variational value of $3.6 \cdot 10^3$ W/(mK). The residual difference

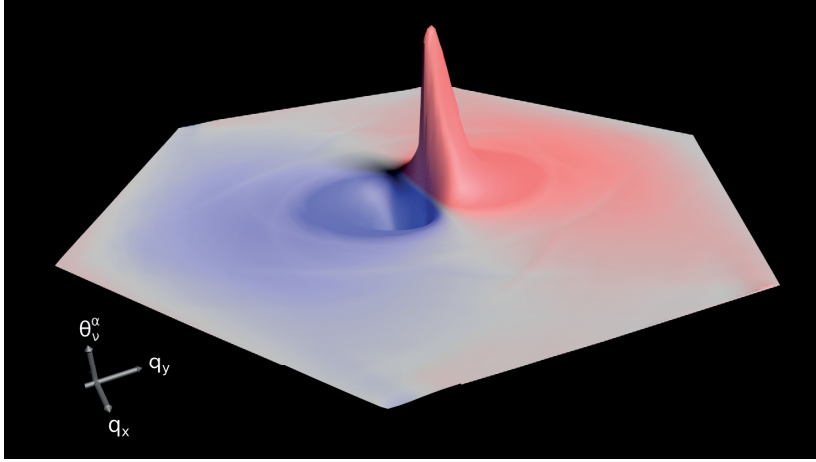


Figure 8.1 – Representation of the relaxon with the longest lifetime in graphene at room temperature. The relaxon eigenvector θ_v^α identifies a collective excitation of phonons $v = (\mathbf{q}, s)$, which we plot as a function of the \mathbf{q} -points of the Brillouin zone for the out-of-plane mode $s=ZA$.

is attributed to roundoff errors in the floating point precision (16 digits), due to the large numerical complexity of the matrix diagonalisation ($O(10^{15})$ operations). This algorithm is therefore much more expensive than a variational approach, if the only goal is to obtain the thermal conductivity. The advantage of the method is to grant inspection to the spectrum of relaxon properties. The diagonalisation procedure provides all the relaxon eigenvectors; notably, few discrete ones have large relaxation times and, for example, the longest-lived relaxon is plotted in Figure 8.1 over the Brillouin zone of graphene, taking into account for simplicity only the component relative to the acoustic out-of-plane branch. So, it becomes possible to understand which phonons are most relevant for a given relaxon; for the case shown in Figure 8.1, we see that the acoustic out-of-plane component is composed mainly by long-wavelength phonons close to the Brillouin-zone center.

8.1 Relaxon properties

We analyse the entire eigenvalue spectrum in Figure 8.2, where the contributions to the SMA or the exact thermal conductivities are plotted as a function of the relaxon or phonon lifetimes. We first note that the spectrum of phonon lifetimes (and phonon velocities and mean free paths) is continuous, with a divergence $\tau_v \rightarrow \infty$ for acoustic ZA phonons at the Γ point [43]. This divergence cannot be accurately described with a finite mesh of points for the sampling of the Brillouin-zone (in our case, a full mesh of 128×128 points), resulting in a sparse tail of long-lived phonons on the right side of Figure 8.2A, whose contribution to k^{SMA} is negligible [43]. Instead, relaxon lifetimes (Figure 8.2B) are discrete and sparse, in particular in the long-lifetime region, so that only a small number of relaxons is sufficient to describe thermal transport with high accuracy. On average, relaxon lifetimes are skewed to larger values with

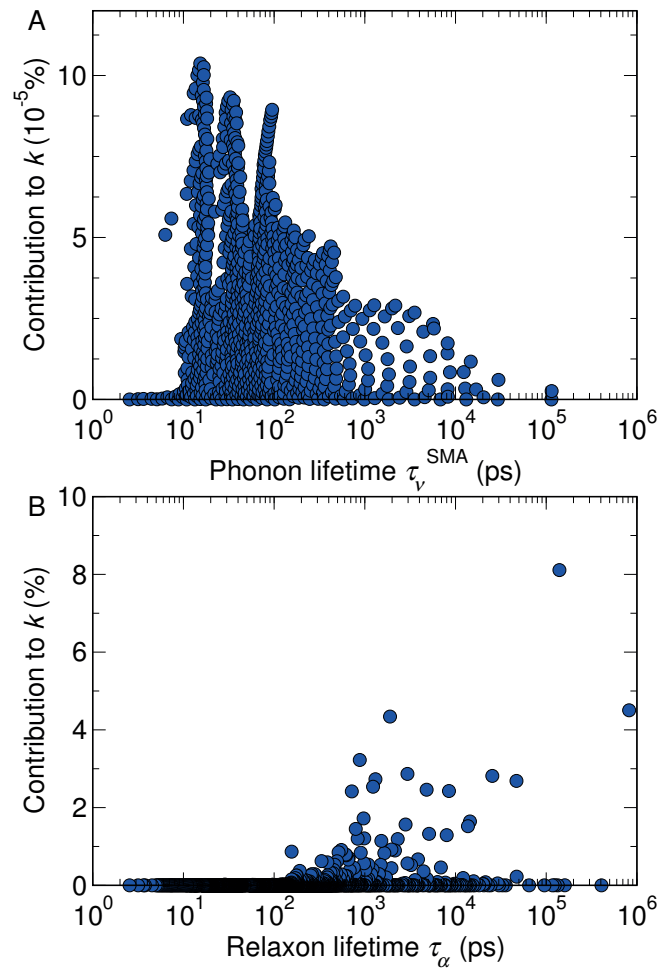


Figure 8.2 – Panel A: spectrum of phonon lifetimes and their contribution to thermal conductivity. Panel B: same for relaxon lifetimes. The relaxons tend to be longer lived than single phonon excitations. The greatest contributions to the thermal conductivity come from relaxons of lifetime larger than 10^3 ps, whereas the phonons have lifetimes mainly in the range 10-100 ps.

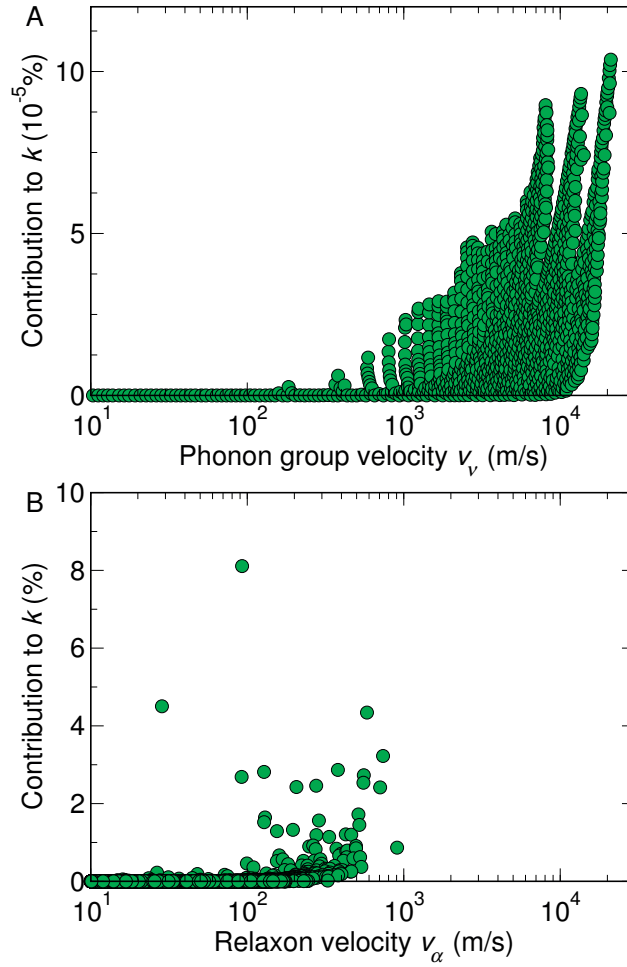


Figure 8.3 – Panel A: spectrum of phonon group velocities and their contributions to thermal conductivity. Panel B: same for relaxon velocities. The relaxons move with velocities much smaller than the speed of sound in graphene (about 20 km/s for the longitudinal acoustic phonon), and most of them move at velocities of 0.1-1 km/s.

respect to phonon lifetimes by at least two orders of magnitude. Therefore, most of the heat flux is dissipated within nano- and micro-second time scales.

Before analysing velocities, we note that the sign of V_α is arbitrary, since both θ_v^α and $-\theta_v^\alpha$ are eigenvectors. As a convention, we select the sign of odd eigenvectors such that V_α is non-negative (and so also Λ_α), noting that in any case the contribution to k would be positive (as V_α^2). Figure 8.3 reveals that the velocities of relaxons are much smaller than those of phonons. The scale of phonon velocities is set by the speed of sound (the group velocity of the longitudinal acoustic phonon is about 20 km/s), whereas the relaxons are slower by two orders of magnitude, indicating that heat is transferred through the material at 0.1-1 km/s.

Finally, we study the relaxon mean free paths in Figure 8.4. As other works reported, phonon mean free paths for graphene are distributed in the 0.1-1 μ m region [60]; this is confirmed

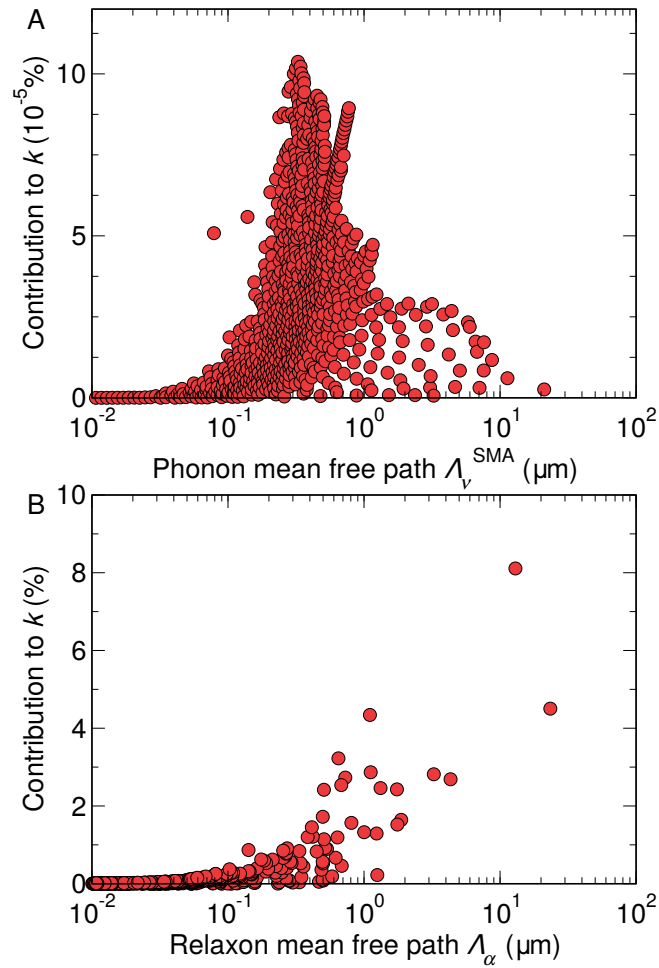


Figure 8.4 – Panel A: spectrum of phonon mean free paths and their contribution to thermal conductivity. Panel B: same for the relaxon mean free paths. Phonon mean free paths are mostly smaller than $1 \mu\text{m}$, whereas relevant relaxon mean free paths are skewed to values larger than $1 \mu\text{m}$. The two largest relaxon mean free paths lie between 10 and $100 \mu\text{m}$.

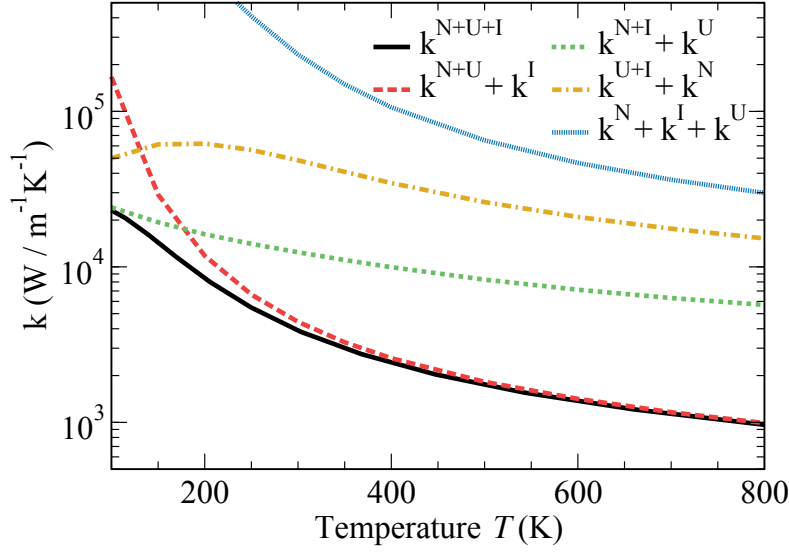


Figure 8.5 – Total thermal conductivity (solid line) and thermal conductivities computed through various Matthiessen sums, where the total sum is given by the sum of the reciprocals (by $k^N + k^U + k^I$ we mean $k^{-1} = (k^N)^{-1} + (k^U)^{-1} + (k^I)^{-1}$). There is no decomposition for which the Matthiessen rule is obeyed at all temperatures.

here and shown in Figure 8.4A. Relaxon mean free paths are longer than phonons' ones, the longest being in the range of tens of μm . The contribution to k is roughly monotonic with the mean free path, and the large increase in τ_α is partly compensated by the decreased V_α . The saturation of relaxons' mean free paths at tens of μm appears to be in contrast with the estimate for saturation lengths of $100\mu\text{m}$ we gave in Section 7.1. However, that estimate is based on the approximated SMA treatment of the surface scattering in graphene ribbons. Since the present study is concerned only with an infinite system, it cannot be properly compared and further studies are required to include the scattering of relaxons at surfaces.

8.2 Failure of the Matthiessen rule

A widely held assumption that is also violated by the exact Boltzmann transport equation is the Matthiessen rule, which states that the total thermal resistivity (i.e. $\frac{1}{k}$) is the sum of the resistivities of each independent scattering mechanism (see Section 3.4). However, the Matthiessen rule is an approximation [132] relying on the possibility of exactly decoupling the scattering mechanisms. To probe numerically this violation, we computed the resistivities of normal, Umklapp and isotopic processes, or any combination of these, and combined them according to Matthiessen rule. In Figure 8.5 we show that, regardless of any particular decomposition, the conductivity obtained by imposing the Matthiessen sum deviates significantly from the exact conductivity. Finally, we verify in our calculations that the total thermal conductivity is always smaller or equal to the Matthiessen sum, as proved in Section 3.4.

Often, modern literature associates Matthiessen's rule to the following relation on the relaxation times:

$$\frac{1}{\tau_v} = \frac{1}{\tau_{1,v}} + \frac{1}{\tau_{2,v}}, \quad (8.1)$$

that is, for each phonon mode its relaxation time can be decomposed into the different scattering sources. This relation is of course derived using the single-mode relaxation time approximation. We remind that in this approximation, the scattering matrix is diagonal:

$$A_{vv'} \approx \frac{\bar{n}_v(\bar{n}_v + 1)}{\tau_v} \delta_{vv'}. \quad (8.2)$$

Since, by construction, the total scattering matrix is just the sum of scattering matrices for the different processes considered, it follows that the total relaxation time of a phonon is the Matthiessen sum of event specific probabilities.

This relation is different from the original formulation from Matthiessen, yet, it still is an approximated relation. In fact, the exact lifetime is the eigenvalue of the scattering matrix, and the exact applicability of Eq. 8.1 on relaxon lifetimes would require that the eigenvalues of the sum of two matrices were the sum of eigenvalues of two matrices - generally not correct when the scattering matrix is not diagonal.

In conclusion, the Matthiessen rule has a varying range of applicability, and when the scattering gives raise to strong correlations between the different mechanisms, which is the case if the relaxon and phonon pictures strongly differ, it is not possible to disentangle them based on the Matthiessen law.

8.3 Divergence of iterative methods

As an added benefit, the direct diagonalisation of the scattering matrix brings clear insight on the numerical stability of the exact solutions of the Boltzmann equation. The iterative method [110, 109, 45] presented in Section 4.3, is often used in literature to study 2D materials, and we remind that it computes the out-of-equilibrium deviation distribution f as a geometric series $f = \sum_{j=0}^{\infty} (-A^{\text{out}})^{-1} A^{\text{in}})^j (A^{\text{out}})^{-1} b$, where A^{out} and A^{in} are respectively the diagonal and the off-diagonal parts of A . The series is convergent if and only if all the eigenvalues λ of $\frac{1}{A^{\text{out}}} A^{\text{in}}$ are $|\lambda| < 1$. In Figure 8.6, we show that in graphene $|\lambda| > 1$ for more than half of the spectrum, proving that the iterative method is numerically unstable for graphene at room temperature. In general, one might expect convergence issues for the iterative method whenever $A^{\text{in}} \gg A^{\text{out}}$, i.e. whenever the relaxon picture differs significantly from the phonon picture.

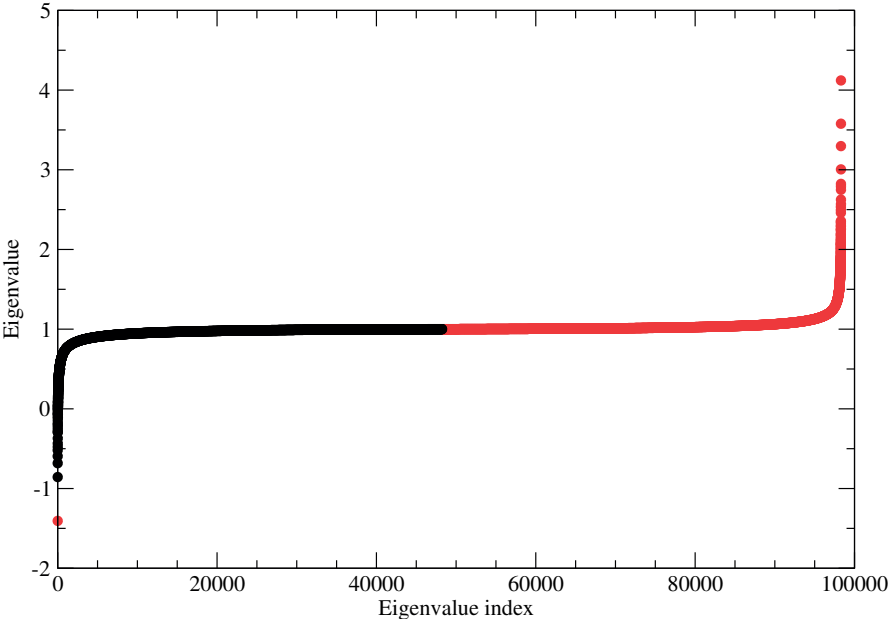


Figure 8.6 – Eigenvalues λ of the matrix $(A^{\text{out}})^{-1} A^{\text{in}}$, for graphene at room temperature, ordered by their magnitude. The red dots, roughly half of the eigenvalue spectrum, indicate eigenvalues $|\lambda| > 1$ that cause a divergence of the iterative solution for the Boltzmann transport equation. Most of the unstable eigenvalues are greater than 1, with only one eigenvalue lower than -1.

9 AiiDA

The last decade has seen computational science rising as a new powerful research paradigm, capable of valuable insights to theories and experiments. This has been possible thanks to the sustained increase in high-performance computational (HPC) capacity and to the accuracy and predictive power of current “quantum engines” (computational codes performing quantum-mechanical simulations). Nowadays simulations are widespread in science and technology and are routinely used in industry and academia to understand, predict, and design properties of complex materials and devices.

Despite this spectacular growth, the researcher’s work has largely remained unchanged, with an approach of managing the simulations manually, where a researcher is preparing calculations and collecting the results in a more or less organised way. This artisanal approach has serious limitation in contemporary research. An example that would be cumbersome to realize is the creation of databases of computational materials properties. The need for such databases arises from the fact that, although there exists versions covering crystal structures, few of them register also properties and they are rarely complete. In particular, the theoretical investigation of this Thesis on thermal properties is part of a larger effort that aims at creating a database of thermal properties. The challenges of this project are twofold: on one hand it needs an understanding of the physical models and the reliability of common approximations, that make calculations faster at the cost of accuracy; on the other hand, it faces the challenges of automatizing the calculation of phonon properties, in order to automatically characterize several thousands of materials.

The creation of such large databases requires a flexible and general, yet easy to use, software infrastructure that helps the user managing the huge amount of data that is created, in particular without the risk of losing information. Moreover, such an infrastructure can be of use even if there is no strict necessity of running a large number of calculations, as in fact has been done for this Thesis. Even in this case, an automating infrastructure provides a significant help to the researcher, by keeping track of the history, ensuring the reproducibility of simulations (quite often missed in computational articles), and facilitating the publishing and sharing of results.

With these considerations in mind, we developed AiiDA [117], an Automated Interactive Infrastructure and Database for computational science. Using AiiDA, the users can access transparently both local and remote computer resources. The platform is easy to use thanks to a high-level python scripting interface and can support different codes by means of a plugin interface. A central goal of AiiDA is the full reproducibility of calculations and of the resulting data chain, which we obtain by a tight coupling of storage and workflow automation. Data analysis and querying of heterogeneous results and of the provenance relationships are made possible and effective by a database design based on directed acyclic graphs and targeted towards data management for high-throughput simulations. Sharing of scientific knowledge is addressed by making it easy to setup and manage local repositories driven by the interests of a given group, providing tools to seamlessly share not only the data itself, but also the full scientific workflows used to generate the results.

In this chapter, we first discuss in detail the general characteristics that any infrastructure should meet to create, manage, analyze and share data and simulations. These requirements are summarized in the four pillars of the ADES model (Automation, Data, Environment, and Sharing). We then describe how these have been addressed by the current open-source implementation of AiiDA, starting from Section 9.3 (one section per pillar). This infrastructure has been intensively developed and used during the Thesis with the goal of simplifying the management of the various results.

9.1 The ADES model for computational science

The aim of this section is to introduce and illustrate the ADES model (see Figure 9.1), in order to motivate our design choices for AiiDA and describe the platform requirements.

The first pillar, **Automation**, responds to the needs of abstracting away the low-level tasks to prepare, submit, retrieve and store large numbers of calculations. It can be subdivided into the following main items:

- **Remote management** Large computations are typically prepared on a user's workstation and executed on HPC clusters. The different steps of job preparation, submission, status check, and results retrieval are repetitive and independent of the specific simulation tool. Therefore, remote management tasks can be abstracted into an Application Programming Interface (API) and automated. Different communication and scheduler implementations can be supported by plugins, all adopting the same API, as we discuss in Section 9.3.
- **Coupling to data** Full reproducibility of calculations requires a *tight coupling of automation and storage*. Decoupling these two aspects leaves the researcher with the error-prone task of manually uploading calculation inputs and outputs to a suitable repository, with the additional risk of providing incomplete information. Instead, if

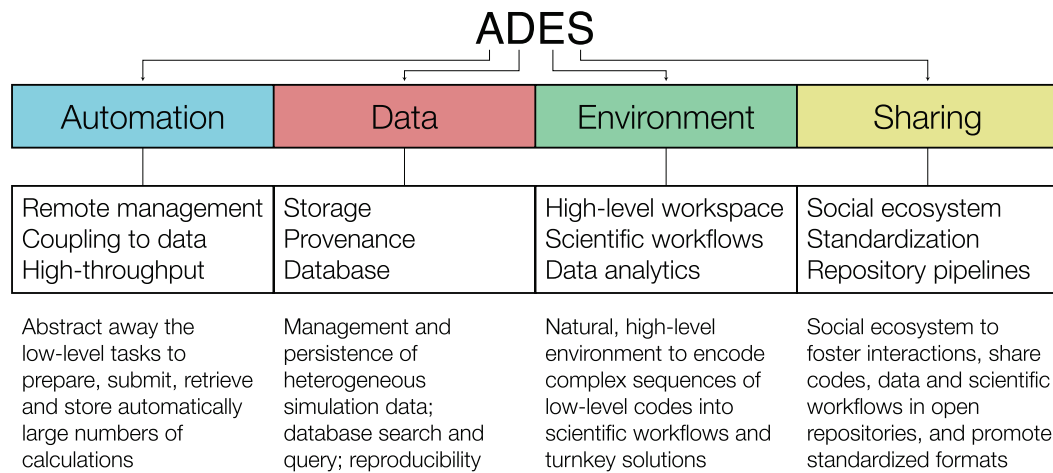


Figure 9.1 – The four pillars of the proposed infrastructure for computational science. At the lower level, an automation framework and an efficient data management solution are needed. At the user level, a high-level environment is coupled with a social ecosystem to stimulate the sharing of codes, data and workflows.

the repository is populated first by the user with all the information needed to run the simulation, the process of creating the input files and running the calculation can be automated and easily repeated. The resulting repositories are therefore necessarily consistent; moreover, almost no user intervention is required to create direct pipelines to shared repositories, as the data is already stored coherently.

- **High-throughput** The main advantage of automation is obtained in situations when screening or parameter sweeps are required, involving thousands of calculations or more. Running and managing them one by one is not feasible. Having a high-level automation framework opens the possibility to run multiple calculations simultaneously, analyze and filter the results. The infrastructure must be able to deal with potential errors arising during the computations, trying to automatically recognize and remedy these whenever possible.

The second pillar, **Data**, concerns the management of the data produced by the simulations and covers the following three core areas:

- **Storage** HPC calculations produce a large amount of heterogeneous data. Files containing input parameters and final results need to be automatically and permanently stored for future reference and analysis. On the other hand, much of the data is required only temporarily (e.g., for check-pointing) and can be discarded at the end of the simulation. Therefore, a code-dependent file-storage policy (optionally customizable by the user) must be adopted to categorize each output file. Anyhow, the existence of intermediate files should be recorded, so that the logical flow of calculations is persisted even when restart files are deleted. If the platform ensures reproducibility of calculations, it is

straightforward to regenerate the intermediate files, if needed. It is also important to store information on the codes that generated the data. If ultimate reproducibility is needed, one could envision to store reference virtual machines or Docker [1] images with the code executables.

- **Provenance** To achieve reproducibility, the platform needs to store and represent the calculations that are executed, together with their input data. An effective data model, though, should not only put emphasis on calculations and data, but also keep track of the causal relationships between them, i.e., the full provenance of the results. For instance, a final relaxed crystal structure is of limited use without knowing how it was obtained. The natural data structure to represent the network of relations between data and calculations is a directed acyclic graph, as we will motivate in greater detail in Section 9.3.
- **Database** Today's typical computational work environment consists of a multitude of files with arbitrary directory structures, naming schemes and lacking documentation. In practice, it is hard to understand and use the information (even by the author after some time) and to retrieve a specific calculation when many are stored. A database can help in organizing results and querying them. The implementation of the data model discussed above, based on directed acyclic graphs, must not be restricted to a specific application, but has to accommodate heterogeneous data. It must be possible to efficiently query any attribute (number, string, list, dictionary, ...) associated to a graph node. Queries that traverse the graph to assess causal relationships between nodes must also be possible. A graph database backend is not required if the requirements above are satisfied. For instance, AiiDA's backend is a relational database with a transitive-closure table for efficient graph-traversal (see Section 9.4).

The first two pillars described above address mainly low-level functionalities. The next two pillars deal instead with user-oriented features. In particular, the pillar **Environment** focuses on creating a natural environment for computational science, and involves the following aspects:

- **High-level workspace** As the researcher's objective is to make new discoveries and not to learn a new code, the infrastructure should be flexible and straightforward to use. For instance, while databases offer many advantages in data-driven computational science, few scientists are expert in their administration. For this reason, the intricacies of database management and connections must be hidden by the an API abstraction layer. Furthermore, by adopting a widespread high-level programming language (such as Python) one can benefit of mature tools for inserting and retrieving data from databases [2, 3, 4]. The infrastructure must also be modular: a core providing common low-level functionalities, and customizable plugins to support different codes.
- **Scientific workflows** Much of the scientific knowledge does not merely lie in the final data, but in the description of the process, i.e., the "scientific workflow" used to obtain

them. If these processes can be encoded, then they can be reused to compute similar quantities in different contexts. A workflow specifies a dependency tree between calculation steps, that may not be defined at the start, but depend on intermediate results (e.g., an iterative convergence with an unpredictable number of iterations). Therefore, the infrastructure should automatically generate dependent calculations only when their inputs are available from earlier steps, evaluating dependencies at run-time. The integration of the scientific workflows with the other infrastructure pillars helps the users to focus on the workflow logic rather than on the details of the remote management. As an additional benefit, the automatic storage of the provenance during execution provides an implicit documentation of the logic behind the results.

- **Data analytics** Application-driven research has the necessity of using dozens of different tools and approximations. Nevertheless, results obtained with different codes often require the same post-processing or visualization algorithms. These data types (e.g., crystal structures or band structures) should be stored in the same common format. The infrastructure can then either provide data analytics capabilities to perform operations on them, or even better facilitate the adoption of existing libraries. This result can be achieved by providing interfaces to external tools for data processing and analytics (e.g. [35, 111] for crystal structures), regardless of the specific simulation code used to generate the data.

The fourth pillar, **Sharing**, envisions the creation of a social ecosystem to foster interaction between scientists, in particular for sharing data, results and scientific workflows:

- **Social ecosystem** The envisioned framework should be an enabling technology to create a *social ecosystem* in computational research. Data access policies must be considered with great care. Researchers prefer at times to keep their data private (while protecting information in pending patents or unpublished data), but sharing with collaborators or on a public repository should occur with minimal effort, when desired. Beside data sharing, a standardized plugin interface should be provided. Plugin repositories can be set up, to which users can contribute to share workflows, handlers for new data formats, or support for new simulations codes. By this mechanism, scientists will be able to engage in *social computing*, parallel to the developments in the mobile app and web ecosystems.
- **Standardization** In order to facilitate data exchange, standard formats should be agreed upon and adopted for data sharing (e.g. [105]). Even when multiple standards exist, a hub-and-spoke configuration can be envisaged, where each new code has the task to provide the data in an established format. On the other hand, it is important that suitable ontologies are defined (i.e., simplifying, the names and physical units of the quantities to store in a given repository, together with their meaning). Ontologies are field-specific and their definition must be community-driven (an example of an ongoing

effort is the TCOOD [5] database). The infrastructure can be useful in this respect both as an inspiration for the ontology, and as a testing environment containing a set of simulated use cases.

- **Repository pipelines** As more repositories emerge, it is important to develop the ability to import or export data directly, either through REST interfaces or via suitably defined protocols. If formats and ontologies are established, the platform must simply convert the data and its provenance in the specified format. Contributing to external databases becomes straightforward and the platform becomes a facilitator for the creation of shared repositories.

9.2 The AiiDA infrastructure

The ADES model described in the previous section aims at defining an integrated infrastructure for automating, storing, managing and sharing simulations and their results. Until now, we discussed the model at an abstract level, so as to highlight the generality of the requirements. In order to provide researchers with an effective tool to manage their efforts, we developed a Python infrastructure, “AiiDA”, (available online at <http://www.aiida.net>) that is distributed open-source. In the following, we describe the implementation details of AiiDA, with particular emphasis on how the requirements of Section 9.1 have been met.

We start by outlining the architecture of AiiDA, schematically represented in Figure 9.2. AiiDA has been designed as an intermediate layer between the user and the HPC resources, where automation is achieved by *abstraction*.

The core of the code is represented by the AiiDA API, a set of Python classes that expose to the user an intuitive interface to interact with the main AiiDA objects — calculations, codes and data — hiding the inhomogeneities of different supercomputers or data storage solutions. The key component of the API is the Object–Relational Mapper (ORM), a layer that maps AiiDA storage objects into python classes. Using the ORM, these objects can be created, modified and queried via a high-level interface which is agnostic of the detailed storage solution or of the SQL query language. The details of the storage, composed of both a relational database and a file repository, are discussed in Section 9.4.

The user interacts with AiiDA in different ways: using the command line tool `verdi`, via the interactive python shell, or directly through python scripts (more details in Section 9.5). Most components are designed with a plugin architecture (Section 9.5). Examples of features that can be extended with new plugins include the support of new simulation codes, management of new data types, and connection to remote computers using different job schedulers.

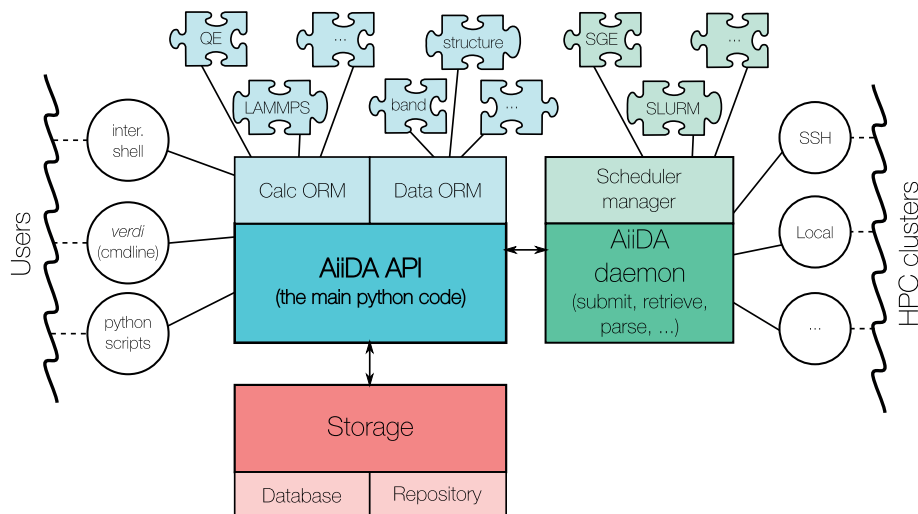


Figure 9.2 – The main components of the AiiDA infrastructure and their interactions. The core AiiDA component is the API, whose ORM represents stored objects as python classes. AiiDA supports any computational code and data type via a plugin interface. The AiiDA daemon is a background process that takes care of most automated operations such as job submission, scheduler state check, file retrieval and parsing. It interacts with the remote clusters via different channels (local, ssh, ...) using the appropriate scheduler plugins.

9.3 Automation in AiiDA

The AiiDA daemon

The daemon is one important building block of AiiDA: it is a process that runs in the background and handles the interaction with HPC clusters (selecting the appropriate plugins for the communication channels — like SSH — or for the different job schedulers) and takes care of all automation tasks. Once the daemon is started, it runs in the background, so that users can even log out from their accounts without stopping AiiDA. Internally, it uses `celery` [6] and `supervisor` [7] to manage asynchronous tasks.

The fundamental role of the daemon is to manage the life cycle of single calculations. The management operations are implemented in the `aiida.execmanager` module and consists in three main tasks: 1) submission of a new job to a remote computer, 2) verification of the remote job scheduler state, and 3) retrieval and parsing of the results after a job completion. These steps are run independently. If several calculations are running on the same machine, they are grouped in order to open only one remote connection and avoid to overload the remote cluster.

The user can follow the evolution of a calculation without connecting directly to the remote machine by checking the `state` of a calculation, an attribute that is stored in the database and is constantly updated by the daemon. In particular, every calculation is initialized in a `NEW` state. A call to the `calc.submit()` method brings `calc` to the `TOSUBMIT` state. As soon as the

daemon discovers a new calculation with this state, it performs all the necessary operations to submit the calculation and then sets the state to `WITHSCHEDULER`. Periodically, the daemon checks the remote scheduler state of `WITHSCHEDULER` calculations and, at job completion, the relevant files are automatically retrieved, parsed and saved in the AiiDA storage. Finally, the state of the calculation is set to `FINISHED`, or `FAILED` if the parser detects that the calculation did not complete correctly. Beside the aforementioned states, other transition states exist (`SUBMITTING`, `RETRIEVING`, `PARSING`) as well as states to identify failures occurred in specific states (`SUBMISSIONFAILED`, `RETRIEVALFAILED` and `PARSINGFAILED`).

Transports and schedulers

As discussed in the “Remote management” section of the “Automation” pillar, in AiiDA we define an abstract API layer with methods to connect and communicate with remote computers and to interact with the schedulers. Thanks to this API, the internal AiiDA code and the user interface are independent of the type of connection protocol and scheduler that are actually used.

The generic job attributes valid for any scheduler (wall clock time, maximum required memory, name of the output files, ...) are stored in a common format. For what concerns schedulers, early work in the specification of a middleware API has been done in the Open Grid Forum [8] with, e.g., the DRMAA [125] and the SAGA APIs, and similar efforts have been done by the UNICORE [9] and gc3pie [10] projects. In AiiDA, we have taken inspiration from these efforts. We provide appropriate plugins to convert the abstract information to the specific headers to be written at the top of the scheduler submission file. Moreover, the plugins provide methods that specify how to submit a new job or how to retrieve the job state (running, queued, ...). Plugins for the most common job schedulers (Torque [11], PBS Professional [12], SLURM [13], SGE or its forks [28]) are already provided with AiiDA.

The scheduler plugins and the daemon, then, rely on the transport component to perform the necessary remote operations (file copy and transfer, command execution, ...). Also in this case, we have defined an abstract API specifying the standard commands that should be available on any transport channel (connection open and close, file upload and download, file list, command execution, ...). Plugins define the specific implementation. With AiiDA, we provide a `local` transport plugin, to be used if AiiDA is installed on the same cluster on which calculations will be executed. This plugin performs directly command execution and file copy using the `os` and `shutil` Python modules. We also provide a `ssh` transport plugin to connect to remote machines using an encrypted and authenticated SSH channel, and SFTP for file transfer. In this case, AiiDA relies on `paramiko` [14] for the Python implementation of the SSH and SFTP protocols.

The appropriate plugins to be used for each of the configured computers are specified only once, when user configures for the first time a new remote computer in AiiDA.

9.4. Data in AiiDA: database, storage and provenance

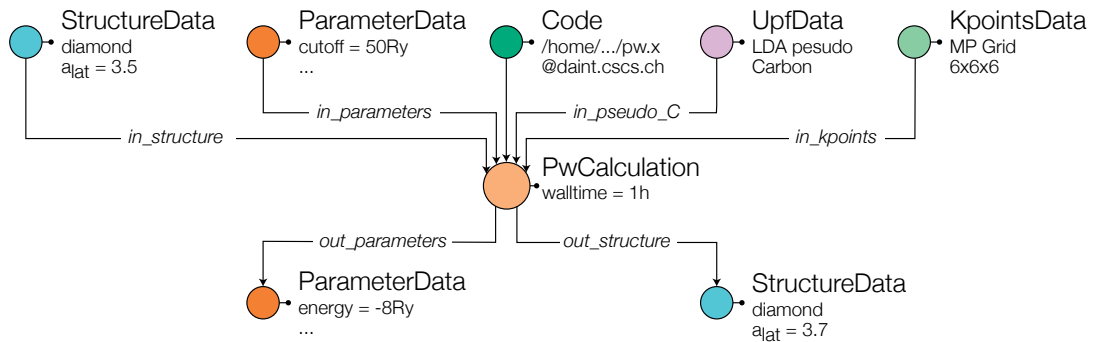


Figure 9.3 – A simple example of how a calculation, the executable code and input/output data are represented as nodes in a graph. Labeled links between nodes represent logical relationships: either inputs or outputs. The code in input of a calculation represents the executable that is launched. In this example, a Quantum ESPRESSO code is used to relax a diamond crystal, using further parameters as input nodes (cutoffs, a mesh of k -points, a pseudopotential in UPF format for carbon, ...). In output, two nodes are produced: a list of result parameters (e.g., the total energy) and an output relaxed structure. This node can in turn be used as input of new calculations.

9.4 Data in AiiDA: database, storage and provenance

The data model in AiiDA

The core concept of the AiiDA data model, partially inspired by the Open Provenance Model [103], is that any calculation acts as a function (with the meaning this word has in mathematics or in a computer language), performing some manipulation on a set of input data to produce new data as output.

We thus represent each fundamental object, `Calculation` and `Data`, as a node in a graph. These nodes can be connected together with directional and labeled links to represent input and output data of a calculation. Direct links between `Data` nodes are not allowed: any operation (even a simple copy) converting data objects to other data objects is a function and must thus be represented by an intermediate `Calculation` node. We define for convenience a third fundamental object, the `Code`, representing the executable file that is run on the HPC resource. Each `Calculation` has therefore a set of `Data` nodes and a `Code` node as input (Figure 9.3). As the output `Data` nodes can in turn be used as input of new calculations, we are effectively modeling a Directed Acyclic Graph (DAG) representing the chain of relationships between the initial data (e.g., a crystal structure from an experimental database) and the final results (e.g., a luminescence spectrum) through all the intermediate steps that are required to obtain the final result: the provenance information of the data is therefore saved. (The graph is acyclic because links represent a causal connection, and therefore a loop is not allowed.)

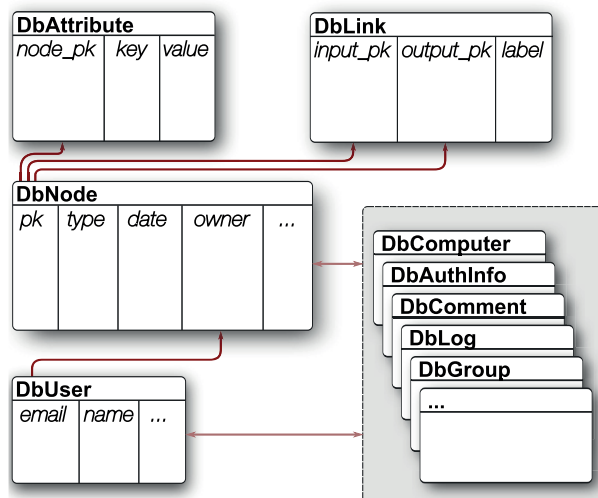


Figure 9.4 – The most relevant tables of the AiiDA database schema. The **DbNode** table contains an entry for each node, with only a limited set of columns such as the ID (or primary key, PK), a string identifying the type of node (Calculation, Data, Code, or a subclass), the creation date, and the owner (a foreign key to the **DbUser** table). All other attributes are stored in the **DbAttribute** table, as described in the text. A third **DbLink** table stores all the links (each link being identified by the PK of the input and output endpoints, and by a label). Other tables exist in the database (to store computers, authorization information, comments, log messages, groups, ...) typically referencing both to nodes and users (e.g., the comment of a given user on a given node).

The AiiDA database

Given that AiiDA represents data in terms of DAGs, we need to choose an efficient way to save them on disk. The objects we need to store are the nodes and the links between them. Each node needs to contain all the information describing it, such as lists of input flags, sets of parameters, list of coordinates, possibly some files, etc. Therefore, the actual implementation must support the storage of arbitrary lists of files, and of attributes in the form `key=value` (of different types: strings, numbers, lists, ...) associated to each node. One simple solution could consist in storing one file per node, containing all node attributes in a suitable format, and then store all the links in another file. However, this storage type is clearly not efficient for querying, because in the absence of a suitable indexing system every search requires disk access to each file. A database, instead, can speed up queries significantly. To have a net benefit however, the database must be suitably configured for the specific type of data and queries that are most likely expected. Moreover, different database solutions exist, each of them tailored to specific types of data.

After benchmarking different solutions, we have chosen to adopt a SQL backend for the AiiDA database. In particular, MySQL [15] and PostgreSQL [16] are fully supported, together with the file-based backend SQLite [17] (even if the latter is not suited for multiple concurrent

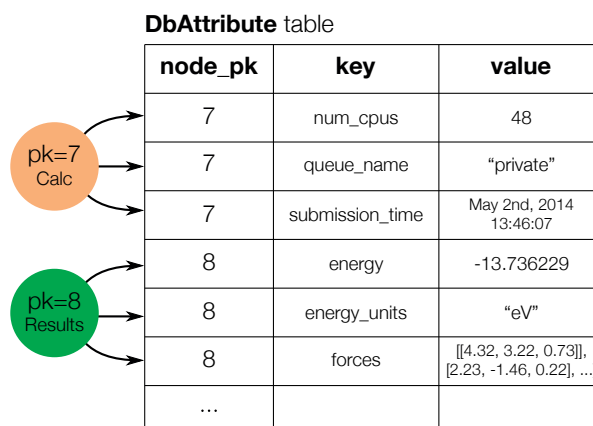


Figure 9.5 – Schematic representation of an arbitrary attribute data in a SQL EAV table by means of our `DbAttribute` table.

accesses, and its usage is limited to testing purposes). The database is complemented by a file repository, where arbitrary files and directories can be stored, useful for large amounts of data that do not require direct querying, and is going to be discussed in details later in Section 9.4. In our implementation, the three main pieces of information of the DAG (nodes, links, and attributes) are stored in three SQL tables, as shown in Figure 9.4.

The main table is called `DbNode`, where each entry represents a node in the database. Only a few static columns are defined: an integer identifier (ID), that is also the Primary Key (PK) of the table; a universally-unique identifier or UUID, a “type” string to identify the type of node (`Calculation`, `Data`, `Code`, or one of their subclasses, see Section 9.5). A few more columns exist for “universal” information such as a label, the creation and modification time, and the user who owns the node (a foreign link to the `DbUser` table, storing user details).

A second table, `DbLink`, keeps track of all directional links between nodes. Each entry contains the PKs of the input and output nodes of the link, and a text field for the link label, that distinguishes the different inputs to a calculation node (e.g., a crystal structure, a set of parameters, a list of k-points, etc.). For instance, link names used for a Quantum ESPRESSO calculation can be seen in Figure 9.3.

A third table, `DbAttribute`, is used to store *any* possible attribute that further characterizes each node. Some examples of attributes could be: an energy value, a string for the chemical symbol of each atom in a crystal structure, a 3×3 matrix for the components of the crystal vectors, an integer specifying the number of CPUs that we want to use for a given calculation, or others.

The `DbAttribute` table is schematically represented in Figure 9.5. Each entry represents one attribute of a node, and for each attribute we store: the PK of the node to which this attribute belongs; the *key*, i.e. a string defining the name of the property that we want to store

(e.g. “energy”, “atom_symbols”, “lattice_vectors”, “num_cpus”, ...); and the *value* of the given property. Internally, the table has a more complicated schema allowing for extended flexibility:

- Different primitive data types can be stored (booleans, integers, real values, strings, dates and times, ...)
- Arbitrary Python dictionaries (sets of key=value pairs) and lists can be stored, and any element of the list or of the dictionary can be directly and efficiently queried (even in case of multiple depth levels: lists of lists, lists of dictionaries, ...)

We emphasize that by means of this table we achieve both flexibility, by being able to store many data types as an attribute, and preserving query efficiency, since any element in the database can be queried directly at the database level (making full use of indexes, etc.).

Since each row of the `DbAttribute` table is an internal property of a single node, we enforce that attributes cannot be modified after the respective node has been permanently stored (for example, we do not want the number of CPUs of a calculation to be changed after the calculation has been stored and executed). However, the user will often find it useful to store custom attributes for later search and filtering (e.g., a tag specifying the type of calculation, the spacegroup of a crystal structure, ...). To this aim, we provide a second table (`DbExtra`) that is identical to the `DbAttribute` table (and therefore it has the same data storage and querying capabilities). The content of the `DbExtra` table, though, is not used internally by AiiDA, and is at complete disposal of the user.

Besides the three tables `DbNode`, `DbLink` and `DbAttribute` that constitute the backbone of the database structure, there are a few other tables that help data management and organization. The most relevant are:

- `DbUser` contains user information (name, email, institution).
- `DbGroup` defines groups of nodes to organize and gather together calculations belonging to the same project, pseudopotentials of the same type, etc.
- `DbComputer` stores the list of remote computational resources that can be used to run the simulations.
- `DbAuthInfo` stores the authorization information for a given AiiDA user (from the `DbUser` table) to log in a given computer (from the `DbComputer` table), like the username on the remote computer, etc.
- `DbWorkflow`, `DbWorkflowData`, `DbWorkflowStep` are the tables that store workflow-related information.
- `DbPath` is the transitive closure table, described in the next section.

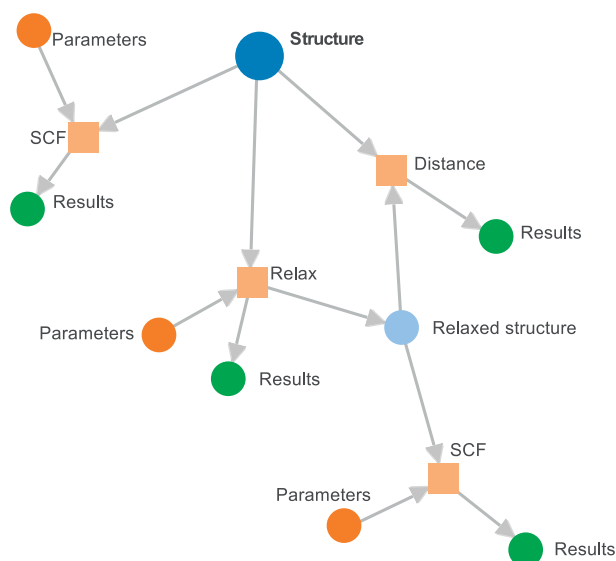


Figure 9.6 – A schematic example of a possible graph inside the AiiDA database. An initial crystal structure (blue node on the top of the figure) is used both for a total energy calculation (SCF) and for a structural relaxation calculation (Relax). Each calculation has a set of input parameters (orange dots) and of output results (dark green dots). The relaxation calculation also produces another crystal structure, used as input for a new SCF calculation. Moreover, the two structures in the graph are both taken as input from a calculation that computes a suitably-defined “distance” between them.

Graph database: querying the provenance

An example of a simple graph that can be stored in AiiDA is shown in Figure 9.6, where four different calculations have been run with different inputs producing a set of output results, and where some output nodes have been used as input of new calculations. Using the database data model described in the previous section, we can store DAGs with arbitrary queryable attributes associated to each node. However, there is another type of query specific to graph databases, related to the graph connectivity: given two nodes, to determine the existence of a path connecting them. This is particularly relevant for simulations in Materials Science: typical queries involve searching for crystal structures with specific computed properties, but the number of intermediate steps (i.e., Calculation nodes) between a structure data node and the final result can be large and not even predictable (e.g., if multiple restarts are required, ...). This type of searches requires in practice to query the provenance of the data in the database.

Sophisticated and efficient *graph traversal* techniques have been developed to discover the existence of a path between two nodes, and graph databases (e.g., Neo4j [18]) implement these functions at the database level, however they require the use of custom querying languages. Instead, we address the graph traversal problem within a SQL database by incrementally evaluating a **transitive closure** table (that we called DbPath). This table lists the “paths”, i.e.,

all pair of nodes (“parent” and “child”) that are connected together in the graph through a chain of links. The table is automatically updated every time a link is added, updated or removed from the `DbLink` table, by means of database triggers that we have developed for the three supported backends (SQLite, MySQL and PostgreSQL). The algorithm for the update of the transitive closure table has been inspired by Ref. [58].

Obviously, the `DbPath` table allows for fast queries on the data “history”, at the expense of occupying additional disk space for its storage. The size of the table can in general become very large; however, in Material Science applications, we typically do not have a single dense graph where all nodes are interconnected; instead, one often creates many small graphs of the type of Figure 9.6. This means that the size of the `DbPath` table will remain roughly linear in the number of nodes in the graph. After benchmarking, we have chosen the solution described above as a good compromise between storage and query efficiency.

Database vs. file repository

The storage of attributes in the database discussed previously allows for query efficiency, at the price of disk space (for additional information like indexes, data types, ...) and of efficiency in regular operations (retrieving a large list from the database is slower than retrieving a file containing the same list). For large matrices, therefore, a threshold exists above which the advantages of faster query speed are not justified anymore. Moreover, the single entries of a large matrix (like the electron charge density discretised on a grid) are often of little interest for direct querying. In such cases it is convenient to store data in a file and rely on the file system for I/O access. This is especially appropriate when the data should be used as an input to another calculation and a fast read access is required.

For these reasons, AiiDA complements the database storage with a file repository (see Figure 9.2), confined within a folder configured during the setup phase of AiiDA. Every time a new node is created, AiiDA automatically creates a subfolder for the specific node. Any file, if present, associated with the node will be stored therein.

Storing information as files or in the database is left as a choice for the developers of the specific subclass of the `Data` of `Calculation` nodes (plugins are discussed in Section 9.5), but in order to maximize efficiency, it should follow the guideline discussed above. Some examples of the choices made for some AiiDA `Data` plugins can be found in Section 9.5.

9.5 The scientific environment in AiiDA

The ORM

AiiDA is written in Python, a powerful object-oriented language. The materials simulation community has been moving towards Python in recent years, due to its simplicity and the large availability of libraries for visualization, text parsing, and scientific data processing [82, 35, 19].

An important component of the AiiDA API is the Object-Relational Mapper (ORM), which exposes to the user only a very intuitive Python interface to manage the database. The main class of the AiiDA ORM, `Node`, is used to represent any node in the graph. Each instance of the `Node` class internally uses Django to perform database operations, and complements it with methods for accessing the file repository. The low-level interaction with the database uses the Django framework [2].

The main functionalities of the `Node` class are:

- It provides a direct access to the node attributes, accessible as a Python dictionary by using the `node.attrs()` method. The method also properly recreates lists and dictionaries that were stored in expanded format at the database level (lists and dictionaries are not natively supported in the chosen databases). Similar methods allow the user to read and write user-defined attributes in the `DbExtra` table.
- It provides direct access to the repository folder containing the files associated to each `Node`.
- It provides a caching mechanism that allows the user to create and use the `Node` even before storing it in the database or on the repository folder, by keeping the files in a temporary sandbox folder, and the attributes in memory. This is particularly useful to test the generation of the input files by AiiDA without the need to store test data in the database. Only after the `node.store()` call, all the data is permanently stored in the AiiDA database and repository and no further modifications are allowed. A similar caching mechanism has also been implemented to keep track of links between nodes before storing.
- It provides an interface for querying nodes with specific attributes or with specific attribute values, or nodes with given inputs or outputs, etc.
- It provides methods (`.inp` and `.out`) to get the list of inputs and outputs of a node and similarly the list of all parent and child nodes using the transitive closure table.

The plugin interface

To support a new type of calculation or a new kind of data (e.g. a band structure, a charge density, a set of files, a list of parameters, ...), one simply needs to write an AiiDA plugin. A plugin is simply a python module file, containing the definition of a subclass of the AiiDA classes, sitting in an appropriate folder; AiiDA automatically detects the new module and uses it.

All different types of nodes are implemented as subclasses of the `Node` class. At a first subclass level we have the three main node types: `Calculation`, `Code` and `Data`. Each of them is further subclassed by plugins to provide specific functionalities. In particular, instances

of Code represent a specific executable file installed on a given machine (in the current implementation, there are no further subclasses). Each subclass of `Calculation`, instead, supports a new simulation software and contains the code needed to generate the software-specific input files starting from the information stored in the AiiDA database. Moreover, it can also provide a set of software-dependent methods (like `calc.restart()`, ...) that make it easier for the user to perform routine operations. Finally, the `Data` class has a subclass for each different type of data that the user wants to represent. The specific subclass implementation determines the possible user operations on the data, and whether the information is going to be stored in the database as attributes or in the file repository. We report here a description of some of the most relevant `Data` subclasses distributed with AiiDA:

- `ArrayData`: it is used to store (large) arrays. Each array is stored on disk as a binary, portable, compressed file using the Python `numpy` module [126]. Some attributes are stored in the `DbAttribute` table for fast querying (like the array name and its size). Subclasses use the same storage model, but define specific methods to create and read the data (e.g., the `KpointsData` class has methods to detect a structure cell, build the list of special k -points in k space and create paths of k -points, suitable for plotting band structures, using for instance the standard paths listed in Ref. [120]).
- `ParameterData`: it is used to store the content of a Python dictionary in the database. Each key/value pair is stored as an attribute in the `DbAttribute` table, and no files are stored in the repository.
- `RemoteData`: this node represents a “link” to a directory on a remote computer. It is used for instance to save a reference to the scratch folder on the remote computer in which the calculation was run, and acts as a placeholder in the database to keep the full data provenance, for instance if a calculation is restarted using the content of that remote folder. No files are written in the AiiDA repository, but the remote directory absolute path is stored as an attribute.
- `FolderData`: this node represents a folder with files. At variance with `RemoteData`, files are stored permanently in the AiiDA repository (e.g., the outputs of a finished calculation retrieved from the remote computer).
- `StructureData`: this node represents a crystal structure. The 3×3 coordinates of the lattice vectors, the list of atoms and their coordinates, and any other information (atomic masses, ...) are saved as attributes for easy querying. (For very large structures, a different data model may be more efficient.) Methods are provided for standard operations like getting the list of atoms, setting their positions and masses, converting structures to and from other formats (e.g. the `Atoms` class of the ASE Atomistic Simulation Environment [35]), obtaining the structure from an external database (like ICSD [20] or COD [67]), getting the spacegroup using SPGLib [19], etc.

Finally, we emphasize that the plugin interface is not limited to the ORM, and a similar plugin-based approach applies to other AiiDA components, like the connection transport channel and the schedulers (as discussed in Section 9.3).

User interaction with AiiDA

We provide a few different interfaces to interact with AiiDA. The most commonly used is the `verdi` command line utility. This executable exposes on the command line a set of very common operations, such as performing the first installation; reconfiguring AiiDA; listing or creating codes, computers and calculations; killing a calculation; starting/stopping the daemon, ... The `verdi` tool is complemented by a Bash completion feature to provide suggestions on valid commands by pressing the TAB key. Moreover, an inline help provides a list of existing commands and a brief description for each of them. The advantage of `verdi` is to expose basic operations to the user without requiring any knowledge of Python or other languages.

In order to access the full AiiDA API, however, the best approach is to write Python scripts. The only difference with respect to standard python scripts is that a special function `load_dbenv()` needs to be called at the beginning of the file to instructs Python to properly load the database. Once this call has been made, any class from the `aiida` package can be loaded and used. If the users do not want explicitly the `load_dbenv()` call in the python code, then they can run the script using the `verdi run` command. In this case, the AiiDA environment and some default AiiDA classes are automatically loaded before executing the script.

A third interface is the interactive python shell that can be loaded using the command `verdi shell`. The shell is based on IPython [115] and has the advantage to automatically load the database environment; at the same time, it already imports by default some of the most useful classes (e.g. `Node`, `Calculation`, `Data`, `Group`, `Computer`, ...) so that they are directly available to the user. TAB completion is available and very useful to discover methods and attributes. Moreover, the documentation of each class or method (written as Python “doc-strings”) is directly accessible.

Scientific workflows

As introduced in Section 9.1, many tasks in scientific research are standard and frequently repeated, and typically require multiple steps to be run in sequence. Common use cases are parameter convergence, restarts in molecular dynamics simulations, multi-scale simulations, data-mining analysis, and other situations when results of calculations with one code are used as inputs for different codes. In such cases, it is beneficial to have a system that encodes the workflow and manages its execution [21, 22, 23, 24, 129].

In order to fully integrate the workflows within the ADES model, we implement a custom engine into AiiDA, by which the user can interact with all AiiDA components via the API.

This engine is generic and can be used to define any computational workflow. Specific automation schemes, crafted for selected applications (equation of states, phonons, etc...) are implemented within each workflow and can be developed directly by the users.

AiiDA workflows are subdivided into a number of steps. One or more calculations can be associated to each step; these are considered to be independent and are launched in parallel. Instead, different steps are executed sequentially and the execution order is specified by “forward” dependency relationships: In other words, each “parent” step must specify the step to be executed next. The execution of the “child” step is delayed until all calculations associated to the parent have completed. We emphasize that dependency relationships are defined only between steps. Dependencies between calculations are implicit, with the advantage of allowing for both parallel and serial simulation streams.

Within a step, beside creating calculations and associating them to the current step, any other Python (and AiiDA) command can be executed. This gives maximum flexibility to define complex workflow logics, especially if the outputs of a calculation in a parent step require some processing to be converted to the new calculation inputs. Moreover, a step can define itself as the next step to be executed, providing support for loops (even conditional ones, where the number of iterations depends on the calculations results).

A key feature, modularity, completes AiiDA workflows: within each step, the user can associate not only calculations, but also subworkflows. The advantage is the possibility to reuse existing workflows that perform specific tasks, so as to develop only missing features. For instance, let us assume that we developed a workflow “A” that performs a DFT calculation implementing code-specific restart and recover routines in order to make sure convergence is achieved. Then, a workflow “B” that calculates the energy of a crystal at different volumes (to obtain its equation of state) does not need to reimplement the same logic, but will just reuse “A” as a subworkflow. “B” can in turn become a subworkflow of a higher-level workflow “C” that, for instance, compares the equation of state calculated at different levels of approximation. The combination of parallel and serial execution, conditional loops, and modularity, makes the workflows general enough to support any algorithm.

From the implementation point of view, the AiiDA workflow engine is provided by a generic `Workflow` class, that can be inherited to define a specific workflow implementation. Workflow steps are special class methods identified by the `@step` decorator. The base class also provides dedicated methods to associate calculations and workflows to the current step. In every step, a call to the `self.next()` method is used to define dependencies between steps. This method accepts as a parameter the name of the following step. The name is stored in the database, and the corresponding method is executed by the daemon only when all calculations and subworkflows of the current step have finished.

In analogy with calculations, AiiDA uses states to keep track of workflows and workflow steps (`RUNNING`, `FINISHED`, ...). The AiiDA daemon handles all the workflow operations (submission of each calculation, step advancement, script loading, error reporting, ...) and the transitions

between different workflow states.

In the long term, we envision integrating into AiiDA many new and existing methods in the form of workflows (e.g., training interatomic potentials [40], crystal structure prediction algorithms [65, 116], ...), so that the researcher can focus on materials science and delegate to AiiDA the management of remote computers, the appropriate choice of code-specific parameters, and dealing with code-specific errors or restarts.

Querying

A relevant aspect of a high-level scientific environment is the possibility of running queries on the data stored in AiiDA without the need to know a specific (and typically complex) query language. To this aim, we have developed a Python class, called the `QueryTool`, to specify in a high-level format the query to run. For instance, it is possible to specify a filter on the node type (e.g., to get only crystal structures); to filter by the value of a specific attribute or `DbExtra` table entry (e.g., to select structures with a specific spacegroup); or to filter by a specific attribute in one of the linked nodes (e.g., to get structures on which a total-energy calculation was run, and the energy was lower than a given threshold). Queries can also take advantage of the transitive closure table, setting filters on attributes of nodes connected to the one of interest by an unknown number of intermediate links (e.g., if the result of the calculation was obtained after an unknown number of restarts). As an example, a complex query that can be run with AiiDA is: *give me all crystal structures containing iron and oxygen and with a cell volume larger than $X \text{ \AA}^3$, that I used as input for a sequence of calculations with codes Y and Z to obtain the phonon band structure, for which the lowest phonon frequency that was obtained is positive, and for which the DFT exchange-correlation functional used was LDA*. Other complex queries can be specified using the `QueryTool` in a format that is easy both to write and to read.

Documentation and unit testing

A key component of a productive scientific environment is a complete and accurate code documentation. For this reason, AiiDA is complemented by an extensive documentation. Each class, method and function has a Python docstring that describes what the function does, the arguments, the return values and the exceptions raised. These docstrings are accessible via the interactive shell, but are also compiled using the Sphinx [25] documentation engine into a comprehensive set of HTML pages (see Figure 9.7). These pages are distributed with the code (in the `docs/` subfolder) and also available online at <http://aiida-core.readthedocs.org>. Moreover, we also provide in the same format, using Sphinx, a complete user documentation of the different functionalities, supported databases, classes and codes, together with tutorials covering the installation phase, the launch of calculations and workflows, data analysis, ... The user guide is also complemented by a developer's guide that documents the API and contains tutorials for the development of new plugins.

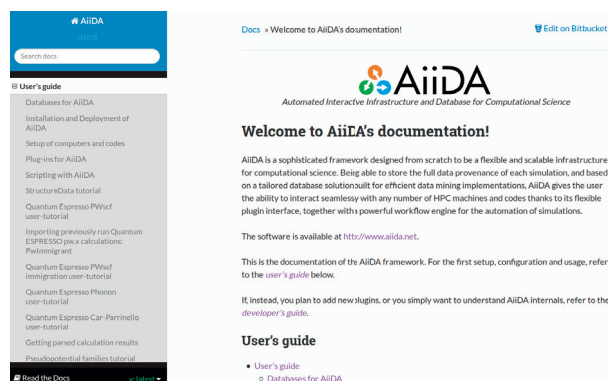


Figure 9.7 – The first page of the AiiDA documentation. Different sections are aimed at the end users (with examples and tutorials) and at developers (with the documentation of classes and methods, and tutorials for new plugin development).

Moreover, to simplify the code maintenance, we implement a comprehensive set of unit tests (using the Python `unittest` module), covering the different components of AiiDA described in Figure 9.2.

9.6 Sharing in AiiDA

The fourth pillar introduced in Section 9.1 aims at enabling a social ecosystem where it becomes easy to share tools and results, such as data, codes, and workflows. In order to preserve the authorship and privacy of the data of each researcher, we implemented a model in which each user or group of users can install their own local AiiDA instance. All data and calculations are accessible only to people with direct access to the instance and therefore remain private. In order to enable sharing of the database (or parts of it) with collaborators, we provide functionality to export a portion of the database to a file, and then to import it in a different instance of AiiDA. In this way several groups in a collaboration may contribute to a common repository, open to the entire project, while retaining their private portions as needed. This approach simplifies issues of user- and group-level security. To avoid conflicts during this procedure, AiiDA assigns a Universally Unique Identifier (UUID) to each node as soon as it is locally created. In fact, while for internal database usage an auto-incrementing integer PK is the most efficient solution to refer to a database row, the PK is not preserved when a node is transferred to a different database. Instead, the first node to be created will always have $PK=1$, the second $PK=2$, and so on. A UUID is instead a hexadecimal string that may look like the following: `e3d21365-7c55-4658-a5ae-6122b40ad04d`. The specifications for creating a UUID are defined in RFC 4122 by IETF [26], and they guarantee that the probability that two different UUIDs generated in different space and time locations can be assumed to be zero. In this way, we can use the UUID to identify the existence of a node in the DB; at import time, it is only verified whether a node with the same UUID already exists before including its contents in the database. We envision one or several centralized repositories, available to the public,

that collect results from different groups. Researchers will be able to share results with colleagues by exchanging just the UUID of the nodes stored on the public repository, rather than sending actual scripts or files. In this collaborative environment the adoption of new codes, the comparison of results, and data disclosure and reproducibility become straightforward, realizing the “social ecosystem” discussed in Section 9.1 and facilitating the reusability of data, codes and workflows. We emphasize that only after having a locally deployed automation infrastructure like AiiDA it becomes feasible to populate public repositories efficiently and in a uniform format, because the user effort to uniform the data, prepare it and upload it is reduced to the minimum.

The standardization of the formats produced by different codes is necessary to maximize the effectiveness of data sharing. This task is outside the scope of the AiiDA project, but we encourage existing and future standardization efforts by the developers of the simulation codes. At the same time, within AiiDA we provide a set of “default” plugins for the most common data structures (crystal structures, paths of k -points in reciprocal space, ...), which can be seamlessly reused in different codes. Implemented classes provide importers and exporters from/to common file formats, so that it is possible to exchange the data also with other infrastructures and repositories that use different data formats. We also emphasize that it is possible to write workflows that perform high-level tasks common to a variety of codes, such as structure optimization or molecular dynamics, even before a standardization of data formats takes place.

Moreover, to encourage the development of the repository pipelines discussed in the “Sharing” pillar, we define in AiiDA a common API for importers and exporters of crystal structures (in the `aiida.tools` package). Also in this case, repositories can be supported by plugin subclasses; plugins for importing structures from some common databases, such as ICSD [20], COD [67], MPOD [27] and TCOD [5] are already distributed with the code.

Conclusion

In the course of this Thesis we studied thermal transport in 2D materials, investigating and developing the concept of collective excitations. We show that the interpretation of thermal transport with a kinetic theory of the phonon gas holds only within the single-mode relaxation time approximation: the phonon relaxation time is not a well defined quantity for describing the thermal conductivity. Scattering events introduce correlations between phonon modes, giving rise to collective phonon excitations called relaxons. Relaxons, at variance with phonons, are characterised by well defined relaxation times and, in case of a homogeneous system, also by a velocity and a mean free path. Therefore, it is possible to recover a kinetic theory description of thermal transport, provided that a gas of relaxons is considered.

The need of properly taking into account collective excitations is strictly connected to the failure of the single-mode relaxation time approximation. While this effect is often negligible in conventional solids at room temperature and becomes apparent only at cryogenic temperatures, collective excitations are fundamental at any temperature in 2D crystals. For the materials examined, the correlation between phonon scatterings is mostly attributed to the dominant presence of normal scattering events. Normal processes play a central role in the transport dynamics, not directly by dissipating the heat flux, but mainly redistributing phonon populations. Only taking into account these collective aspects of the excitations it is possible to obtain large thermal conductivities in 2D systems, that would be otherwise underestimated. Moreover, we show that Callaway's model greatly improves over the single-mode relaxation time approximation and, although discrepancies persist with respect to the exact solution, is an important pointer to the relevance of normal scattering.

We also show that heat conduction cannot always be described by Fourier's law in 2D materials. The statistical nature of this law makes it valid only when the heat carriers are allowed to scatter several time between heat source and sink. Therefore, it cannot be applied when crystal sizes reach the micro or nanoscale and are comparable with the heat-carriers mean free paths. Under these conditions the effective thermal conductivity is not an intrinsic property of the material, but depends on the sample size or shape. In addition, Fourier's law does not apply to describe the response to temperature oscillations. The expected behavior is that of diffusive propagation of heat. Instead, the analysis of the Boltzmann transport equation reveals how heat can propagate as a wave, called second sound, due to the formation of a collective excitation similar to the drifting distribution of Callaway's model. In particular, it should be

possible to observe heat propagating as a thermal wave at room temperature in many 2D materials.

The introduction of relaxons gives us also insights on the validity of Matthiessen's rule. Due to the presence of collective mechanisms, it is not possible to clearly distinguish the contributions to the thermal conductivity (or to a relaxon lifetime) coming from different scattering events, like phonon-isotopes or phonon-phonon processes. Finally, we gained insight on the solvers of the Boltzmann transport equation, showing that the iterative method does not converge for graphene at room temperature and more generally whenever the collective excitations are relevant.

The main conclusion that one can draw from this study is that a complex behavior emerges after shrinking a material to small scales or reduced dimensionality. Laws and approximations that are often used do not hold anymore and care must be taken in describing heat fluxes with macroscopic laws. Instead, a more sophisticated analysis is required and in particular a microscopic description of thermal transport is necessary, as for example that given by the Boltzmann equation used in this Thesis. Most likely, the miniaturization of devices will encounter various unexpected behaviors and there will be several novel phenomena that will need careful investigations.

Although we focused most of the Thesis on the characterisation of thermal transport in 2D materials, this work falls into a broader project for the creation of databases for computational materials properties, which requires a dedicated platform to manage simulations and their results. We first postulated the abstract needs of such a platform with the ADES model, including its fundamental pillars of Automation, Data, Environment and Sharing, and then described its implementation in the open-source infrastructure AiiDA. The AiiDA API provides an intuitive way of interacting with the user, exposing in a simple way the functionalities inherent to Calculation, Data and Code objects. Each logical operation on data is mapped into a custom tailored SQL database, with a schema that allows the storage of directed acyclic graphs and of heterogeneous data. Thanks to the abstraction provided by the API, the user does not need to be aware of the underlying database, the storage solution, or the SQL query language. Procedures for generating new data are encoded in workflows, to provide an efficient turn-key solution for the calculation of properties, and the plugin logic allows for systematically adding new functionalities and support of new codes. The automatic handling of data allows for sharing capabilities across different instances of AiiDA and improving the access to data. We hope that this software will help the transition to a modern approach to computational research, shifting away from the paradigm of error-prone scripting to a systematic methodology based on object programming.

A Computational parameters

First-principles simulations

The second- and third-order force constants for all systems have been calculated using density-functional perturbation theory [38, 55, 56, 91] as implemented in the Quantum ESPRESSO distribution [63], using the local-density approximation and norm-conserving pseudopotentials from the PSLibrary [29]. A summary of the parameters used in the calculations are reported in Table A.1, namely the integration mesh used for the ground state energy calculation (ρ), the mesh for the computation of the dynamical matrix ϕ , and for the anharmonic force constants ψ and the kinetic energy cutoff for the plane wave basis. The structures have been relaxed to minimize the total energy, and we report the final value of the lattice parameter a in the table. The materials have been simulated using 3D periodic boundary conditions in a slab geometry, using an height c sufficiently large to give negligible interactions between periodic images; the c/a factor is reported in the table as well. The force constants, obtained on such coarse grid meshes, are interpolated on finer meshes to be used in the Boltzmann equation using Fourier interpolation.

Thermal conductivity simulations

The Boltzmann transport equation has been solved using the variational method in Chapters 6, 7 and with the diagonalization and iterative method in Chapter 8. The computational parameters (Brillouin zone integration mesh, gaussian smearing and c/a) used to solve it are reported in table A.2. The c/a value is introduced to renormalize the volume of the simulation cell. In fact, the equation for thermal conductivity contains a renormalizing volume whereas, strictly speaking, a 2D system should use a renormalizing surface. However, in order to have a quantity comparable with a 3D thermal conductivity, it is preferable to introduce a volume constituted by the area of the unit cell times the interlayer distance c of the bulk system. In particular, we used the experimental interlayer distances of the corresponding 3D material, whose values have been taken from the ICSD database [20].

Appendix A. Computational parameters

Material	ρ mesh	ϕ mesh	ψ mesh	Pw cutoff	a (Bohr)	c/a
Graphite	16×16×4	8×8×2	4×4×2	90 Ry	4.6077	2.6643
Graphene	24×24×1	16×16×1	4×4×1	90 Ry	4.6074	3.0000
Graphane	24×24×1	16×16×1	4×4×1	90 Ry	4.7621	4.0000
Boron nitride	24×24×1	16×16×1	4×4×1	90 Ry	4.7328	3.0000
Fluorographene	24×24×1	16×16×1	4×4×1	90 Ry	4.8411	3.9347
MoS ₂	24×24×1	16×16×1	6×6×1	100 Ry	6.0081	6.2906
MoSe ₂	24×24×1	16×16×1	6×6×1	100 Ry	6.1898	6.1059
WS ₂	24×24×1	16×16×1	6×6×1	100 Ry	5.8883	4.8139
WSe ₂	24×24×1	16×16×1	6×6×1	100 Ry	6.1279	4.6257

Table A.1 – Computational parameters for density functional theory and linear response calculations.

Material	Integration mesh	Smearing (cm ⁻¹)	c/a
Graphite	64×64×5	10	2.6643
Graphene	128×128×1	10	1.367
Graphane	128×128×1	10	1.367
Boron nitride	128×128×1	10	1.317
Fluorographene	128×128×1	10	1.206
MoS ₂	120×120×1	2	1.945
MoSe ₂	120×120×1	2	1.966
WS ₂	120×120×1	2	1.954
WSe ₂	120×120×1	2	1.974

Table A.2 – Computational parameters used for solving the Boltzmann transport equation.

The isotopic concentrations are chosen to be the natural ones [128]: hydrogen of 99.9885% ¹H, 0.0115% ²H; carbon of 98.93% ¹²C, 1.07% ¹⁴C; boron of 19.9% ¹⁰B, 80.1% ¹¹B, nitrogen of 99.632% ¹⁴N, 0.368% ¹⁵N; fluorine of 100% ¹⁹F; sulphur of 94.93% ³²S, 0.76% ³³S, 4.29% ³⁴S, 0.02% ³⁶S; selenium of 0.0089% ⁷⁴Se, 0.0937% ⁷⁶Se, 0.0763% ⁷⁷Se, 0.2377% ⁷⁸Se, 0.4961% ⁸⁰Se, 0.0873% ⁸²Se; molybdenum of 14.84% ⁹²Mo, 9.25% ⁹⁴Mo, 15.92% ⁹⁵Mo, 16.68% ⁹⁶Mo, 9.55% ⁹⁷Mo, 24.13% ⁹⁸Mo, 9.63% ¹⁰⁰Mo; tungsten of 0.0012% ¹⁸⁰W, 0.2650% ¹⁸²W, 0.1431% ¹⁸³W, 0.3064% ¹⁸⁴W, 0.2843% ¹⁸⁶W.

Tests have been made to assure that the final value of thermal conductivity is converged with respect to the parameters of the calculations.

Most of the calculations that have been made to produce the results shown in this Thesis have been managed using the AiiDA materials' informatics platform [117].

Bibliography

- [1] <https://www.docker.com/>.
- [2] <http://www.djangoproject.com/>.
- [3] <http://www.sqlalchemy.org/>.
- [4] <http://rubyonrails.org/>.
- [5] <http://www.crystallography.net/tcod/>.
- [6] <http://www.celeryproject.org/>.
- [7] <http://supervisord.org/>.
- [8] <http://www.ogf.org>.
- [9] <http://www.unicore.eu/>.
- [10] <http://gc3pie.googlecode.com/>.
- [11] <http://www.adaptivecomputing.com/products/open-source/torque/>.
- [12] <http://www.pbsworks.com/Product.aspx?id=1>.
- [13] <https://computing.llnl.gov/linux/slurm/>.
- [14] <https://github.com/paramiko/paramiko>.
- [15] <http://www.mysql.com/>.
- [16] <http://www.postgresql.org/>.
- [17] <http://www.sqlite.org/>.
- [18] <http://www.neo4j.org/>.
- [19] <http://spglib.sourceforge.net>.
- [20] <http://www.fiz-karlsruhe.com/icsd.html>.
- [21] <http://galaxyproject.org>.

Bibliography

- [22] <https://kepler-project.org>.
- [23] <http://www.knime.org>.
- [24] <http://www.vistrails.org>.
- [25] <http://sphinx-doc.org>.
- [26] <http://www.ietf.org/rfc/rfc4122.txt>.
- [27] <http://mpod.cimav.edu.mx/index/>.
- [28] <http://gridscheduler.sourceforge.net/>.
- [29] Pslibrary. <http://qe-forge.org/gf/project/pslibrary/>.
- [30] C. C. Ackerman, B. Bertman, H. A. Fairbank, and R. A. Guyer. Second sound in solid helium. *Phys. Rev. Lett.*, 16:789–791, 1966.
- [31] P. B. Allen. Improved callaway model for lattice thermal conductivity. *Phys. Rev. B*, 88:144302, 2013.
- [32] A. Alofi and G. P. Srivastava. Thermal conductivity of graphene and graphite. *Phys. Rev. B*, 87:115421, 2013.
- [33] A. Alofi and G. P. Srivastava. Thermal conductivity of graphene and graphite. *Phys. Rev. B*, 87:115421, 2013.
- [34] N. W. Ashcroft and D. N. Mermin. *Solid State Physics*. Thomson Learning, Toronto, 1 edition, 1976.
- [35] S. R. Bahn and K. W. Jacobsen. An object-oriented scripting interface to a legacy electronic structure code. *Comput. Sci. Eng.*, 4(3):56–66, 2002.
- [36] A. A. Balandin. Thermal properties of graphene and nanostructured carbon materials. *Nature Materials*, (8):569–581, 2011.
- [37] A. A. Balandin, S. Ghosh, W. Bao, I. Calizo, D. Teweldebrhan, F. Miao, and C. N. Lau. Superior thermal conductivity of single-layer graphene. *Nano Letters*, 8(3):902–907, 2008.
- [38] S. Baroni, S. de Gironcoli, A. a Dal Corso, and P. Giannozzi. Phonons and related crystal properties from density-functional perturbation theory. *Rev. Mod. Phys.*, 73:515–562, 2001.
- [39] S. Baroni, P. Giannozzi, and A. Testa. Green's-function approach to linear response in solids. *Phys. Rev. Lett.*, 58:1861–1864, 1987.

-
- [40] A. P. Bartók, M. C. Payne, R. Kondor, and G. Csányi. Gaussian approximation potentials: The accuracy of quantum mechanics, without the electrons. *Phys. Rev. Lett.*, 104(13):136403, 2010.
- [41] G. Basile, C. Bernardin, and S. Olla. Momentum conserving model with anomalous thermal conductivity in low dimensional systems. *Phys. Rev. Lett.*, 96:204303, 2006.
- [42] L. S. Blackford, J. Choi, A. Cleary, E. D’Azevedo, J. Demmel, I. Dhillon, J. Dongarra, S. Hammarling, G. Henry, A. Petitet, K. Stanley, D. Walker, and R. C. Whaley. *ScaLAPACK Users’ Guide*. Society for Industrial and Applied Mathematics, Philadelphia, PA, 1997.
- [43] N. Bonini, J. Garg, and N. Marzari. Acoustic phonon lifetimes and thermal transport in free-standing and strained graphene. *Nano Letters*, 12(6):2673–2678, 2012.
- [44] D. A. Broido, M. Malorny, G. Birner, N. Mingo, and D. A. Stewart. Intrinsic lattice thermal conductivity of semiconductors from first principles. *Applied Physics Letters*, 91(23):231922, 2007.
- [45] D. A. Broido, A. Ward, and N. Mingo. Lattice thermal conductivity of silicon from empirical interatomic potentials. *Phys. Rev. B*, 72:014308, 2005.
- [46] D. G. Cahill, P. V. Braun, G. Chen, D. R. Clarke, S. Fan, K. E. Goodson, P. Koblinski, W. P. King, G. D. Mahan, A. Majumdar, H. J. Maris, S. R. Phillpot, E. Pop, and L. Shi. Nanoscale thermal transport. ii. 2003–2012. *Applied Physics Reviews*, 1(1), 2014.
- [47] Joseph Callaway. Model for lattice thermal conductivity at low temperatures. *Phys. Rev.*, 113:1046–1051, 1959.
- [48] P. Carruthers. Theory of thermal conductivity of solids at low temperatures. *Rev. Mod. Phys.*, 33:92–138, 1961.
- [49] H. B. G. Casimir. Note on the conduction of heat in crystals. *Physica*, 5:495–500, 1938.
- [50] A. Cepellotti, G. Fugallo, L. Paulatto, M. Lazzeri, F. Mauri, and N. Marzari. Phonon hydrodynamics in two-dimensional materials. *Nat. Commun.*, 6(6400), 2015.
- [51] A. Cepellotti and N. Marzari. Thermal transport in crystals as a kinetic theory of relaxons. *in preparation*, 2015.
- [52] L. Chaput. Direct solution to the linearized phonon boltzmann equation. *Phys. Rev. Lett.*, 110:265506, 2013.
- [53] M. Chester. Second sound in solids. *Phys. Rev.*, 131:2013–2015, 1963.
- [54] C. Cohen-Tannoudji, B. Diu, F. Laloe, and B. Dui. *Quantum Mechanics (2 vol. set)*. Wiley-Interscience, 2006.

Bibliography

- [55] A. Debernardi, S. Baroni, and E. Molinari. Anharmonic phonon lifetimes in semiconductors from density-functional perturbation theory. *Phys. Rev. Lett.*, 75:1819–1822, 1995.
- [56] G. Deinzer, G. Birner, and D. Strauch. Ab initio calculation of the linewidth of various phonon modes in germanium and silicon. *Phys. Rev. B*, 67:144304, 2003.
- [57] A. Dhar. Heat conduction in the disordered harmonic chain revisited. *Phys. Rev. Lett.*, 86:5882–5885, 2001.
- [58] G. Dong, L. Libkin, J. Su, and L. Wong. Maintaining the transitive closure of graphs in sql. *Int. Journal of Information Technology*, 5:46–78, 1999.
- [59] O. Dubay and G. Kresse. Accurate density functional calculations for the phonon dispersion relations of graphite layer and carbon nanotubes. *Phys. Rev. B*, 67:035401, 2003.
- [60] G. Fugallo, A. Cepellotti, L. Paulatto, M. Lazzeri, N. Marzari, and F. Mauri. Thermal conductivity of graphene and graphite: Collective excitations and mean free paths. *Nano Letters*, 14(11):6109–6114, 2014.
- [61] G. Fugallo, M. Lazzeri, L. Paulatto, and F. Mauri. *Ab initio* variational approach for evaluating lattice thermal conductivity. *Phys. Rev. B*, 88:045430, 2013.
- [62] J. Garg, N. Bonini, B. Kozinsky, and N. Marzari. Role of disorder and anharmonicity in the thermal conductivity of silicon-germanium alloys: A first-principles study. *Phys. Rev. Lett.*, 106:045901, 2011.
- [63] P. Giannozzi, S. Baroni, N. Bonini, M. Calandra, R. Car, C. Cavazzoni, D. Ceresoli, G. L. Chiarotti, M. Cococcioni, I. Dabo, A. Dal Corso, S. de Gironcoli, S. Fabris, G. Fratesi, R. Gebauer, U. Gerstmann, C. Gougoussi, A. Kokalj, M. Lazzeri, L. Martin-Samos, N. Marzari, F. Mauri, R. Mazzarello, S. Paolini, A. Pasquarello, L. Paulatto, C. Sbraccia, S. Scandolo, G. Sclauzero, A. P. Seitsonen, A. Smogunov, P. Umari, and R. M. Wentzcovitch. Quantum espresso: a modular and open-source software project for quantum simulations of materials. *J. Phys.: Condens. Matter*, 21:395502, 2009.
- [64] F. Giustino. *Materials Modelling using Density Functional Theory: Properties and Predictions*. Oxford University Press. Oxford University Press, USA, 2014.
- [65] C. W. Glass, A. R. Oganov, and N. Hansen. Uspex—evolutionary crystal structure prediction. *Computer Physics Communications*, 175(11–12):713 – 720, 2006.
- [66] X. Gonze and J.-P. Vigneron. Density-functional approach to nonlinear-response coefficients of solids. *Phys. Rev. B*, 39:13120–13128, 1989.
- [67] S. Gražulis, A. Daškevič, A. Merkys, D. Chateigner, L. Lutterotti, M. Quirós, N. R. Serebryanaya, P. Moeck, R. T. Downs, and A. Le Bail. Crystallography open database (cod): an

- open-access collection of crystal structures and platform for world-wide collaboration. *Nucleic Acids Research*, 40(D1):D420–D427, 2012.
- [68] M. S. Green. Markoff random processes and the statistical mechanics of time-dependent phenomena. ii. irreversible processes in fluids. *The Journal of Chemical Physics*, 22(3):398–413, 1954.
- [69] R. A. Guyer and J. A. Krumhansl. Solution of the linearized phonon boltzmann equation. *Phys. Rev.*, 148:766–778, 1966.
- [70] R. A. Guyer and J. A. Krumhansl. Thermal conductivity, second sound, and phonon hydrodynamic phenomena in nonmetallic crystals. *Phys. Rev.*, 148:778–788, 1966.
- [71] R. A. H. Hamilton and J. E. Parrot. Variational calculation of the thermal conductivity of germanium. *Phys. Rev.*, 178:1284–1292, 1969.
- [72] R. J. Hardy. Energy-flux operator for a lattice. *Phys. Rev.*, 132:168–177, 1963.
- [73] R. J. Hardy. Lowest-order contribution to the lattice thermal conductivity. *Journal of Mathematical Physics*, 6(11):1749–1761, 1965.
- [74] R. J. Hardy. Phonon boltzmann equation and second sound in solids. *Phys. Rev. B*, 2:1193–1207, 1970.
- [75] L. He, F. Liu, G. Hautier, M. J. T. Oliveira, M. A. L. Marques, F. D. Vila, J. J. Rehr, G. M. Rignanese, and A. Zhou. Accuracy of generalized gradient approximation functionals for density-functional perturbation theory calculations. *Phys. Rev. B*, 89:064305, 2014.
- [76] B. Hehlen, A. Pérou, E. Courtens, and R. Vacher. Observation of a doublet in the quasielastic central peak of quantum-paraelectric srTiO_3 . *Phys. Rev. Lett.*, 75:2416–2419, 1995.
- [77] C. Herring. Theory of the thermoelectric power of semiconductors. *Phys. Rev.*, 96:1163–1187, 1954.
- [78] C. Y. Ho, R. W. Powell, and P. E. Liley. Thermal conductivity of the elements. *Journal of Physical and Chemical Reference Data*, 1(2):279–421, 1972.
- [79] P. Hohenberg and W. Kohn. Inhomogeneous electron gas. *Phys. Rev.*, 136:B864–B871, 1964.
- [80] C. Horie and J. A. Krumhansl. Boltzmann equation in a phonon system. *Phys. Rev.*, 136:A1397–A1407, 1964.
- [81] H. E. Jackson, C. T. Walker, and T. F. McNelly. Second sound in naf. *Phys. Rev. Lett.*, 25:26–28, 1970.

Bibliography

- [82] A. Jain, G. Hautier, C. J. Moore, S. Ping Ong, C. C. Fischer, T. Mueller, K. A. Persson, and G. Ceder. A high-throughput infrastructure for density functional theory calculations. *Comp. Mat. Sci.*, 50(8):2295–2310, 2011.
- [83] P. G. Klemens. Phonon scattering and thermal resistance due to grain boundaries, 1994.
- [84] P.G. Klemens. *Thermal Conductivity and Lattice Vibrational Modes*. Solid State Physics. Academic Press, New York, 1958.
- [85] M. Kohler. Behandlung von nichtgleichgewichtsvorgängen mit hilfe eines extremalprinzips. *Z. Phys.*, 124(772-789), 1948.
- [86] M. Kohler. Transporterscheinungen im elektronengas. *Z. Phys.*, 125(679-693), 1948.
- [87] W. Kohn and L. J. Sham. Self-consistent equations including exchange and correlation effects. *Phys. Rev.*, 140:A1133–A1138, 1965.
- [88] J. A. Krumhansl. Thermal conductivity of insulating crystals in the presence of normal processes. *Proceedings of the Physical Society*, 85(5):921, 1965.
- [89] R. Kubo. Statistical-mechanical theory of irreversible processes. i. general theory and simple applications to magnetic and conduction problems. *Journal of the Physical Society of Japan*, 12(6):570–586, 1957.
- [90] L. D. Landau and Lifshitz E. M. *Statistical physics, vol. 5. Course of theoretical physics*. 1980.
- [91] M. Lazzeri and S. de Gironcoli. First-principles study of the thermal expansion of be(1010). *Phys. Rev. B*, 65:245402, 2002.
- [92] S. Lee, D. Broido, K. Esfarjani, and G. Chen. Hydrodynamic phonon transport in suspended graphene. *Nat. Commun.*, 6(6290), 2015.
- [93] S. Lepri, R. Livi, and A. Politi. Thermal conduction in classical low-dimensional lattices. *Phys. Rep.s*, 377(1):1 – 80, 2003.
- [94] W. Li, J. Carrete, N. A. Katcho, and N. Mingo. Shengbte: A solver of the boltzmann transport equation for phonons. *Computer Physics Communications*, 185(6):1747 – 1758, 2014.
- [95] X. Li, K. Maute, M. L. Dunn, and R. Yang. Strain effects on the thermal conductivity of nanostructures. *Phys. Rev. B*, 81:245318, 2010.
- [96] L. Lindsay and D. A. Broido. Enhanced thermal conductivity and isotope effect in single-layer hexagonal boron nitride. *Phys. Rev. B*, 84:155421, 2011.
- [97] L. Lindsay, D. A. Broido, and N. Mingo. Flexural phonons and thermal transport in graphene. *Phys. Rev. B*, 82:115427, 2010.

-
- [98] L. Lindsay, D. A. Broido, and N. Mingo. Flexural phonons and thermal transport in multilayer graphene and graphite. *Phys. Rev. B*, 83:235428, 2011.
- [99] L. Lindsay, W. Li, J. Carrete, N. Mingo, D. A. Broido, and T. L. Reinecke. Phonon thermal transport in strained and unstrained graphene from first principles. *Phys. Rev. B*, 89:155426, 2014.
- [100] F. Ma, H. B. Zheng, Y. J. Sun, D. Yang, K. W. Xu, and P. K. Chu. Strain effect on lattice vibration, heat capacity, and thermal conductivity of graphene. *Applied Physics Letters*, 101(11):111904, 2012.
- [101] R. M. Martin. *Electronic Structure: Basic Theory and Practical Methods (Vol 1)*. Cambridge University Press, 2004.
- [102] J. C. Maxwell. On the dynamical theory of gases. *Philosophical Transactions of the Royal Society of London*, 157:49–88, 1867.
- [103] L. Moreau, B. Clifford, J. Freire, J. Futrelle, Y. Gil, P. Groth, N. Kwasnikowska, S. Miles, P. Missier, J. Myers, B. Plale, Y. Simmhan, E. Stephan, and J. Van den Bussche. The open provenance model core specification (v1.1). *Future Generation Computer Systems*, 27(6):743–756, 2011.
- [104] X. Mu, X. Wu, T. Zhang, D. B. Go, and T. Luo. Thermal transport in graphene oxide –from ballistic extreme to amorphous limit. *Sci. Rep.*, 4, 01 2014.
- [105] P. Murray-Rust and H. S. Rzepa. Chemical markup, xml, and the world wide web. 4. cml schema. *J. Chem. Inf. Comput. Sci.*, 43(3):757–772, 2003.
- [106] V. Narayanamurti and R. Dynes. Observation of second sound in bismuth. *Phys. Rev. Lett.*, 28:1461–1465, 1972.
- [107] D.L. Nika, S. Ghosh, E.P. Pokatilov, and A.A. Balandin. Lattice thermal conductivity of graphene flakes: Comparison with bulk graphite. *Applied Physics Letters*, 94(20):203103–203103–3, 2009.
- [108] M Omini and A Sparavigna. An iterative approach to the phonon boltzmann equation in the theory of thermal conductivity. *Physica B: Condensed Matter*, 212(2):101 – 112, 1995.
- [109] M. Omini and A. Sparavigna. Beyond the isotropic-model approximation in the theory of thermal conductivity. *Phys. Rev. B*, 53:9064–9073, 1996.
- [110] M. Omini and A. Sparavigna. Heat transport in dielectric solids with diamond structure. *Il Nuovo Cimento D*, 19(10):1537, 1997.
- [111] S. P. Ong, W. D. Richards, A. Jain, G. Hautier, M. Kocher, S. Cholia, D. Gunter, V. L. Chevrier, K. A. Persson, and G. Ceder. Python materials genomics (pymatgen): A robust, open-source python library for materials analysis. *Comp. Mat. Sci.*, 68(0):314–319, 2013.

Bibliography

- [112] L. Paulatto, F. Mauri, and M. Lazzeri. Anharmonic properties from a generalized third-order *ab initio* approach: Theory and applications to graphite and graphene. *Phys. Rev. B*, 87:214303, 2013.
- [113] R. Peierls. Zur kinetischen theorie der wärmeleitung in kristallen. *Annalen der Physik*, 395(8):1055–1101, 1929.
- [114] J. P. Perdew and A. Zunger. Self-interaction correction to density-functional approximations for many-electron systems. *Phys. Rev. B*, 23:5048–5079, 1981.
- [115] F. Pérez and B. E. Granger. IPython: a system for interactive scientific computing. *Computing in Science and Engineering*, 9(3):21–29, 2007.
- [116] C. J. Pickard and R. J. Needs. Ab initio random structure searching. *J. Phys. Cond. Matt.*, 23(5):053201, 2011.
- [117] G. Pizzi, A. Cepellotti, R. Sabatini, N. Marzari, and B. Kozinsky. Aiida: automated interactive infrastructure and database for computational science. *Computational Materials Science*, 111:218 – 230, 2016.
- [118] D. Pohl and V. Irniger. Observation of second sound in naf by means of light scattering. *Phys. Rev. Lett.*, 36:480–483, 1976.
- [119] W. H. Press, S. A. Teukolsky, W. T. Vetterling, and B. P. Flannery. *Numerical Recipes 3rd Edition: The Art of Scientific Computing*. Cambridge University Press, 2007.
- [120] W. Setyawan and S. Curtarolo. High-throughput electronic band structure calculations: Challenges and tools. *Computational Materials Science*, 49(2):299–312, 2010.
- [121] D. Singh, J. Y. Murthy, and T. S. Fisher. Mechanism of thermal conductivity reduction in few-layer graphene. *Journal of Applied Physics*, 110(4):044317, 2011.
- [122] D. Singh, J. Y. Murthy, and T. S. Fisher. Spectral phonon conduction and dominant scattering pathways in graphene. *Journal of Applied Physics*, 110(9):094312, 2011.
- [123] G.P. Srivastava. *The Physics of Phonons*. Taylor & Francis, 1990.
- [124] A. Togo, L. Chaput, and I. Tanaka. Distributions of phonon lifetimes in brillouin zones. *Phys. Rev. B*, 91:094306, 2015.
- [125] P. Tröger, H. Rajic, A. Haas, and P. Domagalski. Standardization of an api for distributed resource management system. In *Proceedings of the Seventh IEEE International Symposium on Cluster Computing and the Grid (CCGrid 2007), Rio de Janeiro, Brazil*, pages 619–626, 2007. <http://www.drmaa.org/>.
- [126] S. van der Walt, S. C. Colbert, and G. Varoquaux. The numpy array: A structure for efficient numerical computation. *Comput. Sci. Eng.*, 13:22, 2011.

- [127] Richard Van Noorden, Brendan Maher, and Regina Nuzzo. *The top 100 papers*, volume 514. 2014.
- [128] M. E. Wieser, N. Holden, T. B. Coplen, J. K. Böhlke, M. Berglund, W. A. Brand, P. De Bièvre, M. Groening, R. D. Loss, J. Meija, T. Hirata, T. Prohaska, R. Schoenberg, G. O'Connor, T. Walczyk, S. Yoneda, and X. K. Zhu. Atomic weights of the elements 2011 (iupac technical report). *Pure Appl. Chem.*, 85(5):883–1078, 2013.
- [129] K. Wolstencroft, R. Haines, D. Fellows, A. Williams, D. Withers, S. Owen, S. Soiland-Reyes, I. Dunlop, A. Nenadic, P. Fisher, J. Bhagat, K. Belhajjame, F. Bacall, A. Hardisty, A. Nieva de la Hidalga, M. P. Balcazar Vargas, S. Sufi, and C. Goble. The taverna workflow suite: designing and executing workflows of web services on the desktop, web or in the cloud. *Nucleic Acids Research*, 41(W1):W557–W561, 2013.
- [130] X. Xu, L. F. C. Pereira, Y. Wang, J. Wu, K. Zhang, X. Zhao, S. Bae, C. Tinh Bui, R. Xie, J. T. L. Thong, B. H. Hong, K. P. Loh, D. Donadio, B. Li, and B. Özyilmaz. Length-dependent thermal conductivity in suspended single-layer graphene. *Nat. Commun.*, 5:3689, 2014.
- [131] L. Yang, P. Grassberger, and B. Hu. Dimensional crossover of heat conduction in low dimensions. *Phys. Rev. E*, 74:062101, 2006.
- [132] J.M. Ziman. *Electrons and Phonons: The Theory of Transport Phenomena in Solids*. Oxford Classic Texts in the Physical Sciences. Oxford University Press, USA, 2001.

Curriculum Vitae

Andrea Cepellotti

Affiliation: Theory and Simulations of Materials (THEOS) and National Center for Computational Design and Discovery of Novel Materials (MARVEL), École Polytechnique Fédérale de Lausanne, Station 12, 1015 Lausanne, Switzerland.

Postal Address: EPFL STI IMX THEOS, Station 12, 1015 Lausanne, Switzerland

Birth: 30th August 1987, Monfalcone, Italy

Nationality: Italian

Email: andrea.cepellotti@epfl.ch

Telephone: +41 21 69 31159

Education

- Nov 2011 – present: Ph.D. in the Institute of Materials of EPFL. Supervisor: Prof. N. Marzari.
Thesis: *Electronic and thermal transport at the nanoscale*
- Sep 2009 – Sep 2011: *Laurea Magistralis in Physics* (M.Sc. equivalent) at the University of Trieste,
Thesis: *Characterization of the NO-NH₃ complex on a Pt (111) surface: an ab-initio study*
110/110 *summa cum laude*, average exam mark: 29.8/30 (see below).
- Sep 2006 – Sep 2009: *Laurea in Physics* (B.Sc. equivalent) at the University of Trieste.
Thesis: *Multistep methods for numerical integration in the simulation of biophysical system.*
110/110 *summa cum laude*, average exam mark: 28.7/30 (see below).

Research Interests

Density Functional Theory, Phonons, Thermal conductivity, Databases, High throughput.

Publications

- A. Cepellotti, and N. Marzari, *Heat transport in crystals as a kinetic theory of relaxons*, (submitted), Nov. 2015
- G. Pizzi*, A. Cepellotti*, R. Sabatini, N. Marzari, and B. Kozinsky, *AiiDA: Automated Interactive Infrastructure and Database for Computational Science*, *Comp. Mat. Sci* 111, 218-230 (2016)
Link
- A. Cepellotti*, G. Fugallo*, L. Paulatto, M. Lazzeri, F. Mauri, and N. Marzari, *Phonon hydrodynamics in two-dimensional materials*, *Nat. Commun.* 6, 7400 (2015). Link
- G. Fugallo*, A. Cepellotti*, L. Paulatto, M. Lazzeri, N. Marzari, and F. Mauri, *Thermal conductivity of graphene and graphite: collective excitations and mean free paths*, *Nano Lett.* 14, 6109 (2014). Link
- A. Cepellotti, A. Peronio, S. Marchini, N. Abdurakhmanova, C. Dri, C. Africh, F. Esch, G. Comelli, and M. Peressi, *NH₃-NO Coadsorption System on Pt(111). II. Intermolecular Interaction*, *J. Phys. Chem. C*, 117 (41), 21196 (2013). Link
- A. Peronio, A. Cepellotti, S. Marchini, N. Abdurakhmanova, C. Dri, C. Africh, F. Esch, M. Peressi, and G. Comelli, *NH₃-NO Coadsorption System on Pt(111). I. Structure of the Mixed Layer*, *J. Phys. Chem. C*, 117 (41), 21186 (2013). Link

*: equally contributed

Invited talks

- Summer School of the Max-Planck-EPFL Center for Molecular Nanoscience & Technology, Schloss Ringberg - Tegernsee, Germany, 27-31 July 2015, *Thermal transport from first-principles: the Boltzmann transport equation*
- Advanced thermoelectrics at nanoscale: from materials to devices, Paris, France, 7-10 July 2015, *Phonon hydrodynamics in two-dimensional materials*
- IntOP2015, Jyväskylä, Finland, 28-29 May 2015, *AiiDA framework and integration*
- SOS 19 Workshop, Park City, Utah, 2 – 5 March 2015, *AiiDA project*
- EUPHONON workshop, Le Mans, France, 1-5 September 2014, *Thermal Conductivity of Graphene and Graphite: Collective Excitations and Mean Free Paths*
- 2nd international conference on Phononics and Thermal Energy Science (PTES), Shanghai, China, 26-31 May 2014, *Collective excitations in the thermal conductivity of graphene*

Contributed Talks

- Psi-k Conference, San Sebastian, Spain, 7 - 10 September 2015, *Phonon hydrodynamics and second sound in 2D materials*.
- German Physical Society (DPG) spring meeting, Dresden, Germany, 30 March - 4 April 2014, *Breakdown of Fourier law in layered materials*.
- XCIX National Congress of the Italian Physics Society (SIF), Italy, 23 - 27 settembre 2013, *The NH₃-NO coadsorption system on Pt(111): structure and intermolecular interactions*.
- European Congress and Exhibition on Advanced Materials and Processes (EUROMAT), Sevilla, Spain, 8-13 September 2013, *Thermal conductivity of graphene from first principles*
- PASC Junior retreat, Männedorf, Switzerland, 9-12 July 2013, *Thermal conductivity of graphene from first principles*
- German Physical Society (DPG) spring meeting, Regensburg, Germany, 10-15 March 2013, *Thermal conductivity of graphene from first principles*.
- German Physical Society (DPG) spring meeting, Technische Universität, Berlin, Germany, 25-30 March 2012, *Structure and characterization of the hydrogen-bonded NH₃-NO coadsorption on Pt(111): an ab-initio study*.

Organisation of Conferences & Tutorials

- *AiiDA tutorial*, CECAM / Psi-k Research Conference: Frontiers of first-principles simulations: materials design and discovery, Berlin, Germany, 5 February 2015.
- *AiiDA tutorial*, Zürich, Switzerland, 31 October 2014.

Awards

- Scholarship "Collegio Universitario per le Scienze Luciano Fonda", 2009, funded by Elettra S.p.A. (Synchrotron light laboratory, Trieste, Italy).
- Final poster competition, Junior Euromat 2014, Lausanne
- Best Poster Presentation, International CAMD'14 Summer School, Technical University of Denmark, Copenhagen

Conferences and Summer Schools

- CECAM workshop, Future technologies in automated atomistic simulations, Lausanne, Switzerland, 8-10 June 2015.
- CECAM school, Excitations in Realistic Materials using Yambo on Massively Parallel Architectures, Lausanne, Switzerland, 13-17 April 2015.
- Psi-k Research Conference, Frontiers of first-principles simulations: materials design and discovery, Berlin, Germany, 1-5 February 2015.
- International workshop on computational physics and materials science: Total Energy and force methods, Trieste, Italy, 15-17 January 2015.
- The CAMD Summer School, Technical University of Denmark, Copenhagen, Denmark, 17-22 August 2014
- 12th Junior Euromat, EPFL, Lausanne, Switzerland, 21-25 July 2014
- CECAM Workshop: Modeling the physical properties of clustering crystals, Lausanne, Switzerland, 4-6 November 2013.
- International workshop on computational physics and materials science: Total Energy and force methods, Trieste, Italy, 10-12 January 2013.
- CECAM Workshop, Vibrational coupling: most important, often ignored, and a challenge for ab-initio theory, CECAM, Lausanne (Switzerland) 6-9 November 2012.
- CECAM Workshop, Validation and Verification in Electronic-Structure calculations: state of the art and perspectives, CECAM, Lausanne (Switzerland) 5-7 September 2012.
- CCMX summer school, Multiscale modeling of materials. EPFL, Lausanne (Switzerland) 29-31 August 2012.
- Hermes summer school 2012, Cumberland Lodge, London (United Kingdom) 27-30 July 2012.

Current research (Ph.D.)

The thermal conductivity of materials is a key property attracting much interest both for its role and relevance to thermoelectric waste heat recovery, and for the scientific questions and technological opportunities that are arising in the field of low-dimensional materials. When dimensionality is reduced or the relevant sizes reach microscopic scales, the knowledge developed in the past on conventional bulk crystals becomes insufficient, and novel properties emerge. By means of solving a semiclassical Boltzmann transport equation based on first-principles phonon properties, I characterize the lattice thermal conductivity of crystals, with a focus on layered and two-dimensional materials, such as graphite, graphene, boron nitride and transition metal dichalcogenides. I have shown that the thermal conductivity in homogeneous two-dimensional materials is dominated by normal scattering events (conserving momentum and energy), rather than heat-flux dissipative events. As a result, collective phonon excitations, and not single phonons, are the main heat carriers in these materials and novel hydrodynamic phonon transport regimes emerge (previously confined only to cryogenic temperatures). With such approach, many peculiar behaviors of 2D materials can be rationalized, such as extremely long heat mean free paths (1mm and above), breakdowns of the Fourier law, and the presence of second sound (i.e. thermal waves).

Another major area of interest encompasses the automatization of calculations. In fact, computational science has seen in the last decades a spectacular rise in the scope, breadth, and depth of its efforts. Notwithstanding this prevalence and impact, it is often still performed using the renaissance model of individual artisans gathered in a workshop, under the guidance of an established practitioner. This model is approaching its limits, since the high performance computational capability is ever increasing and a multitude of calculations and prediction of complex properties can now be run. Great benefits could

come by adopting concepts and tools from computer science to manage, preserve, and share these computational efforts. To this aim, I contributed as a main developer to the open-source AiiDA platform (available online on www.aiida.net), tuned first to the demands of computational materials science. AiiDA is an informatics infrastructure, designed to execute, preserve, and disseminate the simulations, data, and workflows of modern-day computational science. Able to store the full provenance of each object, and based on a tailored database built for efficient data mining of heterogeneous results, AiiDA gives the user the ability to interact seamlessly with any number of remote HPC resources and codes, thanks to its flexible plugin interface and workflow engine for the automation of complex sequences of simulations.

Previous Research (M.Sc.)

Thesis Title: *Characterization of the NO-NH₃ complex on a Pt (111) surface: an ab-initio study.*

Supervisor: Prof. M. Peressi.

In this work, I studied the coadsorption of ammonia and nitric oxide on a Pt(111) surface, that is believed to play an important role as an intermediate state for the catalytic selective reduction of nitric oxide. The theoretical analysis, together with the STM-based experimental observations (CNR-IOM, TASC Laboratory, Trieste), proved the existence of a molecular complex formed on the surface. By means of Density Functional Theory, as implemented in the Quantum Espresso platform, I characterized the electronic structure, identifying the most stable structure, understanding the nature of the bond between the adsorbates, calculating the STM image and the vibrational frequencies, spending particular attention to the comparison with experimental data. I proved theoretically that the interaction between the adsorbates is driven by an hydrogen bond between the N, H and O atoms, stabilized by the interaction with the substrate.

References

- Professor Nicola Marzari (Ph.D. thesis supervisor),
Theory and Simulations of Materials (THEOS) and National Center for Computational Design and Discovery of Novel Materials (MARVEL), École Polytechnique Fédérale de Lausanne, Station 12, 1015 Lausanne, Switzerland.
Email: nicola.marzari@epfl.ch
- Professor Francesco Mauri,
Institut de Minéralogie, de Physique des Matériaux, et de Cosmochimie (IMPMC), Sorbonne Universités, UPMC University Paris 06, UMR CNRS 7590, Muséum National d'Histoire Naturelle, IRD UMR 206, 4 Place Jussieu, F-75005 Paris, France
Email: francesco.mauri@impmc.jussieu.fr
- Professor Maria Peressi (M.Sc. thesis supervisor),
Department of Physics, University of Trieste, via Alfonso Valerio 2, 34127 Trieste, Italy
Email: peressi@ts.infn.it

